



Room 14-0551
77 Massachusetts Avenue
Cambridge, MA 02139
Ph: 617.253.5668 Fax: 617.253.1690
Email: docs@mit.edu
<http://libraries.mit.edu/docs>

DISCLAIMER OF QUALITY

Due to the condition of the original material, there are unavoidable flaws in this reproduction. We have made every effort possible to provide you with the best copy available. If you are dissatisfied with this product and find it unusable, please contact Document Services as soon as possible.

Thank you.

Some pages in the original document contain color pictures or graphics that will not scan or reproduce well.

Investigations at Tal-i Iblis: Evidence for Copper Smelting During the Chalcolithic Period

By
Lesley Frame

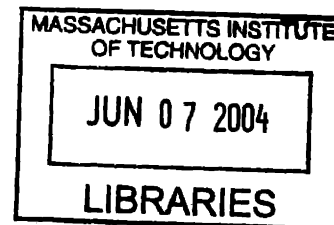
Submitted to the Department of Materials Science and Engineering in Partial Fulfillment of the
Requirements for the Degree of

Bachelor of Science

at the

Massachusetts Institute of Technology

June 2004



© Lesley Frame All rights reserved

The author hereby grants to MIT permission to reproduce and to distribute publicly paper and
electronic copies of this thesis in whole or in part.

Signature of the Author _____
Department of Materials Science and Engineering
May 14th, 2004

Certified by _____
Heather Lechtman
Professor of Archaeology & Ancient Technology
Thesis Supervisor

Accepted by _____
Lorna Gibson
Matoulas S. Salapatas Professor of Materials Science and Engineering
Chairperson, Undergraduate Thesis Committee

ARCHIVES

Acknowledgements

I would like to thank my thesis Advisor, Professor Heather Lechtman for her support, encouragement and insight during the course of this study; her advice has been invaluable as I have explored the topic of ancient technologies. I would also like to thank Dr. Elizabeth Hendrix, whose technical guidance and enduring support have helped to shape my laboratory practices and educational development for the past three years. In addition, my mother, my father and Steven Werlin have provided a strong base of emotional support throughout my years at MIT; thank you for helping me through the hard times.

This thesis was produced through the employment of several analytical methods, and therefore, I would like to thank the many laboratory supervisors for their expert advice. Especially helpful were Dr. Anthony Garratt-Reed, Dr. Nilanjan Chatterjee, Dr. Harold Larson, Joseph Adario, Dr. Fengcheng Chou. I would also like to thank the following people for their exemplary guidance as I studied the artifacts from Tal-i Iblis: Professor Merton Flemings, Professor Linn Hobbs, Professor Dorothy Hosler, Professor John Germaine, Jennifer Meanwell, my family and the Wild Women of WILG.

Abstract

This thesis examines a small corpus of artifacts from Tal-i Iblis, Iran dating to the mid-6th millennium BCE. When excavated in the late 1960s, these artifacts were presumed to be evidence of an early copper smelting technology on the Iranian Plateau, and they were delivered to MIT for further analysis. In this thesis I briefly describe the origins of early metallurgical activity in the Old World focusing mainly on the Iranian Plateau. This will provide a basis for the significance of the thesis and of the early date associated with the metallurgical objects. I have studied six of the Tal-i Iblis artifacts curated at MIT through extensive qualitative and quantitative analytical methods. These methods are described in Chapter IV. The results and discussion are presented in Chapters V and VI. I have found that these Iblis sherds provide substantial evidence for the presence of a copper smelting technology during the early occupation levels at Tal-i Iblis, Iran.

Table of Contents

	Page Number
List of Figures	9
List of Tables	16
Chapter I: Introduction to Early Metallurgy	
1.1 Background	19
1.2 History of Metallurgy	19
1.3 Metal Production during the Chalcolithic Period	23
Chapter II: Tal-i Iblis region	
2.1 Metals on the Iranian Plateau and at Tal-i Iblis	27
2.1.1 The Ore Geology of the Iranian Plateau	29
2.2 Tal-i Iblis	30
Chapter III: Motivation for research	
3.1 Purpose of the research	36
3.2 Preparation for the research	40
Chapter IV: Methodology	
4.1 Methods for Analysis	44
4.2 Microscopy	44
4.2.1 Environmental Scanning Electron Microscopy	45
4.2.2 Petrographic Thin Section Microscopy	47
4.3 Thermal Analysis	49
4.3.1 Differential Thermal Analysis	49
4.3.2 Re-firing Experiments with Modern Crucible Replica	51
4.4 Compositional Analysis	52
4.4.1 Bulk Chemical Compositional Analysis	52
4.4.2 X-Ray Diffraction Analysis	53
4.4.3 SEM X-Ray Mapping	54
4.4.4 Electron Microprobe Analysis	54
Chapter V: Results	
5.1 Macroscopic Description of the Crucible Sherds	56
5.1.1 Photography and Drawings	57

	Page Number
5.1.2 Environmental Scanning Electron Microscopy	64
5.1.3 Summary	68
5.2 Comparison: Tal-i Iblis Sherds and Modern Crucible Replica	68
5.2.1 Thin Section Analysis of Archaeological and Replica Crucibles	70
5.2.2 X-Ray Diffraction of Archaeological and Replica Crucibles	75
5.2.3 Bulk Chemical Analysis of Archaeological and Replica Crucibles	82
5.2.4 Dissimilarities Between Archaeological and Replica Crucibles	82
5.2.5 Summary	84
5.3 Thermal Analysis	85
5.3.1 Differential Thermal Analysis of Archaeological and Replica Crucibles	85
5.3.2 Re-firing Experiment using Modern Replica Crucible (MIT No. 5277)	89
5.3.3 Summary	100
5.4 Characterization of Zones 3 and 4 from Tal-i Iblis Crucible Sherds	100
5.4.1 Scanning Electron Microscopy and Elemental X-Ray Mapping	100
5.4.2 Photomicrography and Electron Microprobe Analysis	102
5.5 Summary	109
Chapter VI: Discussion	
6.1 Copper at the Site of Tal-i Iblis	113
6.2 The Use of the Crucibles at Tal-i Iblis	113
6.3 Temperatures Reached in the Crucible Fabric during Use	117
6.4 Significance of Zone 4 in the Ancient Crucibles	118
Chapter VII: Conclusion	
Appendix A	127
Appendix B	149
Appendix C	157
References Cited	159

List of Figures

Figure Number	Caption	Page Number
1.1	Some examples of carbonate copper ores. (a) Malachite; (b) azurite. < http://minerals.gps.caltech.edu/COLOR_Causes/Metal_Ion/ >	20
1.2	Archaeological sites in Iran (Pigott 1999:75).	22
1.3	An example of a pit smelting operation in Ambelikou, Cyprus drawn by Tylecote (1982:233). No date or site information provided.	23
2.1	Modern copper ore bodies in Anatolia and Iran (Pigott 1999:83).	28
2.2	The five main copper districts of Iran (Bazin and Hübner 1969:10).	29
2.3	Ore bodies near Tal-i Iblis (Bazin and Hubner 1969:119), with overlain circles at 50km and 100 km from Tal-i Iblis. The carbonate ore sources are indicated in green.	31
2.4	Photograph of Tal-I Iblis taken by Stein (1937: Fig.55) from North-west view.	32
2.5	Photograph taken by Caldwell in 1964 (1967:10). The center of the mound was dug out.	33
3.1	Drawing of a crucible restored from a large fragment found in level II (Caldwell Cat. No. 277, 1967:185).	36
3.2	Photograph of a replica (MIT No. 5277) of an Iblis crucible made in 1966 by Hildegard Wulff at Tal-i Iblis, using local clay.	37
3.3	Set-up for on-site experiment conducted by Pleiner (1967:369) (a) the shallow pit dug out of the earth; (b) the replica crucible made of local clay; (c) charcoal fuel; (d) tuyere; (e) simple bellows.	38
4.1	Figure 4.1. Schematic drawing of Scanning Electron Microscope (MIT 3.081 lecture notes 2001).	46

Figure Number	Caption	Page Number
4.2	Kaolin clay platelets at a magnification of 3700 (Rice 1987: 46).	47
4.3	Schematic of DTA experiments.	50
4.4	Schematic diagram of the re-firing experiments.	52
4.5	Schematic drawing of x-ray diffraction apparatus.	53
5.1	Zones of heat alteration across a section of a crucible fragment (Traced from section photograph of MIT No. 240).	56
5.2	MIT No. 5279: Modern crucible sherd used in experiment at Tal-i Iblis in 1967. Left: top view; Right: profile view showing slumped rim.	57
5.3	(a) MIT No. 5277: Modern crucible replica; Top: view of interior from above; Bottom: profile view; (b) MIT No. 5277: Section of modern crucible replica; Carbon coring provides proof that this replica was fired at a low (below 600°C) temperature when constructed.	59,60
5.4	MIT No. 240: Tal-i Iblis Crucible sherd, Level I. Left: profile view; Right: view of interior wall and portion of base.	61
5.5	MIT No. 241η: Tal-i Iblis crucible sherd, Level I and II profile wall. Left: profile wall; Right: view of interior surface.	61
5.6	MIT No. 5274: Tal-i Iblis crucible sherd, collected by Prof. Smith. Left: profile wall; Right: view of interior surface.	62
5.7	MIT No. 241β: Tal-i Iblis crucible sherd, Level I and II profile wall. Left: profile wall; Right: view of interior surface exhibiting a thick green accretion.	63
5.8	MIT No. 241ε: Tal-i Iblis crucible sherd, Level I and II profile wall. Left: profile wall; Right: view of interior surface showing green accretion.	63
5.9	MIT No. 241γ: Tal-i Iblis crucible sherd, Level I and II profile wall. Left: view of interior heavily vitrified surface; Middle: profile wall with slumped rim shown; Right: view of exterior surface.	63

Figure Number	Caption	Page Number
5.10	MIT No. 245: Tal-i Iblis crucible sherd, Level V. Left: profile wall; Right: view of interior surface (this sherd is much larger than any of the other ones, and it is also from a much later level).	64
5.11	Profile of MIT No. 241 β with locations of ESEM images indicated with arrows.	65
5.12	ESEM image of MIT No. 241 β at a magnification of 650, in Zone 3 near the interior surface, within the thick green accretion. (1) These streaks are artifacts of sample preparation. (2) The platelets are fused together in this area, (3) but not as much so in this area. (4) These pores are due to vitrification.	66
5.13	ESEM image MIT No. 241 β at a magnification of 800, on the boundary between the green residue zone and Zone 2, 0.8mm from the interior surface. The arrow indicates where the platelets are more distinct (less fused).	66
5.14	ESEM image of MIT No. 241 β at a magnification of 1000, within Zone 2 (reduced core), 2.5mm from the interior surface. The arrow indicates stacks of clearly defined platelets.	67
5.15	ESEM image of MIT No. 241 β at a magnification of 1000, within Zone 2, 5mm from the interior surface. Notice the complete lack of fused particles.	67
5.16	ESEM image of MIT No. 240 at a magnification of 100, Zone 4 on the interior surface. There are no discernable platelets. Notice the smooth surfaces of the void interiors and the large spherical voids.	69
5.17	ESEM image of MIT No. 240 at a magnification of 100, Zone 4 on the interior surface. Even at broken sections through void wall, no platelets can be identified.	69
5.18	ESEM image of MIT No. 241 β at a magnification of 250. At interior surface, Figure 13 is a detail of this photomicrograph.	70
5.19	Bivariant plot of thin section mineralogy. Clay Matrix vs. All Inclusions.	71
5.20	Bivariant plot of thin section mineralogy. Clay Matrix vs. Voids.	73

Figure Number	Caption	Page Number
5.21	Bivariant plot of thin section mineralogy. Clay Matrix vs. Quartz.	73
5.22	Bivariant plot of thin section mineralogy. Clay Matrix vs. Plagioclase.	74
5.23	Bivariant plot of thin section mineralogy. Quartz vs Voids.	74
5.24	Bivariant plot of thin section mineralogy. Quartz vs. Plagioclase.	74
5.25	XRD spectrum of MIT No. 5277 (Modern crucible replica).	76
5.26	XRD spectrum of MIT No. 241 β (Tal-i Iblis crucible).	77
5.27	X-ray diffraction spectra for common clay types. (a) illite of the illite group; (b) monmorillonite of the smectite group. Notice the shift in the initial peak at 2θ value of 7 when the sample is heated to 400°C. This peak is also greatly diminished when the clay is heated; (c) kaolinite of the kaolinite group.	78
5.28	Geological map of area surrounding Tal-i Iblis, with key (Haghipour and Aghanabati 1985).	80,81
5.29	Hypothetical DTA curve for ceramic material over the range of 0-1000°C (Tite 1972:296).	86
5.30	DTA curve for modern replica (MIT No. 5277); arrows indicate loss of calcite and slumping temperature.	87
5.31	DTA curve for Zone 1 of Iblis crucible (MIT No. 240); arrow indicates slumping temperature.	87
5.32	DTA curve for Zone 4 of Iblis crucible (MIT No. 240); arrow indicates slumping temperature.	88
5.33	DTA curve for sherd of experimental modern crucible replica (MIT No. 5279); arrow indicates slumping temperature.	88
5.34	Photographs of furnace-heated samples from MIT No. 5277. MIT No. 5277D heated to 300°C in re-firing experiment; MIT No. 5277N heated to 1100°C; MIT No. 5277J heated to 1125°C; MIT No. 5277U heated to 1150°C; MIT No. 5277Q heated to 1175°C; MIT No. 5277T heated to 1200°C.	90

Figure Number	Caption	Page Number
5.35	(a-n) Optical activity changes with temperature. All images are taken at a magnification of 100, images on the left are in cross-polarized light; images on the right are in plane-polarized light.	82,93
5.36	Void morphology of no heat, 1100°C, 1125°C, 1150°C, 1175°C and 1200°C. Plane-polarized light, taken at a magnification of 50.	94
5.37	Presence of calcite in re-fired samples. (a) MIT No. 5277H (not heated); (b) MIT No. 5277B (500°C); (c) MIT No. 5277G (700°C). All images are in cross-polarized light at a magnification of 50.	95
5.38	Zone 1 of Iblis sherd (MIT No. 240) does not possess optical activity. Cross-polarized light, magnification of 50.	95
5.39	Zone 1 of Iblis sherd (MIT No. 241δ) does possess optical activity in one region. Cross-polarized light at a magnification of 50.	95
5.40	Zone 1 of Iblis sherd (MIT No. 241δ) contains calcite in one region. Cross-polarized light at a magnification of 50.	95
5.41	Voids present in Zone 3 of Iblis sherds. (a) MIT No. 240; (b) MIT No. 241β; (c) MIT No. 241γ; (d) MIT No. 241δ all taken in plane-polarized light at a magnification of 50.	96
5.42	Voids present in Zone 4 of Iblis sherds. (a) MIT No. 240; (b) MIT No. 241γ; (c) MIT No. 241δ all taken in plane-polarized light at a magnification of 50.	97
5.43	Temperature profile for Iblis crucible (MIT No. 240). Dotted line indicates the extent of the thin section sample. This sherd is also shown in Figure 5.4.	98
5.44	Temperature profile for Iblis crucible (MIT. No. 241β). This sherd is also shown in Figure 5.7.	98
5.45	Temperature profile for Iblis crucible (MIT. No. 241γ). This sherd is also shown in Figure 5.9.	99
5.46	Temperature profile for Iblis crucible (MIT. No. 241δ). This sherd is also shown in Appendix A.	99

Figure Number	Caption	Page Number
5.47	X-ray map of MIT No. 241 β in Zone 3. Copper and chlorine concentrated in the same regions of this surface zone, which I have interpreted to signify the presence of copper chloride. (a) SEM image at interior surface of MIT No. 241 β at location of green accretion; (b) chlorine concentrations; (c) copper concentrations.	101
5.48	Copper prills found in (a) MIT No. 241 β , at a magnification of 500, Zone 3; (b) MIT No. 241 δ at a magnification of 100, Zone 4; (c) MIT No. 241 γ at a magnification of 100, Zone 4.	103,104,105
5.49	Copper sulfide inclusions in the largest prill; MIT No. 241 γ , at a magnification of 200.	106
5.50	Dendrites in MIT No. 241 δ Zone 4 (a) photomicrographs at a magnification of 500; and (b) SEM image with scale bar indicated.	108
5.51	Clast and needle phases in MIT No. 241 δ . SEM image with scale bar shown.	109
5.52	Matrix phases for MIT No. 241 δ Zone 4, taken at a magnification of 500 (Matrix for MIT No. 241 δ can also be seen in Figures 5.48b, 5.50 and 5.51).	110
5.53	Matrix phases for MIT No. 241 γ Zone 4, SEM image with scale bar indicated.	111
6.1	An example of a pit smelting operation in Ambelikou, Cyprus drawn by Tylecote (1982:233). No date or site information provided.	114
6.2	Plot of the effect porosity on the thermal conductivity of clay at temperatures of 70.5-120.5°C. Clay samples were taken from three source areas (Kuchin, Singapore; Beskhudnikov (location unknown); and Ashkabad, Turkmenistan). Five samples were taken from each source area with different degrees of porosity. Data are taken from standards presented in Touloukian (1970:806).	116

Figure Number	Caption	Page Number
6.3	Schematic drawing for crucible smelting or melting operations. The region indicated by the arrow on the crucible wall would experience the contact between the contents of the crucible and the fuel source piled on top.	117
6.4	Temperature profile for fragment of replica crucible (MIT No. 5279) used in the on-site experiment.	118
6.5	MIT No. 241 δ : Normalized composition of dark phase of Zone 4, plotted on SiO ₂ –Al ₂ O ₃ -CaO phase diagram.	120
6.6	MIT No. 241 δ : Normalized composition of light phase of Zone 4, plotted on SiO ₂ -FeO-CaO phase diagram.	121
6.7	MIT No. 241 δ : Normalized composition of dendrite phase of Zone 4,, plotted on Fe-Cu-Si phase diagram.	122
6.8	MIT No. 241 γ : Normalized composition of dark phase of Zone 4, plotted on SiO ₂ -MgO-CaO phase diagram.	123
6.9	MIT No. 241 γ : Normalized composition of light phase of Zone 4, plotted on SiO ₂ -Al ₂ O ₃ -CaO phase diagram.	124

List of Tables

Table Number	Caption	Page Number
1.1	Approximate dates for the onset of some ancient technologies (BCE).	20
2.1	Chronology and dates for the levels of occupation at Tal-i Iblis.	34
2.2	Copper metal objects excavated from Tal-I Iblis and documented in Caldwell's preliminary report (Chase et al. 1967:153,168,185-6).	35
3.1	Artifacts curated at MIT via Caldwell and Smith.	42
3.2	The artifacts examined in this thesis.	43
4.1	Methods of analysis for each object studied.	45
4.2	Artifacts studied with thin section analysis and the finishing methods for each.	48
4.3	Grain size ranges for category groupings.	48
5.1	Artifacts examined in this thesis with description and find spot.	58
5.2	Point count data for thin sections based on 1000 data points per sample (%Volume Fraction).	72
5.3	Bulk Chemical analysis of Zones 1 and 2 (wt%).	79
5.4	Porosity of Tal-I Iblis crucible sherds and modern crucible replica.	82
5.5	Morphological changes predicted for a ceramic as a function of temperature (Tite 1972:296).	85
5.6	Morphological changes in the ceramic of modern replica crucible (MIT No. 5277) as a function of temperature.	91

Table Number	Caption	Page Number
5.7	(a) Weight % of elemental composition for phases in Zone 4; (b) Weight % of elements reported as oxides for phases in Zone 4.	107
6.1	Melting Temperatures for phases present in Zone 4.	119
6.2	MIT No. 241 δ : recalculated dendrite composition.	122
6.3	Estimated composition for Zone 4 of 241 δ and 241 γ based on volume fraction of phases.	125

Chapter I: Introduction to Early Metallurgy

1.1 Background

This thesis is focused on the analysis of ceramic crucibles recovered from the 6th to 1st millennium BCE Iranian site of Tal-i Iblis. These crucibles provide some of the earliest evidence for the onset of extractive copper metallurgy on the Iranian Plateau. They each have been examined with thermal and chemical compositional analyses to determine the nature of this technology developed by the inhabitants of Tal-i Iblis.

1.2 History of Metallurgy

This section outlines the background information that will help to establish the historical significance of the Tal-i Iblis crucibles. In this thesis, a materials technology (such as metallurgy) is defined as any process involving the use of tools with the intent to manipulate materials found in the environment. The advent of a true metallurgical technology—i.e., a technology in which metal ore is heated with the intention of reducing it to a pure metallic form—is a debated topic even today. There is evidence for early metallurgical activity in many areas of the Old World, and as materials archaeologists it is our job to interpret this evidence to determine where, when, and how such technologies began. Prior research concludes that the earliest metallurgical technologies resulted from familiarity with the properties of both stone and fire. Beyond that, however, the development of metallurgy took different paths in different geographic regions (both in the Old World as well as the New World). Approximate dates for the advent of the earliest metallurgical technologies in the Old World are reported in Table 1.1.

Despite the relatively small amount of archaeological evidence for early metal technologies, there are multiple proposals as to exactly how the crucial transition from stone working to the production of metal objects occurred. One proposal is that the use of colorful copper ores for

Table 1.1. Approximate dates for the onset of some ancient technologies (BCE)

Technological onset	Mesopotamia	Levant	Anatolia	Iranian Plateau
Lithic	30 000	30 000	30 000	30 000
Agriculture	8 500	9 000	8 000	8 500
Pottery	8 500	5 500	6 500	8 500
Native copper	8 500	8 700	7 200	9 000
Smelting	3 800	3 200	5 500	3 800
Bronze	3 000	3 000	3 000	3 000

Dates for this table have been taken from:

Lamberg-Karlovsky and Sabloff 1995: 62-66, 80-84; Craddock 2001:153,157; Tylecote 1976:5,9

decoration on pottery triggered the onset of a new technology (Tylecote 1976). Tylecote believes that the well-documented use of green and blue copper ores in Neolithic societies provides some verification of this idea. Azurite has been found in Crete at levels dating to as early as 6000 BCE (Tylecote 1976:1; Charles 1979:9). If copper oxide or carbonate minerals such as azurite or malachite (Figure 1.1) were used as powdered pigments to decorate pottery before firing, these early potters would have noticed the effects of heat on the mineral. In an oxidizing atmosphere, the mineral turns black (Tylecote 1976), but if the pottery were fired in a sufficiently reducing atmosphere, the mineral could instead transform to nodules of metal on the surface of the fired vessel. Although this relationship between heat and the appearance of metals may have been noticed in conjunction with the firing of pottery, the transformation of ore to metal was not likely to occur in pottery kilns because early kilns did not create suitably reducing atmospheres (Craddock 2001). Furthermore, it is not necessary that a *sophisticated* pottery technology be developed before the onset of a metallurgical one because a ceramic crucible necessary for smelting ore requires thermal and structural properties that are different from those necessary for a cook pot (Tylecote 1982).

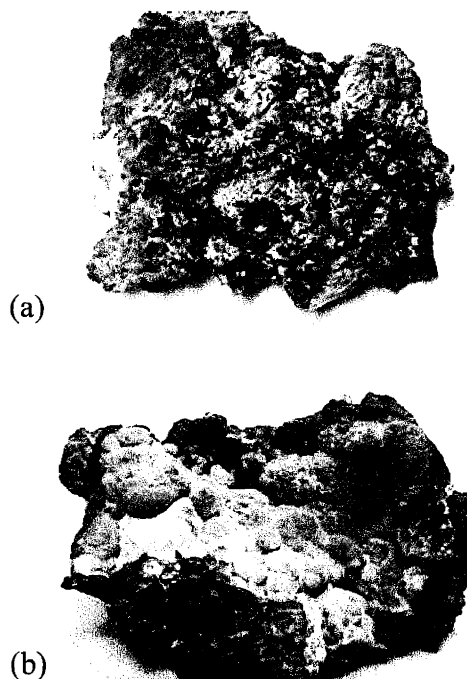


Figure 1.1. Some examples of carbonate copper ores. (a) Malachite; (b) Azurite

http://minerals.gps.caltech.edu/COLOR_Causes/Metal_Ion/

Another possible scenario for the advent of metallurgy could stem from the discovery of native copper—a metal that occurs naturally as an outcrop when sulfide ores have been leached by corrosive ground water, or when heavily saturated ground water courses through fissures in rocks to deposit metallic copper in the crevices (Craig and Vaughan 1981). Craftsmen of the Neolithic age were experts in materials selection because their livelihood was based on being able to knap certain kinds of rock efficiently to produce desired tools. It is quite possible that upon collecting stone to use for various tools, native copper was collected as well (either by accident, or intentionally as a novelty item). It would have become obvious immediately that this material possessed properties distinct from those of other rocks. Presumably for this reason, native copper objects appear very early in the archaeological record (9th to 7th millennium BCE) at Ali Kosh in western Iran and at Çayönü Tepesi in Anatolia (Tylecote 1976; Craddock 2001). Figure 1.2 provides the locations of these sites and other sites mentioned in this thesis.

Following the discovery of native copper, craftsmen also realized that they could increase the malleability of native copper by heating it at low temperatures. Temperatures of 600°C (Thompson 1958) are easily attainable with a charcoal fire; anything hotter would require a forced draught. These temperatures are well above the temperatures used to anneal copper, which can be done as low as at 300°C, but not high enough to melt it ($T_m = 1083^\circ\text{C}$). It is likely that melting native copper followed this annealing process (Tylecote 1976). Some scholars argue that smelting followed melting (Craddock 2001; Charles 1979). Even though these suggestions make logical sense, they rely on general theories concerning the evolution of metal technologies, and these theories cannot be proven with the little evidence that we have. There are many isolated cases of copper use early in prehistory, but these few isolated cases do not determine the onset of a new technology. Rather they determine the presence of inquisitive craftsmen. Therefore, we cannot make the leap from observing the use of native copper objects by a prehistoric society to determining this society's role in the evolution of some metal technology.

For this reason, we can only establish an approximate date for the onset of metallurgical technology in the Near East and Central Asia. Scholars do not currently agree on a specific date for

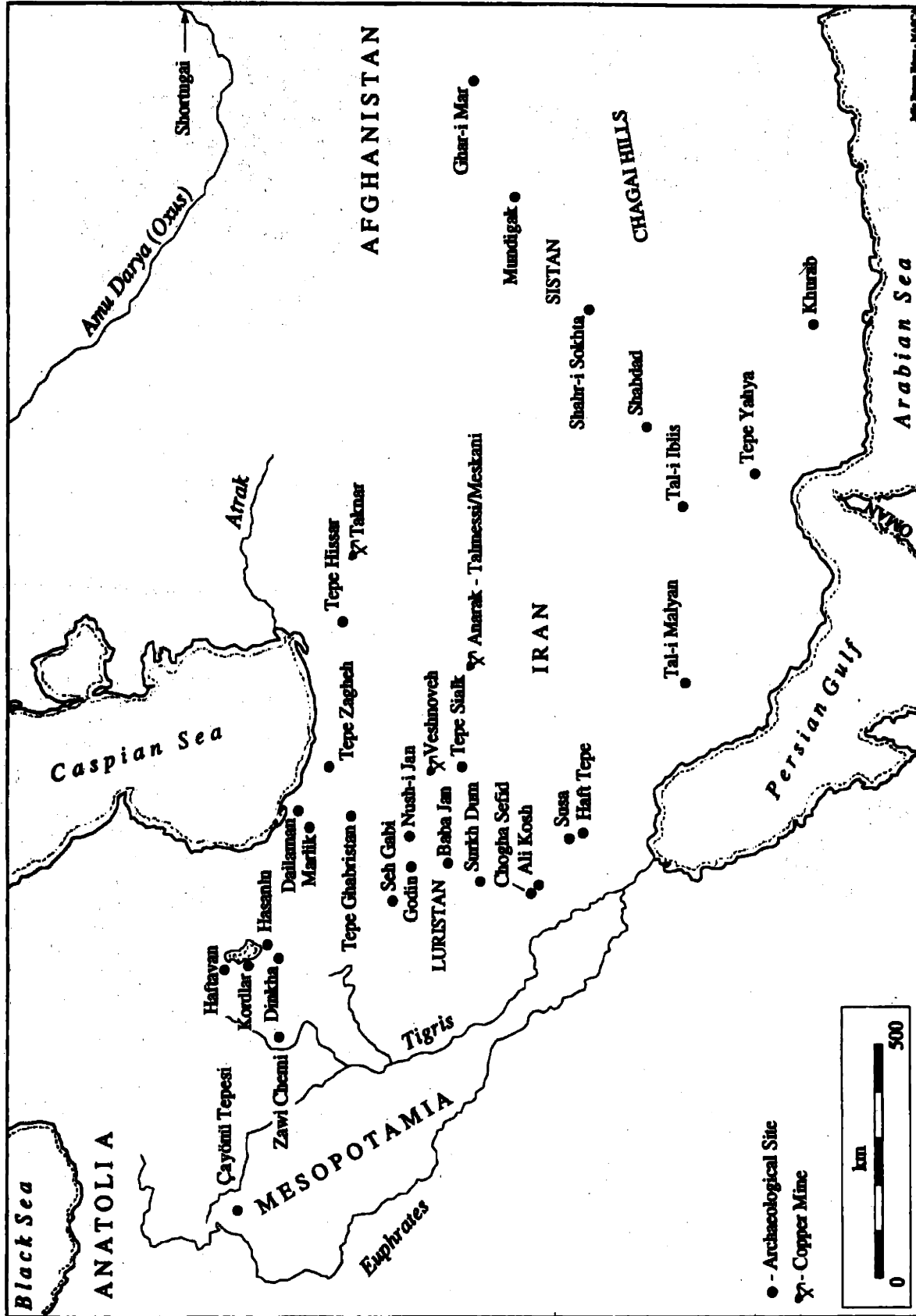


Figure 1.2. Archaeological sites in Iran. (Pigott 1999:75)

this onset. Tylecote (1976) suggests that smelting began in the 4th millennium BCE, while Pigott (1999) suggests an older date of 5th millennium BCE. Craddock (2001) theorizes that smelting of copper ore began during the Neolithic period in the 6th millennium BCE, but states that the “first firm evidence for smelting in the Middle East” comes from the 4th millennium BCE (Craddock 1985:126). The uncertainty in establishing this date stems from both the difficulty in identifying the origin of copper objects (i.e., were they formed from melted or smelted copper) and from the vague definition of *metallurgical technology*. Tylecote suggests that the transition from lithic to metal technologies should be defined as the presence of copper smelting, not by the ability of ancient craftsmen to recognize and shape native copper by cold hammering and annealing. In the Old World, this period of early copper smelting technology is often referred to as the Chalcolithic period. It corresponds to the transition from the Neolithic to the Copper Age (or sometimes, the transition from the Neolithic to the Bronze Age). “Chalcolithic” literally means “copper-stone” and is not a term used ubiquitously even by archaeologists in the Old World. It is sometimes called Eneolithic, or omitted altogether. In this thesis the Chalcolithic period is taken to span the period from 5500 to 3200 BCE (Pigott 1999).

1.3 Metal production during the Chalcolithic period

The Chalcolithic period is characterized by a very basic method of copper smelting. This early smelting technology involved the reduction of copper oxide or carbonate ores in small ceramic crucibles to produce copper metal.

Crushed ore and charcoal were placed within the crucibles and heated to low temperatures—at least 600°C (Thompson 1958). A schematic of this setup can be seen in Figure 1.3. When the carbon fuel source burns, carbon monoxide is created. As long as the atmosphere is

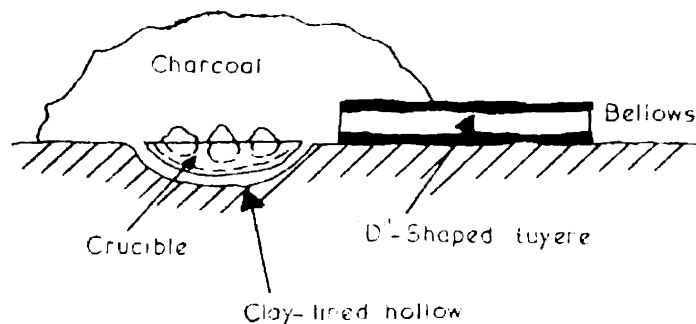
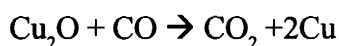
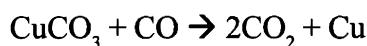


Figure 1.3. An example of a pit smelting operation in Ambelikou, Cyprus drawn by Tylecote (1982:233). No date or site information provided.

reducing, the CO readily combines with the oxygen present in the ore, leaving behind copper metal. If the ore is cuprite (Cu_2O), the chemical reduction reaction is given by:



The reduction of copper carbonate ores like azurite and malachite (azurite: $\text{Cu}_3(\text{CO}_3)_2(\text{OH})_2$; malachite: $\text{Cu}_2(\text{CO}_3)(\text{OH})_2$) follows a similar reaction, but more CO_2 is produced:



If the reduction of the copper ore is carried out at these low temperatures, the metal exists in the crucible containers in the form of “sponge copper” (Charles 1979). Unfortunately there seems to be no published metallographic analysis of the microstructure of sponge copper, but Charles (1979:9) states that it can be “melted and agglomerated” to form a solid piece of copper metal. If the crucible is heated to slightly higher temperatures, the copper will exist as small, scattered spheres of copper, or prills, within a vitrified matrix. To put this copper in a usable form, the prills need to be isolated by first mechanically crushing the vitreous matrix of charcoal and crucible material that holds the prills. Then these prills are hand sorted or panned and winnowed (Tylecote 1976:5). The prills are melted together in a crucible to form a larger piece of copper (sometimes referred to as an ingot).

These procedures leave behind evidence that allows archaeologists to estimate the level of production and sophistication of the technology in use. For example, slag—the vitrified by-product of melting or smelting—is produced both when smelting copper ore and when melting copper in a crucible. However, the slag formed from each of these operations is slightly different, and these differences enable us to determine which of these procedures was used. Non-smelting slags are those derived from the melting of copper metal. Tylecote (1976) informs that these slags develop from the reaction between alkali in the fuel ash and silicates in the ceramic crucible. Large amounts of entrapped copper are usually contained within this slag. Tylecote distinguishes smelting slags (from slags formed upon melting) as ferrous silicates containing small amounts of copper. (The cut-off for “large” versus “small” amounts of copper is roughly 4wt%.) Similarly Craddock (1985) says that the main difference between smelting and non-smelting metallurgical slags is that smelt-

ing slags are uniform and darker in color than the “more glassy” non-smelting slags.

The earliest evidence for slaggy copper material is at Çatal Hüyük in Anatolia (*c.* 7000-6000 BCE). However, because there are no iron silicates found in the material, there is debate as to whether this constitutes evidence for the earliest smelted copper production (Tylecote 1976). If nothing else, the presence of this slaggy material and associated ore fragments indicates that these peoples were on the verge of discovering copper smelting technologies as early as the 6th millennium BCE (Craddock 2001).

The earliest metallurgical technology (*i.e.*, the smelting of copper ores) is believed to have developed during the early 4th millennium BCE (see section 1.2). This is largely due to the associative evidence in the Middle East and the eastern Mediterranean from this period. For example, early copper artifacts produced from smelting have been excavated from Tepe Yahya in Iran (*c.* 3800 BCE). These artifacts include awls and chisels and are made of arsenical copper (Tylecote 1976). Similar artifacts (such as axes) were also excavated at Egypt dating to *c.* 4000 BCE and were made of “impure smelted copper” (Tylecote 1976:9). There is abundant evidence of copper smelting after 3500 BCE, and it seems that a metallurgical technology spread rapidly throughout the Near East after multiple Sumerian city-states were established (Tylecote 1976:5). However, there is little evidence of earlier peoples using anything more than pieces of raw ore and cold hammered native copper. The date and location for the onset of this early copper smelting technology is difficult to establish because our evidence for copper smelting sites is sparse, both spatially and temporally.

By the 3rd millennium BCE the smelting of copper ores was widespread, and many places began to employ a more sophisticated method than that utilizing crucibles. Furnaces designed to maintain a reducing environment replaced crucibles as the containers for ore and fuel (Craddock 2001). The presence of this furnace smelting technique is usually implied when labels such as Copper Age or Bronze Age denote a time period, although this is not always the case.

The presence and development of an early extractive metallurgical technology throughout the Old World was closely related to the local geology. Metallurgical activity is evident earlier in

regions with higher concentrations of copper ore deposits, and many scholars agree that smelting took place at settlements existing only a short distance from mines or source areas (Craddock 2001). We know today that it was not mere coincidence that the Iranian Plateau, a region containing a high concentration of copper ore, is also a region with a high concentration of early metallurgical sites.

The next Chapter will focus more closely on the metals and metallic ore bodies in the Iranian Plateau and on early metallurgical sites, such as Tal-i Iblis, where the artifacts for this thesis were excavated.

Chapter II: Tal-i Iblis Region

2.1 Metals on the Iranian Plateau and at Tal-i Iblis

This section concentrates on the general setting of the Iranian Plateau, both geologically and archaeologically. The site of Tal-i Iblis lies in the southern region of this plateau in the Kerman Province (Figure 1.2), and its place in metallurgical history can be understood better once one has a general knowledge of the surrounding area.

We find the earliest evidence of metallurgical technology on the Iranian Plateau in the form of smelting debris (ore and crucible fragments as well as metal objects). It is not surprising to find this evidence in this particular setting, because the region is an “ore-rich metallogenic zone” (Pigott 1999:73). Figure 2.1 reveals the concentration of copper ore bodies identified in Iran and Anatolia. There are five main copper districts in Iran, one of which is located in the Kerman Province (Figure 2.2). Being a zone rich with copper, the Iranian Plateau was a perfect environment for the development and use of metals. This development proceeded in generally the same way as in other regions of the Old World. During the Neolithic period (7500-5500 BCE on the plateau), cultures became familiar with the appearance and properties of both native copper and metal ores. The reduction of oxide ores to produce copper is a technology that first appears in the archaeological record during the Chalcolithic period (5500-3200 BCE). One site showing evidence of this technology is Tepe Ghabristan, which dates to the 6th millennium BCE¹ and is located on the Iranian Plateau (Thornton et al. 2002). Another site, Tal-i Iblis (6th millennium BCE), produced metallurgical evidence similar to that found at Tepe Ghabristan. The location of both sites can be identified in Figure 1.2.

¹ Pigott (1999:77) states that the smelting technology at this site dates to the late 5th millennium BCE.

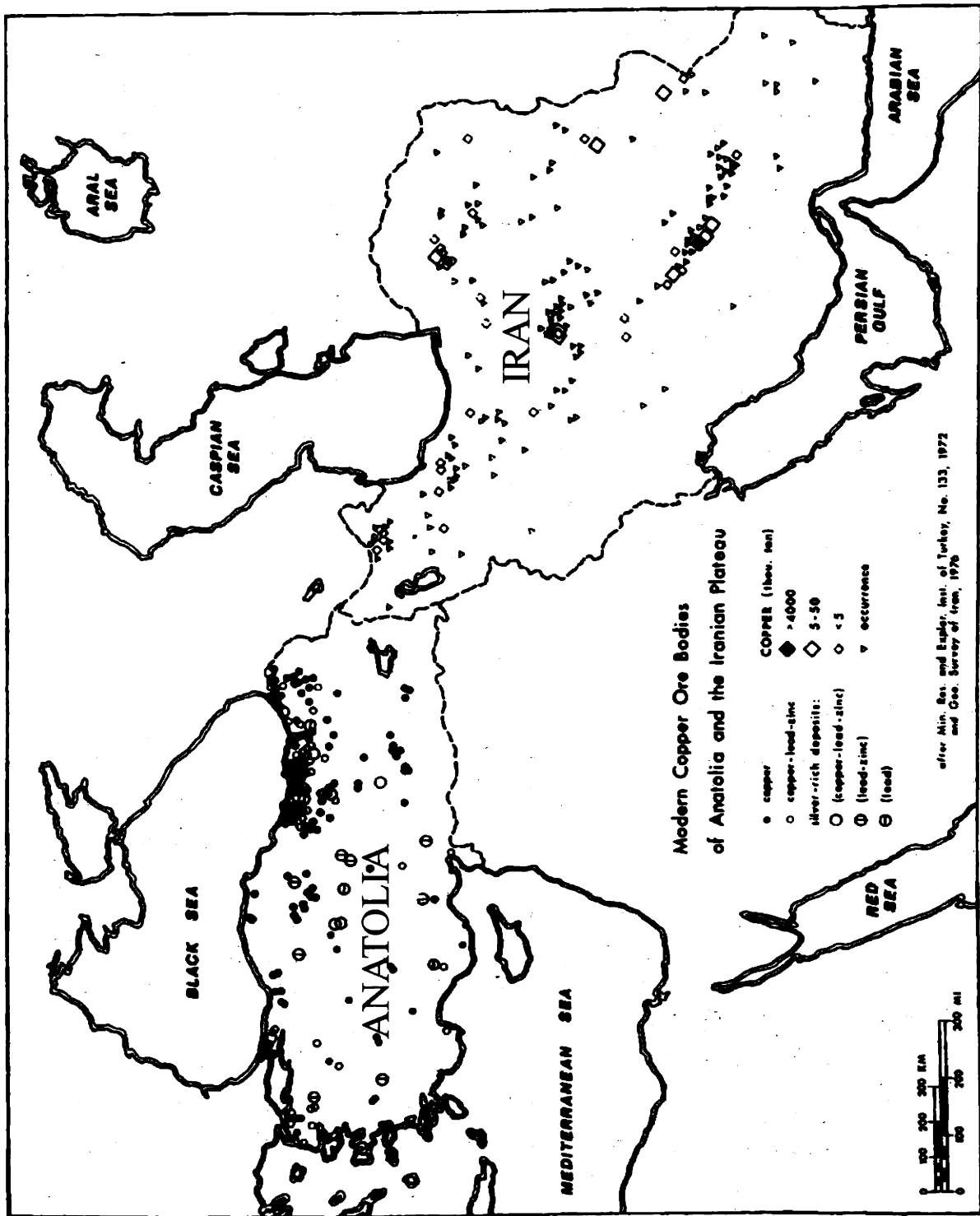


Figure 2.1. Modern copper ore bodies in Anatolia and Iran. (Pigott 1999:83)

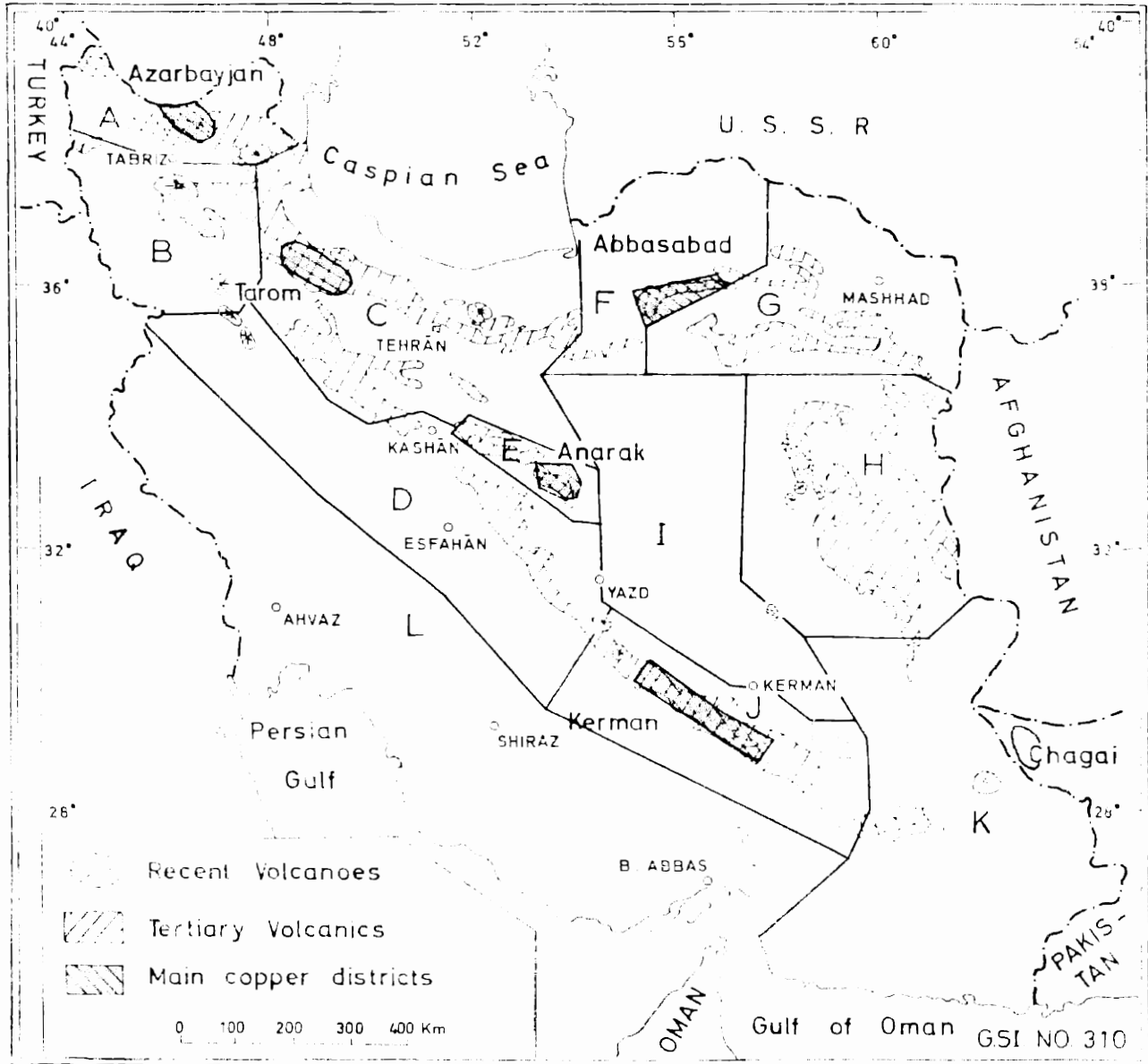


Figure 2.2. The five main copper districts of Iran (Bazin and Hübner 1969:10)

2.1.1 The Ore Geology of the Iranian Plateau

The copper district located in the Kerman province includes numerous copper ore deposits, which presumably would have also been accessible during the Chalcolithic period. Many of these deposits occur in sedimentary and volcanic rock outcrops, and are the product of copper-rich ground water seeping through cracks and forming mineralized veins (Lur'ye 1986). Concerning metallurgy on the Iranian Plateau alone, there are three major mines that were used in prehistory: Anarak, Veshnovah and Taknar. However, these mines are located in close proximity to each other, and

little research has been carried out on the possibility of other sources of ores mined in prehistory. Today most of our knowledge of the geological setting of Iran comes from studies of oil fields, and only one extensive study, carried out in 1969, focused primarily on copper deposits (Bazin and Hübner 1969). We must assume that, in addition to the the ore bodies shown in Figure 2.1, there are a number of unknown ore sources, some of which could have been used in prehistory. This assumption is based on the fact that there has been little systematic geological and archaeological research to document ore deposits in Iran, and we have no reason to suspect that we have discovered all ore sources used by societies of the distant past. There may have also been ore sources fully exploited in prehistory, leaving no evidence to indicate mining or other extraction operation.

The three major mines of the Iranian Plateau mentioned above, are located a great distance from the site of interest for this thesis. Tal-i Iblis is located 500 km from the nearest of these three mines (Anarak); therefore it is highly unlikely that the Iblis occupants were obtaining their ores from this prehistoric mine. Rather, there are many local deposits of carbonate copper ore that were more easily accessible to the inhabitants of Tal-i Iblis. In a 100 km radius, there are 40 known deposits of copper metal or copper ore. Of these 40, 27 contain carbonate copper ores. Within a 50 km radius, there are 13 sources, eight of which are carbonate ore (Figure 2.3, Bazin and Hübner 1969). Because smelting for non metallurgical purposes is believed to have occurred largely by accident (section 1.2), it is likely that the Iblis occupants were obtaining these colorful carbonate ores for decorative purposes as they found them during regular gathering activities, and only later discovered their functional properties.

It is possible that once smelting became an established technology, raw material from the three major mines was transported to many corners of the Iranian Plateau along Neolithic trade routes (Pigott 1999), but we lack evidence to establish this unequivocally.

2.2 Tal-i Iblis

This investigation focuses on Tal-i Iblis as one of the earliest metallurgical sites in the world. Understanding the metallurgical technology present at this site may help archaeologists

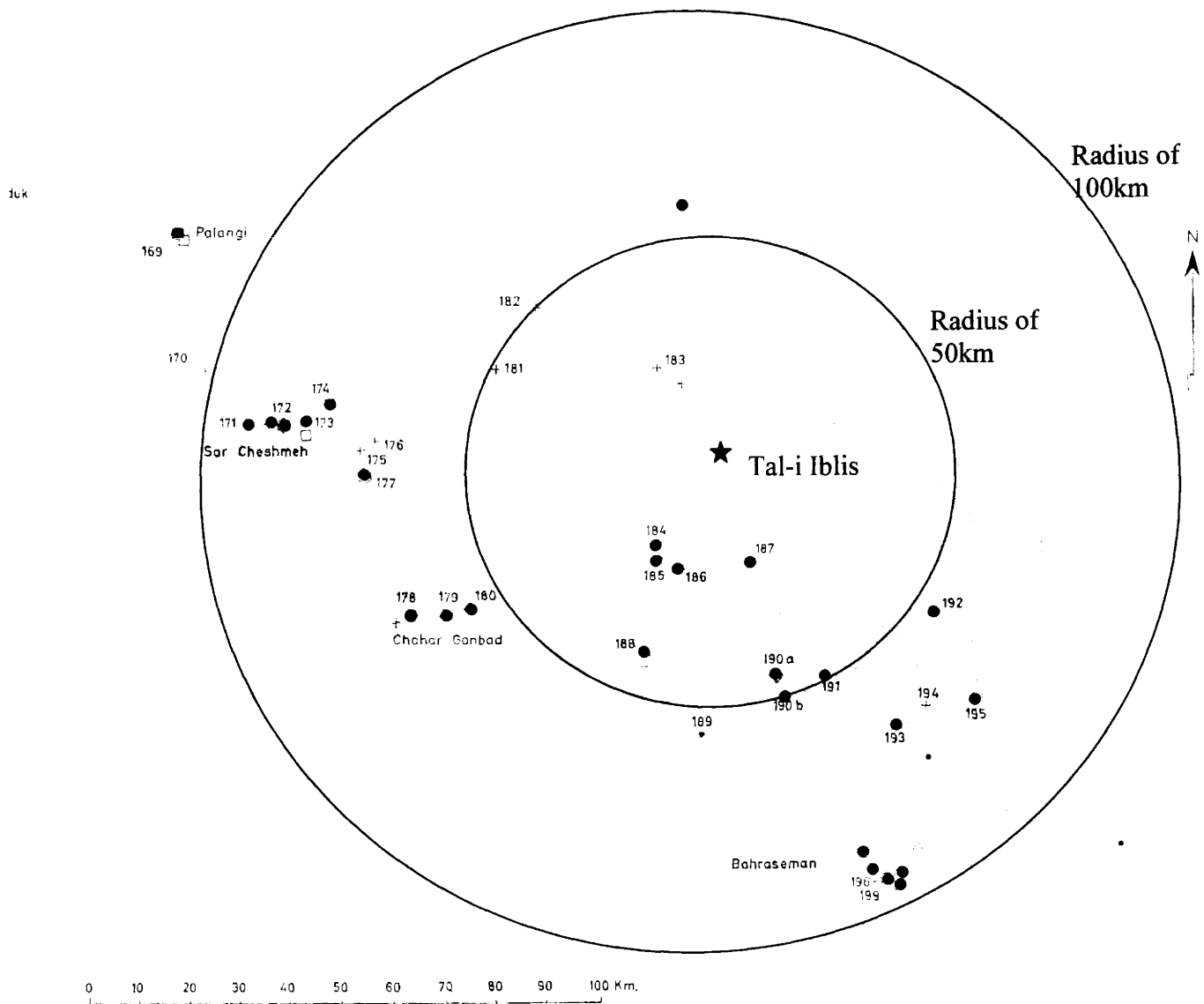


Figure 2.3. Ore bodies near Tal-i Iblis (Bazin and Hubner 1969:119), with overlain circles at 50km and 100 km from Tal-i Iblis. The carbonate ore sources are indicated in green.

interpret the effects of a more advanced pyro-technology, such as metallurgy, upon the development of society, the formation of trade networks and the exchange of information in prehistory. Because it is such an early site, the examination of its artifacts and metallurgical material must be treated with utmost care. Therefore, I will provide a complete description of the relevant history of the site, as well as its artifacts of consequence.

Tal-i Iblis is located in the Mashiz Valley (also known as the Bard Sir Valley, or the Lalehzar Valley) southwest of the Kerman mountains in southern Iran. The name means “Devil’s Mound,” (Stein 1937) and it is an ob-

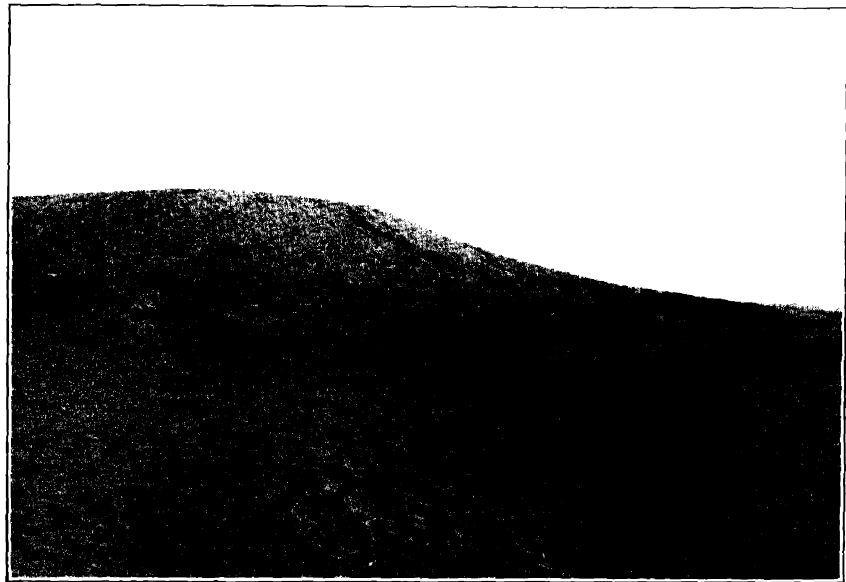


Figure 2.4. Photograph of Tal-I Iblis taken by Stein (1937: Fig.55) from North-west view.

long tell site that measured approximately 118m by 100m and rose over 11m in height at its zenith during the late 12th century BCE (Caldwell and Shahmirzadi 1966). Sir Mark Aurel Stein took these measurements when he studied the site in 1933 (Figure 2.4); however, he noted that the mound “may have been considerably reduced by prolonged digging for manuring earth” (Stein 1937:166). It is fortunate that Stein documented the tell site in 1933, for when Joseph Caldwell rediscovered the site in 1964 he found that the “entire center of this large mound had been dug out and destroyed” (Caldwell 1967:9, Figure 2.5). Local farmers had slowly carted away the fill of the mound to use for fertile soil in their valley fields. The farmers’ excavation of the middle of this tell did, however, reveal the site’s stratigraphy. Immediately, Caldwell was able to decipher six distinct deposits of cultural material. Radiocarbon dates were determined based on the abundant charcoal contained within each level².

² Throughout this thesis the term “level” denotes the occupation periods as defined in Table 2.1. In other publications (Caldwell 1967; Voigt and Dyson 1992; Pigott 1999; Pigott and Lechtman 2003) this term is sometimes replaced with “Iblis.” For example, in this thesis, level 1=Iblis 1.

Table 2.1 summarizes these dates, which range from the mid-5th millennium BCE to the late 12th century BCE.

This cultural material includes an unusually large amount of artifacts related to metallurgical activities.



Figure 2.5. Photograph taken by Caldwell in 1964 (1967:10). The center of the mound was dug out.

These artifacts include metallurgical crucible fragments, pieces of copper ore, small copper objects, and some slag. Because of its overwhelming abundance, much of this material was discarded; however, hundreds of artifacts were kept and are currently curated in the Georgia Museum of Natural History at

the University of Georgia at Athens. The late Cyril Stanley Smith (MIT Institute Professor, Department of Materials Science and Engineering) also collected a small amount of material during his visit to the site in 1966. In addition, Caldwell later sent a selection of his catalogued artifacts to Professor Smith at MIT for further analysis. Some of the metal artifacts sent to MIT were analyzed 35 years later by Professor Heather Lechtman (Pigott and Lechtman 2003). These artifacts include a tack (MIT No. 249), a pin (MIT No. 247) and two hand tools (MIT Nos. 248, 250). However, the crucible and slag artifacts were not studied extensively prior to the research reported here. The crucibles were concentrated most heavily in the early levels of the site, indicating the early development of metallurgy at Tal-i Iblis.

Level I (5290-4420 BCE, see Table 2.1) contained the first crucibles at the site with a characteristic “green stain of copper residue” on their interior surfaces (Caldwell and Shahmirzadi 1966:11). A dumping area excavated in level II (5205-4685 BCE) contained crucibles at a concen-

Table 2.1: Chronology and dates for the levels of occupation at Tal-i Iblis

Period	Date (BCE)	Correction from Voigt and Dyson (BCE) (1992)
	From Caldwell's radiocarbon dating	
Iblis VI	1130±120	Not determined
Iblis V	Unknown	Not determined
Iblis IV	2869±57 (questionable)	4415-3365
Iblis III	3792±60	4460-4400
Iblis II	4110±150 - 4090±74	5205-4685
Iblis I	4287±40	5290-4420
Iblis 0	4502±72 - 4410±165	Does not exist

Note: When a range in radiocarbon dates is shown here, it indicates the earliest and latest date from that period. One date indicates only one reliable sample tested for that level. (Caldwell 1967:24,32,34,36; Voigt and Dyson 1992:131)

tration of 128/m³, which is a considerably higher concentration than that found in the dumping areas of level I (Caldwell 1967:34). Ralph C. Dougherty, a chemist at Ohio State University, was asked by Caldwell to examine one of the crucible sherds found at Tal-i Iblis. He concluded that these crucibles were used for smelting copper ore and that, therefore, they provided some of the earliest evidence of copper smelting in the Iranian Plateau (Caldwell and Dougherty 1966). Caldwell interpreted the substantial number of crucible fragments in the level II occupation as indicative of a production quantity exceeding that necessary for local needs. He suggested that Tal-i Iblis might have been a production center for a surrounding copper-trade network (Caldwell 1967).

Most of the crucibles found at Tal-i Iblis came from levels I and II; Iblis level 0 appeared only in some excavation trenches at the site and contained only a small amount of pottery. Voigt and Dyson (1992:143) go so far as to say that level 0 “cannot stand as a time unit distinct from Iblis I, and...should be rejected.” In addition to these crucibles in levels I and II, one small hearth was found in level II. This hearth was “scooped out of the ground” (Caldwell 1967:35). I have interpreted this description to be similar to that described by Tylecote (1982), reproduced here as Figure 1.3. The hearth at Tal-i Iblis contained small fragments of copper oxide, copper ore and one crucible fragment, but the presence of this single hearth does not provide substantial indication of the process used for the metallurgical technology present (Caldwell 1967:35). There was also a substantial number of small copper objects found in Iblis levels I and II; Table 2.2 summarizes these as well as the copper objects found in subsequent levels.

Iblis level III (4460-4400 BCE) was badly destroyed and contained fine pottery but no coarse crucibles; this level also contained the first furnace at the site, which was a “gypsum-burning furnace” (Caldwell 1967:36). However, level IV (4415-3365 BCE) also contained evidence of copper metallurgy (copper objects, malachite ore fragments and fragments of larger and deeper crucibles), giving Caldwell reason to speculate that copper-processing technology had continued to grow and flourish at the site (Caldwell 1967). Caldwell clearly states that more excavation is necessary at levels IV and V to improve our understanding of the cultural detail during these periods. In fact, Caldwell says that level I is the only level at Tal-i Iblis where sufficient detail has been obtained (Caldwell 1967:39). The pressing question for Caldwell, and the issue addressed by this thesis, is whether the level I and level II crucibles were being used for copper smelting or for copper melting.

Table 2.2. Copper metal objects excavated from Tal-i Iblis and documented in Caldwell’s preliminary site report (Chase et al. 1967:153,168,185-6).

Object	Caldwell Cat. No.	Level	Find spot
Copper pin (tack)	6	Iblis I	Area A, Section A
Copper pin (awl)	32	Iblis I	Area A, Section B
Copper pin (tack)	35	Iblis I	Area A, Section B
Copper pin (bent awl)	38	Iblis I	Area A, Section B
Copper pin fragment	39	Iblis I	Area A, Section B
Copper ring	12	Iblis I	Area A, Section B
Copper pin (tack)	36	Iblis I	Area A, Section B
Copper bead	43	Iblis I	Area A, Section B
Copper pin (tack)	217	Iblis II	Area C, 270-310cm
Copper pin (tack)	275	Iblis II	Area C, 270-310cm
Flat-ended copper pin (awl)	274	Iblis II	Area C, 270-310cm
Copper pin (nail)	25	Iblis III	Area A, Section A
Copper pin (tack)	122	Iblis III	Area E, Section F
Copper pin (nail)	121	Iblis III	Area E, Section F
Copper pin (awl)	99 (MIT No.248)	Iblis IV	Area E, Section F
Copper pin (awl)	98	Iblis IV	Area E, Section F
Copper pin fragments	Unknown	Iblis IV	Area C, 160-190cm
Copper ornament	222	Iblis IV	Area C, 120-150cm
Copper pin (awl)	84	Iblis IV	Area C, 120-150cm
Copper fragment	86	Iblis IV	Area C, 120-150cm
Flat-ended copper pin (awl)	56	Iblis IV	Area C, 90-110cm
Flat-ended copper pin (awl)	51	Iblis IV	Area C, 60-90cm

Descriptions in parentheses are provided by the author of this thesis and are defined as follows: a pin with a flat head is described as a tack; a pin with no head and little variation in width is described as an awl, and a pin with a small head is described as a nail.

Chapter III: Motivation for the Research

3.1 Purpose of the research

This section outlines the need for further analytical materials research on the crucibles from Tal-i Iblis that we presume provide evidence for metallurgy during the 6th millennium BCE. Ralph Dougherty and Joseph Caldwell (1966) invested research efforts into determining the extent of the metallurgical technology available to the Iblis occupants. Unfortunately, their studies were limited in both scope and analysis. I have at my disposal today more analytical and historical resources than were available to them in 1966. I have also found that some of my findings differ from those of Dougherty (Dougherty and Caldwell 1966) and therefore these results deserve attention.

Previous research conducted on the metallurgical crucibles recovered from Tal-i Iblis was carried out at the site as well as in a controlled laboratory environment. Prior to Dougherty's laboratory analysis of a single crucible sherd, Caldwell assembled an international team of metallurgists to visit Iran with the goal of understanding the metallurgical role of the site of Tal-i Iblis.

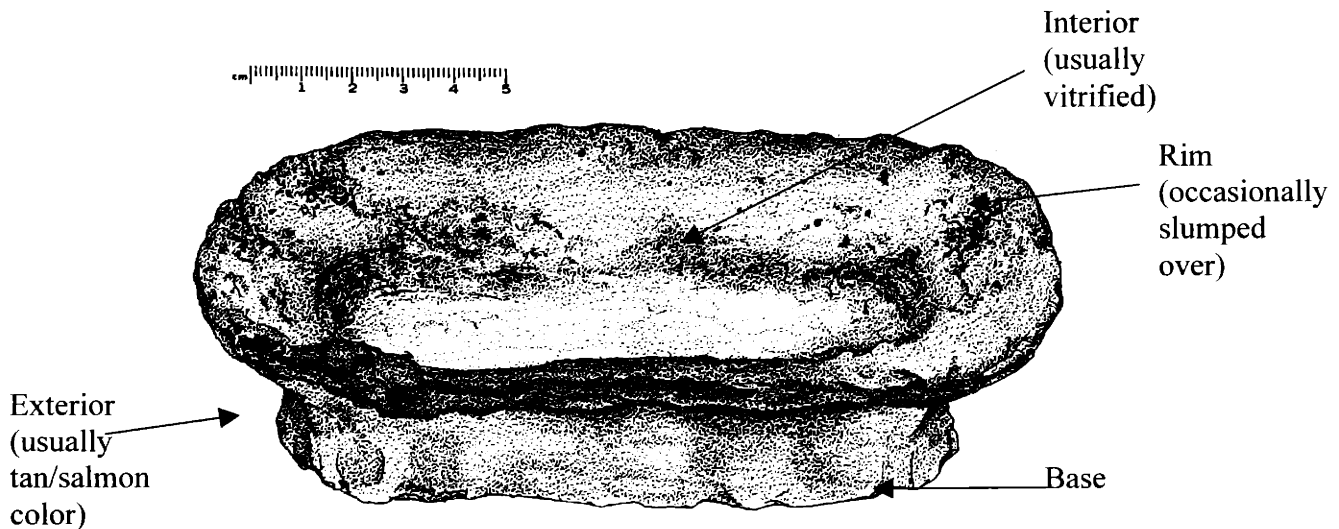


Figure 3.1. Drawing of a crucible restored from a large fragment found in level II (Caldwell Cat. No. 277, 1967:185)

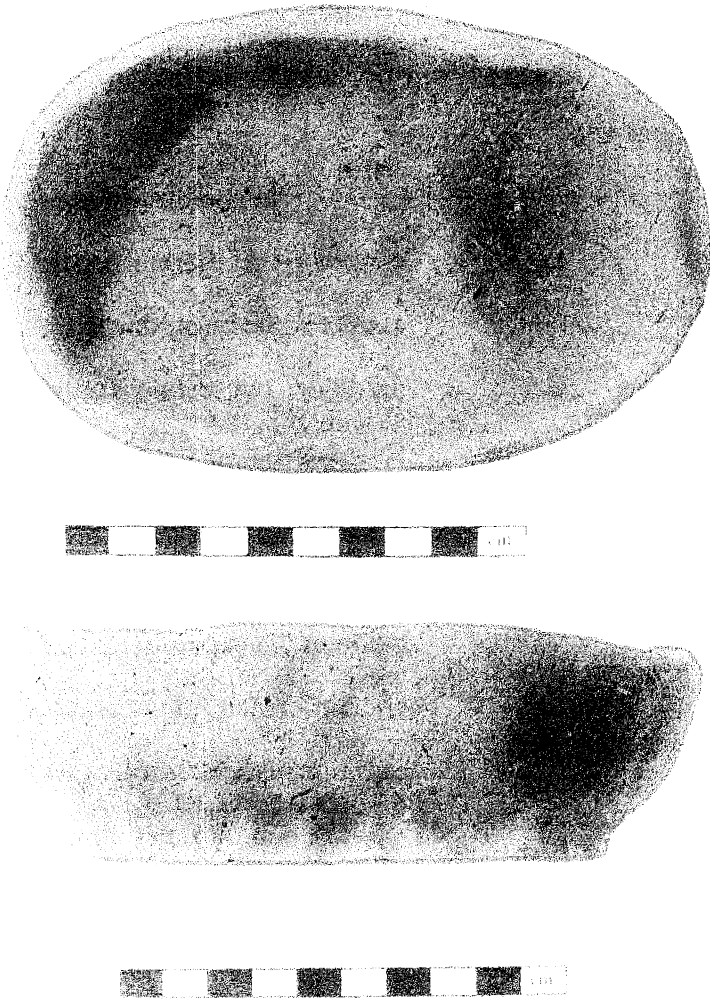


Figure 3.2. Photograph of a replica (MIT No. 5277) of an Iblis crucible made in 1966 by Hildegard Wulff at Tal-i Iblis, using local clay.

This team included the noted metallurgists Cyril Stanley Smith of MIT's Department of Materials Science and Engineering and Radomir Pleiner of the Archaeological Institute, Prague. Geologist Gholam-Hossein Vossouzadeh with the Ministry of Economy of Iran, Theodore Wertime of the Smithsonian Institute, and Joseph Caldwell completed the team (Pleiner 1967:340). This team of professionals conducted a smelting experiment at the site of Tal-i Iblis to assess the possibility that the Tal-i Iblis crucibles could have been used for the reduction of copper oxide ores. One of their colleagues, Hildegard Wulff, constructed a replica

(Figures 3.1 and 3.2) of the Iblis level I and level II-type crucible using "local clay," which she fired at low temperatures (Caldwell 1967:35). The experimental setup is shown in Figure 3.3. The crucible was placed in a simple bowl-shaped hearth similar to one found in Iblis level II (see section 2.2). The metallurgists placed small pieces of malachite found around the site into the crucible and piled charcoal above the ore. They heated the crucible for approximately one-half hour with a forced draught from a "simple bellows" while monitoring the temperature³ with a thermocouple

³ It is unclear as to whether the temperature measured by the thermocouple was the temperature at the center of the fire, or at the contact point with the crucible.

placed at the end of a tuyere (Pleiner 1967:375). This experiment produced only a few small pieces of copper and completely melted the crucible. The temperature measured by the thermocouple reached 1100°C during the experiment (Pleiner 1967).

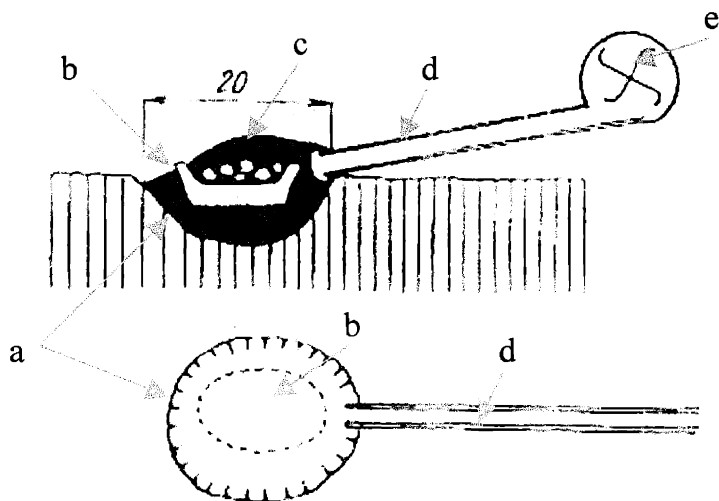


Figure 3.3. Set-up for on-site experiment conducted by Pleiner (1967:369) (a) the shallow pit dug out of the earth; (b) the replica crucible made of local clay; (c) charcoal fuel; (d) tuyere; (e) simple bellows.

The experiment was successful in that it demonstrated that copper could be produced from an oxide ore by heating in a simple Iblis-type crucible in the setting described. Unfortunately, the experiment, or at least the documentation of the experiment, had several deficiencies: (1) the only description of the construction of the replica crucible stated that it was made from “local clay” (Caldwell

1967:35). This clay was not analyzed to determine its mineral type, porosity or mineral inclusion concentrations, nor were we told the original firing temperature for the replica vessel. (2) The ore used in the experiment was described as coming from the site of Tal-i Iblis, but it was not analyzed to determine its mineralogy or chemical composition. (3) Since no tuyeres were found at Tal-i Iblis, they should not have been used in the experiment. (4) None of the ancient crucibles is described in the literature as having melted to the extent of the crucible used in the experiment, suggesting that the temperature reached during the smelting experiment exceeded that obtained by the Iblis metal workers.

In addition to this on-site experiment, Dougherty analyzed one crucible sherd from Iblis level I at the Argonne National Laboratory in Chicago. The results of this analysis were first published in *Science* (Dougherty and Caldwell 1966) and later reproduced in the Tal-i Iblis site report (Dougherty and Caldwell 1967). Based on his analysis, described below, Dougherty came to the

conclusion that the Iblis crucibles had been used for the “reduction [smelting] of a copper ore” (Dougherty and Caldwell 1966:985).

Dougherty obtained samples from three regions of the crucible cross-section: from the interior surface, the inner core, and the exterior surface. He heated them on a tungsten filament while temperatures were monitored with an optical pyrometer⁴. Dougherty determined that the interior surface melted at $1150\pm 50^{\circ}\text{C}$, the inner core melted at $990\pm 50^{\circ}\text{C}$, and the exterior surface melted at $990\pm 50^{\circ}\text{C}$ (Dougherty and Caldwell 1966:984). Dougherty explains the difference in melting temperature between the interior surface of the crucible and the rest of the ceramic material as related to a difference in composition of the interior surface. Dougherty argues that such a change in a chemical composition caused a change in the melting temperature and that the increase in melting temperature on the interior surface indicates that the crucible was used for smelting copper ore. He states that melting native copper in the crucible would have involved heating the interior of the vessel without changing its composition sufficiently to result in the measured difference in melting point temperatures.

In addition, Dougherty pointed out that the melting point range of the crucible fabric that he measured ($990\text{-}1100^{\circ}\text{C}$) is close to the melting point of copper metal (1083°C). Therefore, he argued, if the Iblis crucibles were being used to melt native copper, they likely would have vitrified and collapsed before the process was complete. Dougherty claims that it is possible to smelt pure copper oxide ore at temperatures that are considerably lower ($700\text{-}800^{\circ}\text{C}$) than the predicted melting point of the ceramic fabric. This suggests the possibility that the Iblis crucibles may have been used for smelting copper oxide or carbonate ore without loss of their integrity (Dougherty and Caldwell 1966). Thompson (1958) previously determined that this low smelting temperature is possible. He states that smelting a carbonate ore such as malachite at temperatures as low as $500\text{-}600^{\circ}\text{C}$ will produce a “spongy mass of metallic copper” (Thompson 1958:3). Furthermore, Thompson argues that a campfire can reach temperatures upwards of 600°C , suggesting that one would not

⁴ Dougherty also provides as a footnote, that these temperatures were “uncorrected” (Dougherty and Caldwell, 1966: 985), though the exact meaning of this is unclear.

even need bellows to create enough heat for the smelting reaction to occur. Charles (1979) has verified a similarly low smelting temperature of 700°C experimentally.

Finally, Dougherty noted that the core of the ceramic crucible sherds exhibit a grey/black color, whereas the exterior surface is usually colored tan/salmon. This information suggests that the crucibles were “intentionally” (Dougherty and Caldwell 1966:984) fired in a reducing atmosphere. He uses the word “intentionally,” because other pottery at the site was fired well enough to have oxidized the organic materials present in the clay, yielding a uniform tan/salmon color across the entire cross-section of the potsherds (Dougherty and Caldwell 1966). Dougherty uses this evidence to assert that a reducing atmosphere is necessary for smelting copper oxide or carbonate ores, but it is not necessary for melting copper. Dougherty does not point out, however, that one can melt copper in a reducing atmosphere, even if it is not *necessary* to do so.

These conclusions drawn by Dougherty leave several questions unanswered, both about the analytical methods employed in his research and more significantly, regarding the technological level of the metallurgy practiced at the site during this time period. A more complete analysis of the sherds is necessary to understand fully the use and history of these Tal-i Iblis crucibles.

3.2 Preparation for the research

This thesis reports my experimental and analytical investigations of a small collection of crucible sherds excavated at Tal-i Iblis and now in the collections of the MIT Center for Materials Research in Archaeology and Ethnology. This collection of materials arrived at MIT shortly after Cyril Smith’s visit to Tal-i Iblis in 1966. Smith collected some items on-site in addition to those that were sent to him later by Caldwell for further analysis. Until recently it was believed that the materials received by MIT in 1967 (and still curated there) were the only ones from the site available for study. However, during the spring of 2003, it was discovered that many cartons of artifacts excavated by Caldwell at Tal-i Iblis are held in storage at the University of Georgia in Athens, GA. These artifacts have not been examined and will not be addressed here.

The collection of Tal-i Iblis artifacts at MIT includes nineteen artifacts sent by Caldwell,

and eight artifacts collected separately by Smith (see Table 3.1). Ten of these have been studied for this thesis; they are described briefly in Table 3.2. These ten are illustrated in Appendix A, and are discussed in more detail in section 5.1. In his original site report, Caldwell refers to these ceramic vessels as “crucibles” (Dougherty and Caldwell 1966:984), and I will continue to use that designation throughout this thesis. The reconstruction of the crucibles (Figures 3.1 and 3.2) (Pleiner 1967:369,374) shows that the length is approximately 1.5 times the width, and the height is approximately 0.5 times the width. The convention I use to describe the areas of the artifacts is also indicated in Figure 3.1. Because there are so few of them, the documentation of these artifacts is extremely important. For this reason, I have carefully chosen methods of analysis to optimize the information I gather in exchange for the amount of the artifact that I am forced to sacrifice. The aim of this research is to present a clear and complete understanding of the role of these artifacts in the development of metallurgy at the site of Tal-i Iblis.

Table 3.1. Artifacts curated at MIT via Caldwell and Smith.

MIT No.	Caldwell Cat No.	Description	Find Spot
--	79	Copper ore (?)	Structure B 3-8; floor of room 4
242	326	Hematite	Structure B 3-8; corner of room 4
247	173	Copper pin	Floor of B 13
243	199	Hematite	B-19
240	--	Crucible fragment	Level 1 (collected by Smith)
244	--	Fragments of ore and slag	West profile, level 1
241 α *	--	Crucible fragment	West profile; levels 1 and 2
241 β *	--	Crucible fragment	West profile; levels 1 and 2
241 γ *	--	Crucible fragment	West profile; levels 1 and 2
241 δ *	--	Crucible fragment	West profile; levels 1 and 2
241 ϵ *	--	Crucible fragment	West profile; levels 1 and 2
241 ζ *	--	Crucible fragment	West profile; levels 1 and 2
241 η *	--	Crucible fragment	West profile; levels 1 and 2
249	295	Copper pin	Area C, level 2
248	99	Copper pin	Area E, section F, level 4
245	63	Crucible fragment (larger than others)	Level 5a
250	51	Copper pin with flattened end	level 5b
--	--	Copper ore	Level 5b
246	--	Copper oxide (?)	Level 5b
252	--	Ore (?)	Area B, level unknown
251	--	Fused cupriferous bead	Unknown
5274	--	Crucible fragment	Unknown
5275	--	Crucible fragment	Unknown
5276	--	Crucible fragment	Unknown
5277	--	Modern replica crucible	Constructed on-site with local clay
5278	--	Crucible fragment	From on-site experiment
5279	--	Crucible fragment	From on-site experiment

*These seven objects were contained within the same bag, and when the material was received in 1967, Professor Smith assigned the MIT No. 241 to the entire bag. I have amended the numbers for these objects to be able to distinguish them from one another.

Table 3.2. The Tal-i Iblis artifacts examined in this thesis.

MIT No	Caldwell's Cat. No/Sample No.	Description	Level
240	--	Ancient crucible fragment including rim, ext, and int. wall, and base. Green residue present on interior base.	Level I
241β	--/7	Ancient crucible fragment including ext. and int. wall. And a unique 4mm thick deposit of copper corrosion product interspersed with Zones 2 and 3 on interior surface of sherd.	West profile wall of levels I and II
241γ	--/7	Ancient crucible fragment including rim, ext. and int. wall. Most heavily vitrified of all ancient sherds.	West profile wall of levels I and II
241δ	--/7	Ancient crucible fragment including rim and ext. and int. wall. Green residue and nodules present on interior wall and base..	West profile wall of levels I and II
241ε	--/7	Ancient crucible fragment including ext. and int. wall and base. Green residue present on interior of base.	West profile wall of levels I and II
241η	--/7	Ancient crucible fragment including rim, ext. and int. wall, and base. Green residue and nodules present on interior wall.	West profile wall of levels I and II
245	63/10	Ancient crucible fragment, much larger than all others. Includes thick rim, ext. and int. wall. Green residue and nodules present on interior wall	Level V
5274	--	Ancient crucible fragment containing rim, ext. and int. wall, and base. Green residue present on interior wall and base.	Unknown, probably collected by Prof. Smith
5277	--	Complete crucible replica constructed by Miss Wulf in 1966 at Tal-i Iblis.	Modern
5279	--	Experimental crucible. A fragment of the crucible used for the experiment performed by the team of metallurgists at Tal-I Iblis. Fragment includes rim, ext. and int. wall, and base.	Modern

Chapter IV: Methodology

4.1 Methods for Analyses

I used many analytical methods to determine the likely function of these crucibles. These methods can be roughly divided into three categories: (1) microscopy: low power optical examination of the crucible sherds; micrographic analysis; scanning electron microscopy examination of sherd cross-sections; petrographic microscopic examination of sherd thin sections; (2) thermal analysis: differential thermal analysis, furnace experiments; (3) compositional analysis: x-ray diffraction, electron microprobe analysis; inductively coupled plasma optical emission spectroscopy. These three categories of analysis provide a well-rounded view of the fabrication and use of these crucible sherds. The suite of microscopic methods was essential both in developing an overall plan for my analytical procedure and in determining mineralogical differences within various zones of the sherds caused by heat alteration. Thermal analysis methods were employed to compare the ancient sherds with heated samples of the modern crucible replica (MIT No. 5277). Compositional analysis methods were employed to determine the compositional similarities and differences among the crucible sherds at both a macro and microscopic level.

4.2 Microscopy

It was necessary to acquire a thorough knowledge of the appearance and characteristics of the artifacts in this study. This was achieved through a number of methods of visual inspection. The crucible sherds examined over the course of this study are outlined in Table 4.1 with the corresponding methods of analysis used for each sherd. They were examined initially using the incident light, low power microscopes located in the CMRAE Graduate Laboratory. Opaque sections were

Table 4.1: Methods of analysis for each artifact studied.

Object (MIT No.)	Visual Analysis	Thermal Analysis	Composition Analysis
240	Micrographic ESEM Thin Section	DTA	Bulk Analysis EDS/WDS
241β	Micrographic ESEM Thin Section		Bulk Analysis XRD SEM EDS/WDS
241γ	Micrographic Thin Section		Bulk Analysis EDS/WDS
241δ	Micrographic ESEM Thin Section		Bulk Analysis EDS/WDS
241ε 241η 245 5274			Bulk Analysis Bulk Analysis Bulk Analysis Bulk Analysis
5277	Micrographic Thin Section	DTA Re-firing Experiments	Bulk Analysis XRD EDS/WDS
5279	Thin Section	DTA	

Key of terms:

- ESEM** Environmental Scanning Electron Microscopy
- DTA** Differential Thermal Analysis
- EDS** Energy Dispersive Spectroscopy with microprobe
- WDS** Wavelength Dispersive Spectroscopy with microprobe

constructed for some of the sherds and documented with the micrographic microscope in the CMRAE photography facility.

4.2.1 Environmental Scanning Electron Microscopy

The sherds were cut with a gem saw and the cut surfaces were ground smooth on silica carbide strip grinding papers. The cut-and-ground surfaces were examined with the Environmental

Scanning Electron Microscope (ESEM) in the Center for Materials Science and Engineering at MIT under the supervision of Dr. Anthony Garratt-Reed. The samples were not mounted or carbon coated because the ESEM employs a low-vacuum environment to prevent charging. This microscope

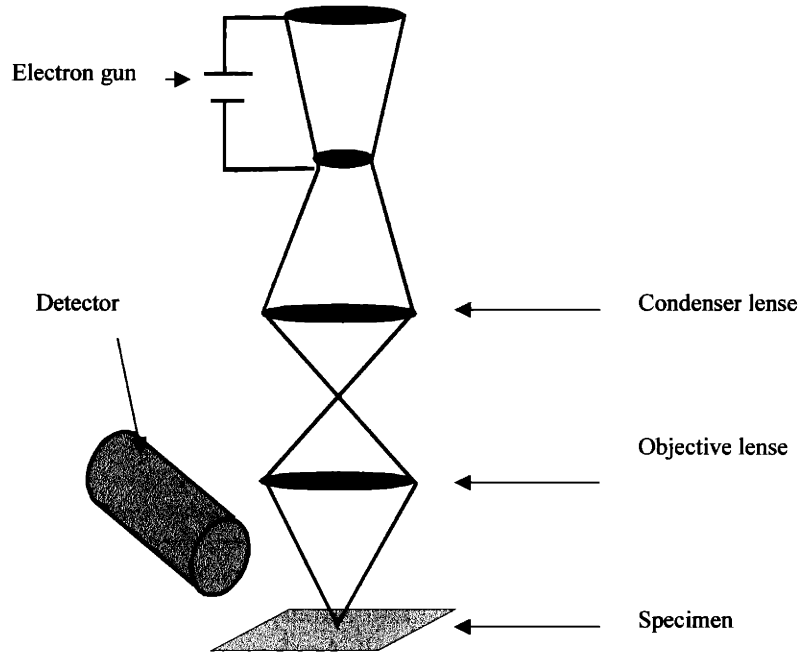


Figure 4.1. Schematic diagram of Scanning Electron Microscope (MIT 3.081 lecture notes 2001)

scope emits an electron beam, which is collimated and directed onto the surface of the sample (see Figure 4.1). The electron beam is absorbed and deflected by the material it hits. These deflections are detected by electron “collectors” and are then interpreted to create a digital image of the sample surface.

Rice (1987:46) illustrates an SEM image of clay platelets at a magnification of 3700. The

photomicrograph is reproduced here as Figure 4.2. These hexagonal discs are contained in all types of clay and normally fuse at approximately 1000°C. I used this photomicrographic image from Rice as a guide during my microscopic examination of the crucible sherds. My goal was to compare the microstructure of each crucible at various points along its cross-section to characterize the heating history of the material. The platelets should be present and unaltered in zones that have not been subject to temperatures in the range of 1000°C, and they should appear fused, or be absent in the vitrified areas.

The SEM images were collected at a beam voltage of 10-15kV and a vacuum pressure of 1.4torr in an atmosphere environment. In addition to gathering SEM images, this microscope is set up to determine the elemental composition of the material. This determination is achieved by detecting the X-rays emitted as a result of the interactions of the electrons with the sample rather



Figure 4.2. Kaolin clay platelets at a magnification of 3700 (Rice 1987: 46).

than by detecting only the deflected electrons. Once this preliminary ESEM examination was finished, I mounted the samples in Epotek Epoxy and returned to undertake the second stage of SEM work. This was performed with the goal of providing an elemental analysis of the sherd material and is described in section 4.4.

4.2.2 Petrographic thin section microscopy

Thin section analysis is a microscopic method of identifying minerals in rocks, ores or in clay bodies. It involves the passage of polarized light through a thin section of rock or ceramic, which has been ground and polished to a thickness of 30 microns. As the polarized light passes through the minerals, it is refracted depending on the crystal structure of the mineral. Minerals have characteristic colors and textures when observed in polarized light, allowing an observer to distinguish them. All of the crucible sherd thin sections were prepared following the method out-

Table 4.2. Artifacts studied with thin section analysis and the finishing methods for each.

MIT No.	Finishing Method
240	Fine polish
241 β	Cover slip
241 γ	Cover slip
241 δ	Cover slip
5277H	Fine polish
5277B	Fine polish
5277G	Cover slip
5277L	Cover slip
5277N	Cover slip
5277J	Cover slip
5277U	Cover slip
5277Q	Cover slip
5277T	Fine polish
5279	Fine polish

lined in the CMRAE thin section protocol. Thin sections were constructed from each of the artifacts listed in Table 4.2 with finishing methods (cover slip or fine polishing) indicated. The petrographic analyses were carried out with an Olympus polarizing microscope under 50, 100 and 200 magnifications. Minerals were identified using both plane and cross-polarized light.

In order to determine the volume fraction of the minerals identified in each sherd thin section, I performed point counts on the cru-

cible thin sections that were large enough to obtain 1000 data points. Point counting was carried out in the CMRAE Ceramics Research Laboratory. During point counting, the microscope stage moves automatically by increments of 200 microns upon identifying the mineral in the cross hairs of the microscope field of view. The analytical categories I used included: Clay matrix, Void, Quartz (including both polycrystalline and monocrystalline), Plagioclase Feldspar, Amphibole (usually hornblende), Biotite, Opaque minerals, Basalt clumps, Calcite, Pyroxene (usually orthopyroxene), Other (including both unidentifiable minerals and minerals not listed above).

The grain size distribution was also studied. The grain size of each identified mineral was recorded in terms of how many data points it occupied. For example, if a quartz grain was large enough to receive two clicks in a row, then it was marked under the category "2." The relationship

between category (number of "clicks" for one mineral) and the size range for the minerals in that category is shown in Table 4.3. This method of grain size analysis provided a rough estimate of the grain size distribution. I chose to look at grain size in this fashion because the distribution looked homogenous for most minerals. The results of the mineral identifications

Table 4.3. Grain size ranges for category groupings.

Category #	Grain size range (μ)
1	0-400
2	200-600
3	400-800
4	600-1000
5	800+

and grain size determinations appear in section 5.2.1. After point counting was complete, I studied the morphology of the minerals to become familiar with the appearance of the minerals at locations across a complete cross-section (i.e., from the interior to the exterior surface) of a crucible sherd, since they experienced different levels of heat depending upon their location in the vessel fabric.

4.3 Thermal Analysis

Determining the temperatures to which the regions of these ceramic vessels were heated is critical to understanding how they were used in prehistory. It is also necessary to understand the highest temperatures that these ceramic containers are capable of sustaining in order to determine the metallurgical processes for which they could be used. Since the sherds often present a vitrified interior surface, one might assume that the ceramic crucibles were near their limit in terms of the maximum temperature to which they could be heated before collapsing. My goal was to determine this maximum temperature while also examining any other morphological changes that occur in the ceramic as a function of temperature.

4.3.1 Differential Thermal Analysis

My first attempt to determine the melting temperature of the ceramic of the crucible sherds was through Differential Thermal Analysis (DTA). This method involves monitoring the temperatures by means of thermocouples of two samples heated simultaneously (a schematic drawing of this method of analysis is shown in Figure 4.3). One sample is a non-reactive standard (aluminum oxide), and the other is the test sample. As the samples are heated the test sample may go through changes where heat is released (exothermic reactions) or absorbed (endothermic reactions) but the standard does not. Therefore, a temperature difference (ΔT) is created between the two samples, and while the temperature of the standard increases linearly the test sample will show peaks and dips in its heating curve. These curves are then plotted on a graph of temperature vs ΔT .

It has been well established that endothermic and exothermic events occur at predictable temperatures in ancient ceramics depending on the original firing temperature of the clay. There-

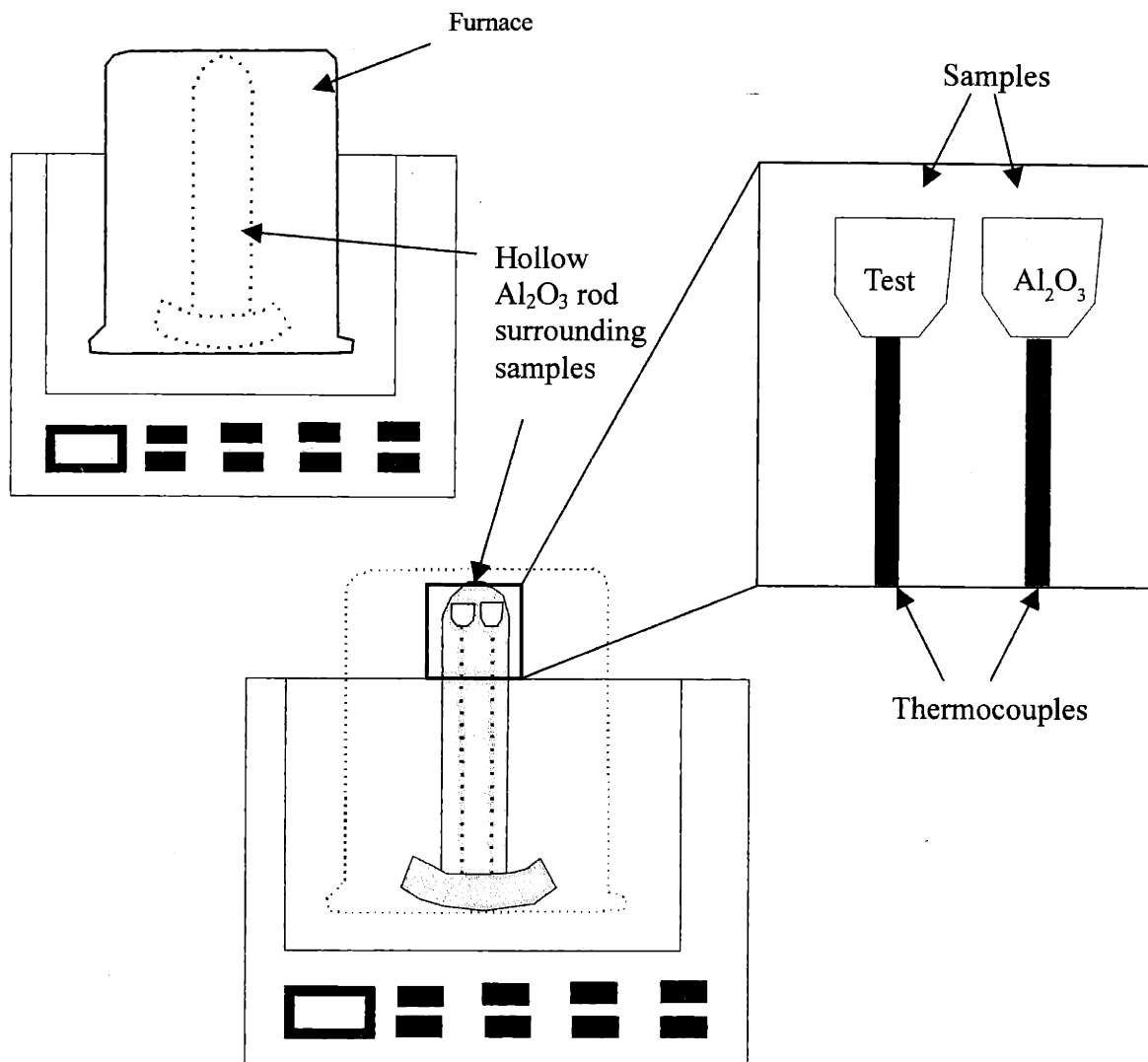


Figure 4.3. Schematic of DTA experiments.

fore DTA is a useful method in determining the original firing temperature of a ceramic (Kingery 1974). This technique is useful because clay will undergo a series of alterations when it is fired. For example, one can detect low firing temperatures if DTA peaks correspond to the combustion of organic material (e.g. chaff) in the clay, or if the peaks signal the loss of water from the clay minerals during firing. The presence of these peaks on a DTA curve of an Iblis sherd would reveal that the ancient ceramic was never heated to these temperatures in prehistory. However, if the ceramic was heated to higher temperatures (above 950°C), it would only be possible to detect the temperature at which the material melts. At these higher temperatures there are no further thermodynamic indicators corresponding to structural changes in the clay. In the present study I am interested in

determining the melting temperature of the Tal-i Iblis ceramic crucibles, and determining if there is a difference in the melting temperature of the exterior and interior zones.

The test samples for DTA were prepared by scraping with a scalpel blade, the vitrified region of a Tal-i Iblis crucible sherd (MIT No. 240) as well as the region unaltered by heat. The coarse ceramic sample was then powdered using a mortar and pestle. A small amount of this powdered sample was loaded into an aluminum oxide test crucible, and surrounded by Al_2O_3 powder so that the powdered Iblis sherd sample did not make contact with the walls of the test crucible. This sample and a standard sample (Al_2O_3 crucible filled with only Al_2O_3 powder) were then loaded into the Perkin Elmer DTA furnace associated with the Center for Materials Science and Engineering (CMSE) Crystal Growth Facility and under the supervision of Dr. Fangcheng Chou. The samples were run utilizing two different heating programs. The highly vitrified zones of the crucibles were heated from 500°C to 1500°C at a rate of 40°C per minute, held at 1500°C for one minute, then cooled back to 500°C at the same rate. The exterior zones of the crucibles, which were unaltered by heat, were heated from 100°C to 1200°C at the same rate.

4.3.2 Re-firing experiments with modern replica crucible

To determine the morphological changes occurring within the matrix of the crucible sherds as a function of temperature, I monitored the heat alteration experienced by samples cut from the modern crucible replica (MIT No. 5277). Portions of the modern replica were cut into cubes measuring 1-2 cm on a side. Each cube was placed on a fire brick and loaded into a CM Rapid Temperature Furnace located in Professor Thomas Eagar's Joining Laboratory at MIT. Under the instruction of Dr. Harold Larson, I positioned a Type K Thermocouple inserted into the back of the furnace, 1 cm above the crucible sample (see Figure 4.4 for a schematic drawing of the experimental setup). Nitrogen gas flowed into the furnace to create a neutral environment. Sample cubes were heated in 100°C intervals from 300°C to 1100°C and in 25°C intervals from 1100°C to 1200°C. Once the desired temperature was reached, each sample was maintained at that temperature for 20 minutes.

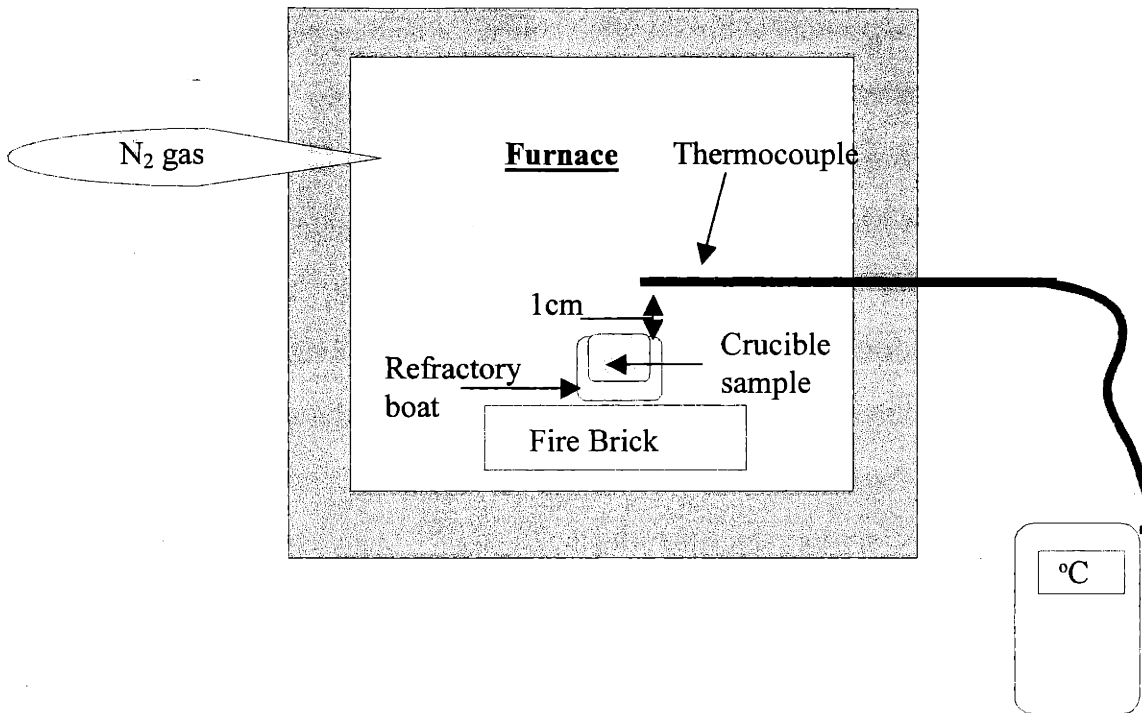


Figure 4.4. Schematic diagram of the re-firing experiments.

4.4 Compositional Analysis

Compositional analyses were carried out with three objectives: (1) to compare the bulk chemical composition of the modern crucible replica and the ancient sherds (2) to determine the mineralogical composition of the crucible sherds and of the modern replica (both (1) and (2) will provide evidence to validate the use of the modern replica as a proxy in the furnace experiment and in thin section mineral comparisons); and (3) to provide a highly specific, quantitative chemical analysis of the constituents of the vitrified regions of the Tal-i Iblis crucible sherds.

4.4.1 Bulk chemical compositional analysis

The composition of the crucibles was determined through inductively coupled plasma optical emission spectroscopy (ICP-OES) at the Activation Laboratories Ltd. under the supervision of C. Douglas Read. These results were reported as oxides, and the protocol for the Actlabs analysis are included in Appendix C.

4.4.2 X-Ray Diffraction

X-Ray Diffraction (XRD) was also used to compare the mineral components of the ceramic material in a Tal-i Iblis crucible sherd and in the modern crucible. All XRD was performed at MIT's CMSE. Under the guidance of Joseph Adario, I analyzed the samples using a Rigaku Rotoflex RTP 500 RC XRD unit at settings of 1° convergence slit, 1° scatter slit, 0.3 mm receiving slit, 60 kV and 300 mA. 2θ values were set at $5-50^\circ$, and the sampling interval was set at 0.02° . The scan speed was $10^\circ/\text{min}$ for the initial scans and $2^\circ/\text{min}$ for the slower scans. The samples were prepared in powdered form and dry-mounted on a glass slide.

XRD determines the crystalline structures of minerals and compounds. As an x-ray beam is incident upon a sample and as the angle of incidence changes, the crystalline lattice of the material diffracts the beam in a unique pattern, and the diffraction pattern can then be analyzed to determine the lattice spacing and the compounds present in the sample. A schematic of this method is shown in Figure 4.5. In this way we were able to determine the major minerals present in the ceramic samples.

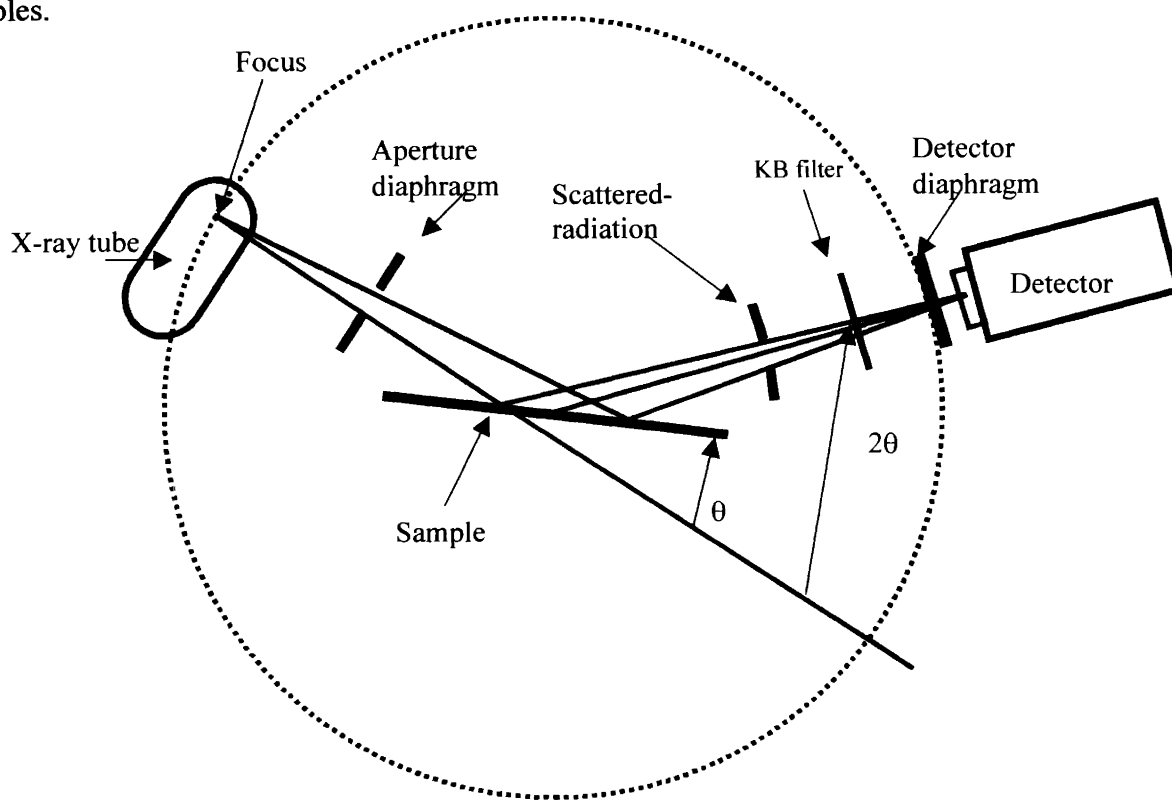


Figure 4.5. Schematic diagram of x-ray diffraction apparatus

4.4.3 SEM X-Ray Mapping

Samples cut from the sherds were mounted in Epotek Epoxy and polished with 6-micron synthetic diamond paste. They were carbon coated and examined with a JEOL 6320FV Scanning Electron Microscope in its high-resolution mode with a beam voltage of 5kV. The examination was carried out at CMSE under the supervision of Dr. Anthony Garratt-Reed. The energy dispersive x-ray detector was used to create x-ray maps of the sample cross sections. This helped to develop an understanding of the elemental distribution in the matrix of the material. For example, it would be valuable to know if elements were evenly dispersed across the section or tightly focused in one region of the section. A montage of SEM and X-ray map images were created of the cross-section from MIT No. 241 β to provide a better view of the morphological changes in the sherds from the interior zone to the exterior zone.

4.4.4 Electron Microprobe Analysis

Several sherd samples were examined at the Electron Microprobe facilities in the Department of Earth, Atmospheric and Planetary Sciences at MIT. Electron microanalysis was performed under the guidance of Dr. Nilanjan Chatterjee on a JEOL JXA-733 Superprobe. This method was employed to determine the purity of metallic copper prills visible in MIT No. 241 γ at the macroscopic level. In addition, this method provided a more complete analysis of the vitrified region, which was in direct contact with the contents of the crucible in prehistory and therefore may provide evidence as to what those contents were.

The analyses were performed with Energy Dispersive Spectrometry (EDS, a qualitative analytical method) and Wavelength Dispersive Spectrometry (WDS, a quantitative analytical method). In both analytical modes a beam of electrons is incident orthogonally onto a sample. As the beam penetrates the inner shell electrons, they gain energy and are displaced. The outer shell electrons move to fill the vacancies in the inner shells and release X-rays as they do so. The energy released is unique to each element and provides an energy spectrum for the sample. As the x-rays

are collected either by EDS or WDS, one can determine the elemental composition of the small (1micron in diameter) sample areas. The minimum detection limit is 10ppm, and elements with atomic number of 4 or greater can be analyzed (EMPA website).

The methods outlined here are the relevant procedures employed during the research period of this project. The next chapter, Results, will present the outcomes of these procedures.

Chapter V: Results

5.1: Macroscopic Description of the Crucible Sherds

During my initial examination of the crucible fragments, it became necessary to develop a nomenclature to describe the zones of the heat alteration within the sherd fragments. These zones are visible at the macroscopic level across a section of the sherd fragments. This nomenclature is shown in Figure 5.1 as it relates to a schematic rendition of a section through a crucible sherd. The crucible sherds possess four distinct zones, though not all zones are present in each sherd. Zone 1 exhibits a tan/salmon color, and usually appears as a thin layer on the exterior wall of the crucible sherds. This oxidized zone seems to be the least affected by the heat applied during the metallurgical use of the crucibles. Zone 2 is a reduced core, and every sherd contains this grey-colored region; when Zone 1 exists, Zone 2 is found adjacent to it. This means that the reducing environment present for Zone 2 did not reach the exterior of the crucible. Therefore the reducing atmosphere must have been created within the interior of the crucible, and this environment was not sustained at the exterior.

In addition to these oxidized and reduced zones, two vitrified zones may also be present on the sherds. Zone 3 is found along the rims and interior base of the crucible sherds. It also serves as a transition

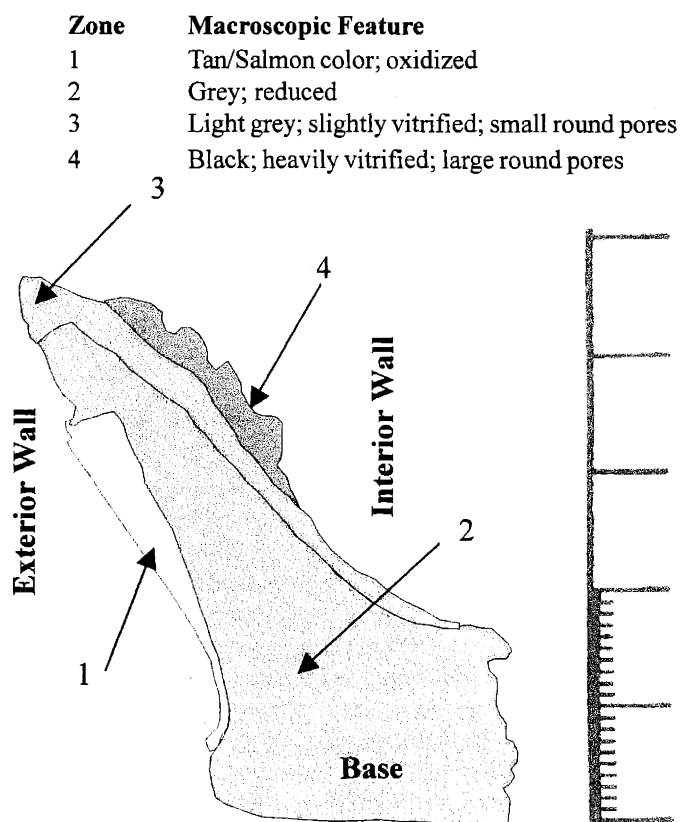


Figure 5.1. Zones of heat alteration across a section of a crucible fragment. (Traced from section photograph of MIT No. 240).

zone between Zone 2 and Zone 4. Zone 4 lies on the upper interior wall of the crucibles, and is glassy in appearance. Zone 3 is lighter grey in color and contains many small spherical pores. Zone 4 is almost black in color and contains large pores. The larger pores and vitrified appearance indicate that the sherd reached a higher temperature at this location (see section 5.3.2). Zone 4 is referred to as heavily vitrified and Zone 3 as slightly vitrified.

5.1.1 Photography and Drawings

Each of the 10 artifacts described in Table 5.1 was drawn and photographed before analyses were performed. This table lists the find spot of the artifacts as well as a brief description of each. Accompanying photographs and drawings of each can be found in Appendix A. Replicas of these ancient crucibles were constructed by Hildegard Wulff at Tal-i Iblis in 1967 with “local clay” (Caldwell 1967:35). One of these (MIT No. 5279) was used for the onsite experiment mentioned in

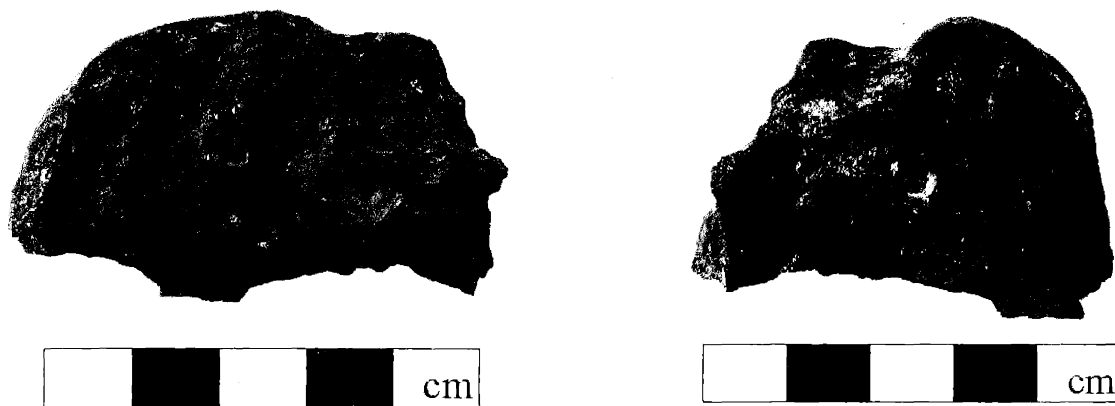


Figure 5.2. MIT No. 5279: Modern replica crucible sherd used in experiment at Tal-i Iblis in 1967. Left: top view; Right: profile view showing slumped rim.

section 3.1, and fragments of it were subsequently sent to MIT for analysis. This *used* replica is more heavily vitrified than any Tal-i Iblis crucible sherd held at MIT, and this fragment can be seen in Figure 5.2. Another replica (MIT No. 5277) that was not used for experimentation was also sent to MIT; however, this modern replica was fired at a low temperature on site. This is apparent from the carbon core found within the crucible. As a ceramic vessel is fired, the organic material contained within the clay matrix combusts. As firing temperatures reach 200°C and above, the carbon

Table 5.1. Artifacts examined in this thesis with description and find spot.

<u>MIT No</u>	<u>Size</u>	<u>Description</u>	<u>Zones</u> (% Volume fraction of cross section)	<u>Level</u>	<u>Caldwell's Cat. No./Sample No.</u>
240	41.25g 4.3x4.8x0.3cm	Ancient crucible fragment including rim, ext, and int. wall, and base. Green residue present on interior base.	Zone 1: 7 Zone 2: 81 Zone 3: 5% Zone 4: 7%	Level I	--
241β	8.8g 3x2.2x1.8cm	Ancient crucible fragment including ext. and int. wall. And a unique 4mm thick deposit of copper corrosion product interspersed with Zones 2 and 3 on interior surface of sherd.	Zone 1: 0% Zone 2: 90% Zone 3: 10% Zone 4: 0	West profile wall of levels I and II	--/7
241γ	4.8g 2.3x0.8x1cm	Ancient crucible fragment including rim, ext. and int. wall. Most heavily vitrified of all ancient sherds.	Zone 1: 7% Zone 2: 20% Zone 3: 13% Zone 4: 60%	West profile wall of levels I and II	--/7
241δ	41.7g 7x1.8x4.9cm	Ancient crucible fragment including rim and ext. and int. wall. Green residue and nodules present on interior wall and base..	Zone 1: 40% Zone 2: 45% Zone 3: 7% Zone 4: 8%	West profile wall of levels I and II	--/7
241ε	24.0g 0.9x3.6x5.2cm	Ancient crucible fragment including ext. and int. wall and base. Green residue present on interior of base.	Zone 1: 0% Zone 2: 100% Zone 3: 0% Zone 4: 0%	West profile wall of levels I and II	--/7
241η	32.8g 1.2x5.7x5.2cm	Ancient crucible fragment including rim, ext. and int. wall, and base. Green residue and nodules present on interior wall.	Zone 1: 3% Zone 2: 77% Zone 3: 5% Zone 4: 15%	West profile wall of levels I and II	--/7
245	77.3g 7.8x6.7x2.2cm	Ancient crucible fragment, much larger than all others. Includes thick rim, ext. and int. wall. Green residue and nodules present on interior wall	Zone 1: 62% Zone 2: 13% Zone 3: 9% Zone 4: 16%	Level V	63/10
5274	21.3g 3.5x.35x3.5/0.9cm	Ancient crucible fragment containing rim, ext. and int. wall, and base. Green residue present on interior wall and base.	Zone 1: 7% Zone 2: 90% Zone 3: 3% Zone 4: 0%	Unknown, probably collected by Prof. Smith	--
5277	373.2g	Complete crucible replica constructed by Miss Wulf in 1966 at Tal-i Iblis.	Zone 1: 100% Zone 2: 0% Zone 3: 0% Zone 4: 0%	Modern	--
5279	25.1g 1.4x4.8x3.6cm	Experimental crucible. A fragment of the crucible used for the experiment performed by the team of metallurgists at Tal-I Iblis. Fragment includes rim, ext. and int. wall, and base.	Zone 1: 3% Zone 2: 5% Zone 3: 32% Zone 4: 60%	Modern	--

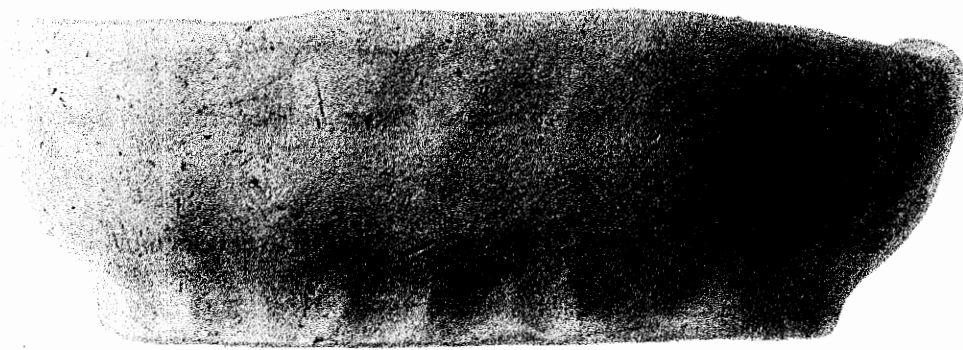
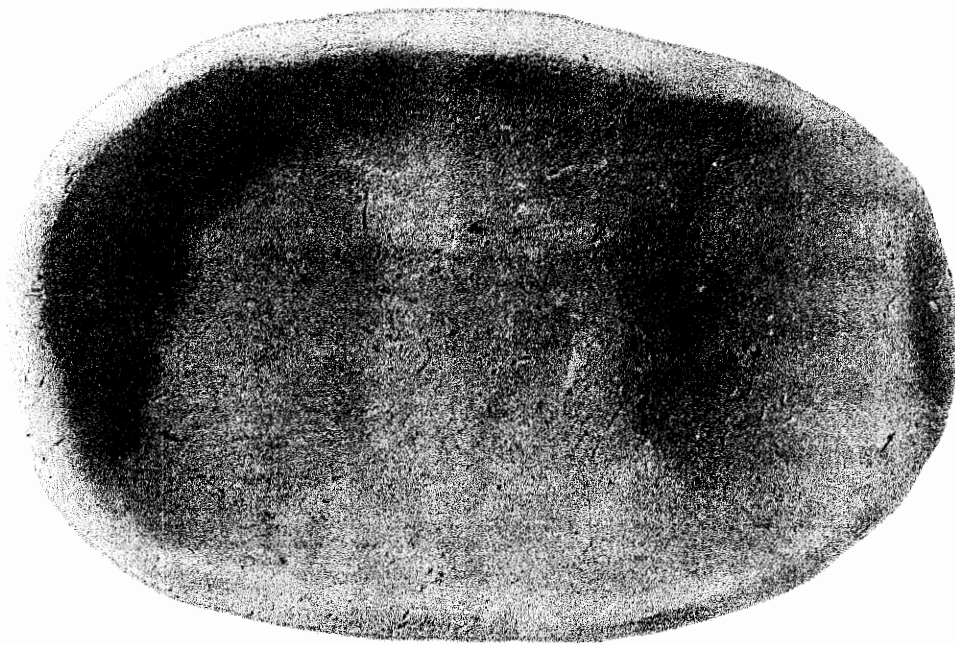


Figure 5.3a. MIT No. 5277: Modern crucible replica; Top: view of interior from above; Bottom: profile view

within the clay begins to burn out and oxidize. This causes the carbon to travel from the interior to the surface leaving a blackened core. This core will only fully disappear when the ceramic material is heated to above 600°C in a fully oxidizing environment (Rice 1987:88). This modern replica is shown in Figure 5.3a, and the carbon coring can be seen in Figure 5.3b.

Figure 5.4 illustrates the most representative of the ancient sherds (MIT No. 240). It includes a preserved base, wall and rim. Most of the artifacts examined here are fragmentary and include at least the walls and rims of the ancient metallurgical crucibles of which they were a part. Only MIT



Nos. 240, 241η, 5274 and 5279 contain bases as well (Figures 5.4, 5.5, 5.6 and 5.2, respectively).

Figure 5.3b. MIT No. 5277: Section of modern crucible replica; Carbon coring provides proof that this replica was fired at a low (below 600°C) temperature when constructed.

MIT Nos. 241β and 241ε do not contain any part of the rim, though 241ε contains a base (Figures 5.7 and 5.8).

MIT Nos. 241γ and 245 (Figures 5.9 and 5.10) are the only ancient sherds that exhibit heavy vitrification at their rims (Zone 4); all of the other sherd rims are slightly vitrified (Zone 3). Figure 5.9 shows the extreme vitrification of MIT No. 241γ at the rim and along the interior wall. Zone 4 occurs along the interior wall of all sherds except MIT Nos. 241β and 241ε (Figures 5.7 and 5.8). MIT No. 240 exhibits a hybrid of Zones 3 and 4 on its interior surface. Many large pores typical of Zone 4 characterize the interior surface, but it is light grey in color, like Zone 3.

The interior surfaces of the lower walls and the bases of most of the sherds are covered with a green residue. This residue is characteristic of copper corrosion and was believed by Caldwell to be indicative of an early smelting technology at Tal-i Iblis; however I will discuss this in section

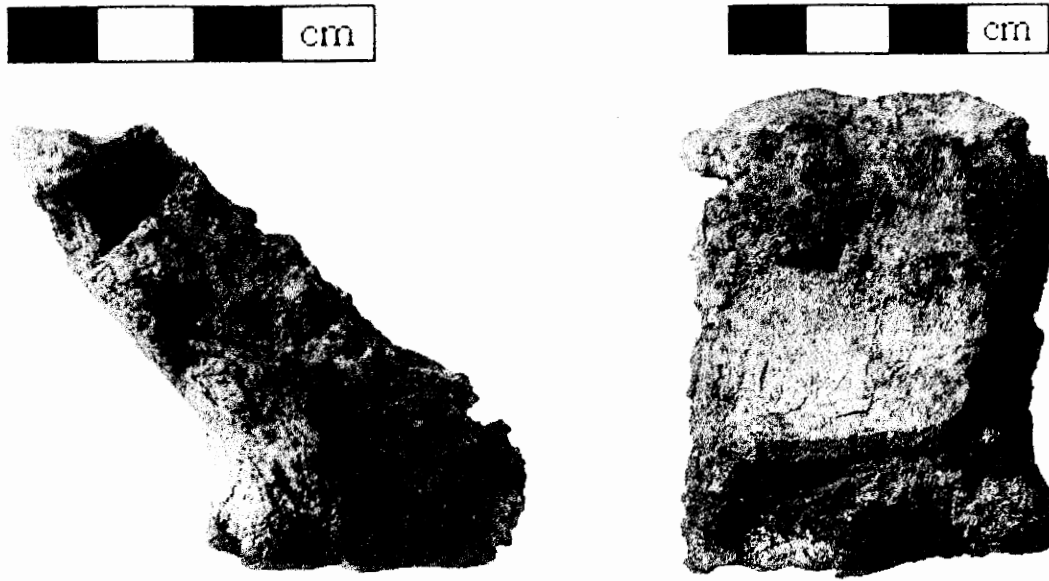


Figure 5.4. MIT No. 240: Tal-i Iblis Crucible sherd, Level I. Left: profile view; Right: view of interior wall and portion of base.

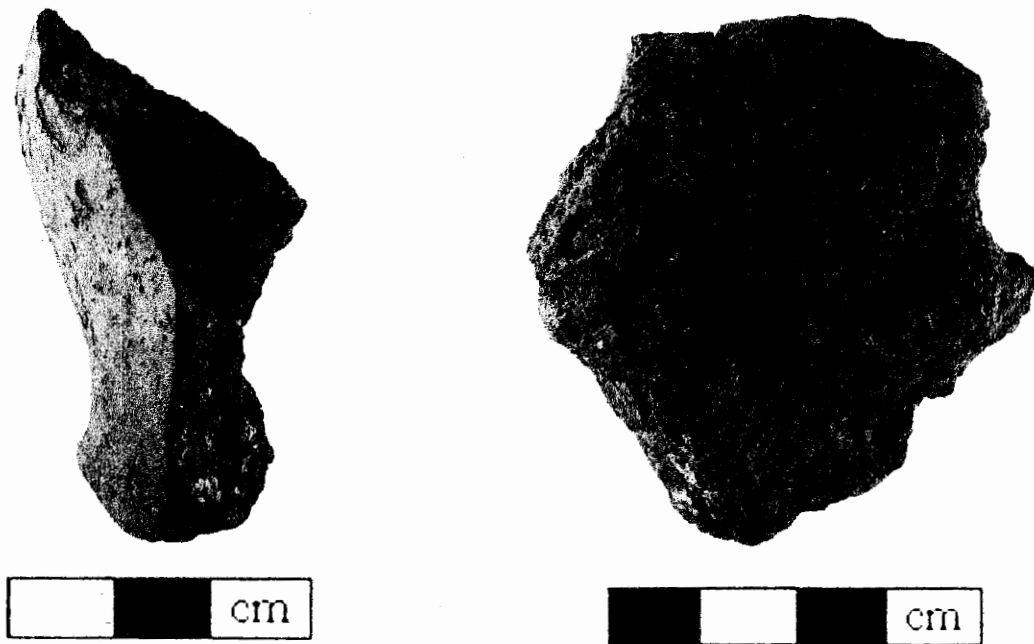


Figure 5.5. MIT No. 241η: Tal-i Iblis crucible sherd, Level I and II profile wall. Left: profile view; Right: view of interior surface.

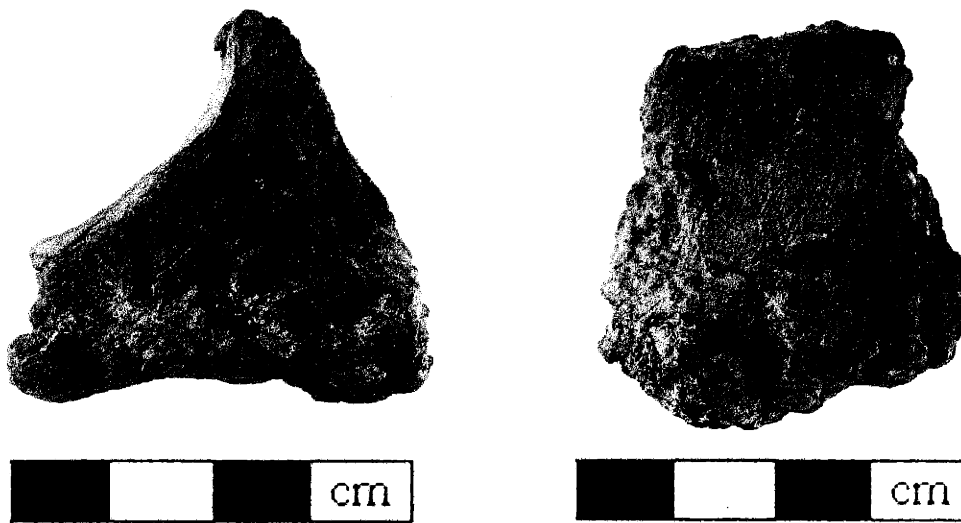


Figure 5.6. MIT No. 5274: Tal-i Iblis crucible sherd, collected by Prof. Smith. Left: profile view; Right: view of interior surface.

6.2. In addition to this green residue, the interior bases and lower walls occasionally exhibit a thin layer of Zone 3, but the interior bases and lower walls never show the morphology typical of Zone 4. Zone 2 is present in all of the ancient crucible sherds, and Zone 1 can be located on the exterior wall for every sherd with an identifiable wall, but it is not present on any identified bases. Interestingly, MIT Nos. 241 β and 241 ϵ (Figures 5.7 and 5.8) are the only two sherds that do not exhibit Zone 4 morphology and do not contain a rim, but they are completely reduced, with green accretions on their interior surfaces. Notice that this accretion is especially thick on the interior surface of MIT No. 241 β (Figure 5.7). This leads me to suspect that these two fragments (MIT Nos. 241 β and 241 ϵ) are from the interior bases of their respective crucibles, and I return to this argument in the next chapter (section 6.2).

In addition to these visual indications of the sherds' contact with copper metal and that they were heated to temperatures that resulted in zonal vitrification, many mineral inclusions and voids can be seen in the ceramic matrix of the sherds. Voids are also present as pseudomorphs of chaff added to the clay as temper. It is likely that this temper was added to increase the refractory properties of the clay, allowing it to become a better heat insulator. This discussion is addressed in the next chapter (6.3).

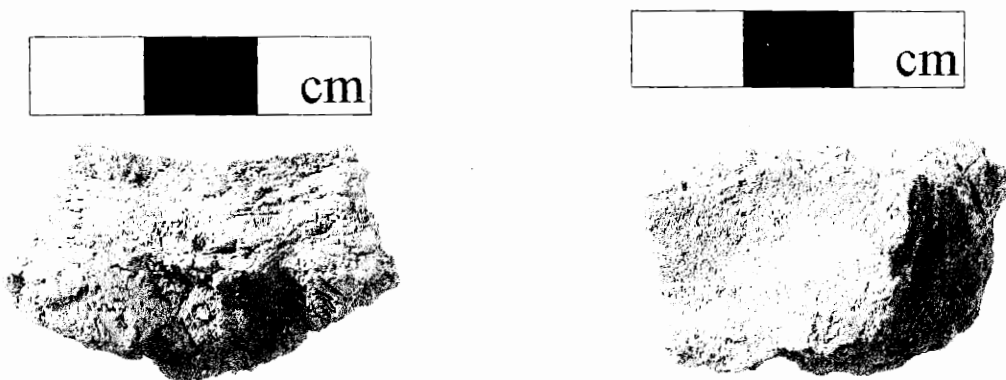


Figure 5.7. MIT No. 241β: Tal-i Iblis crucible sherd, Level I and II profile wall. Left: profile view; Right: view of interior surface exhibiting a thick green accretion.

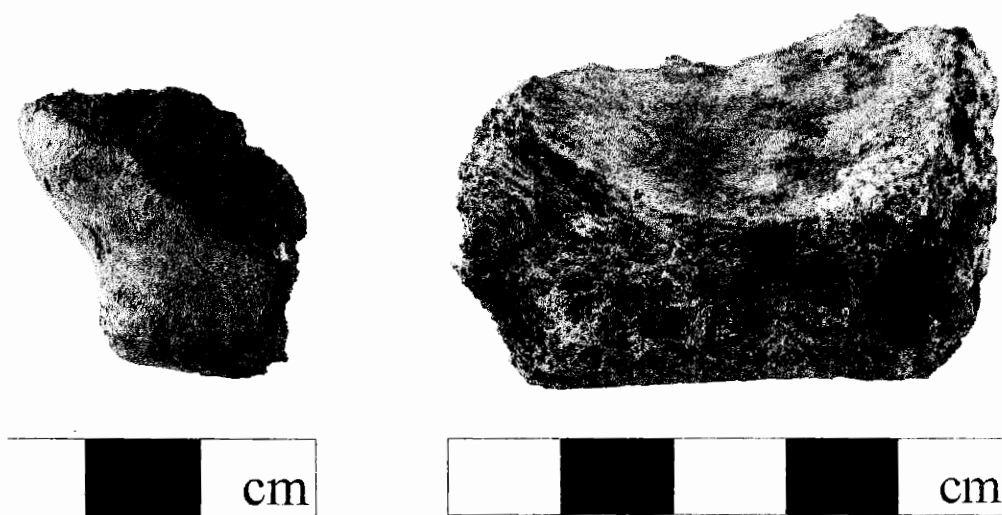


Figure 5.8. MIT No. 241ε: Tal-i Iblis crucible sherd, Level I and II profile wall. Left: profile view; Right: view of interior surface showing green accretion.

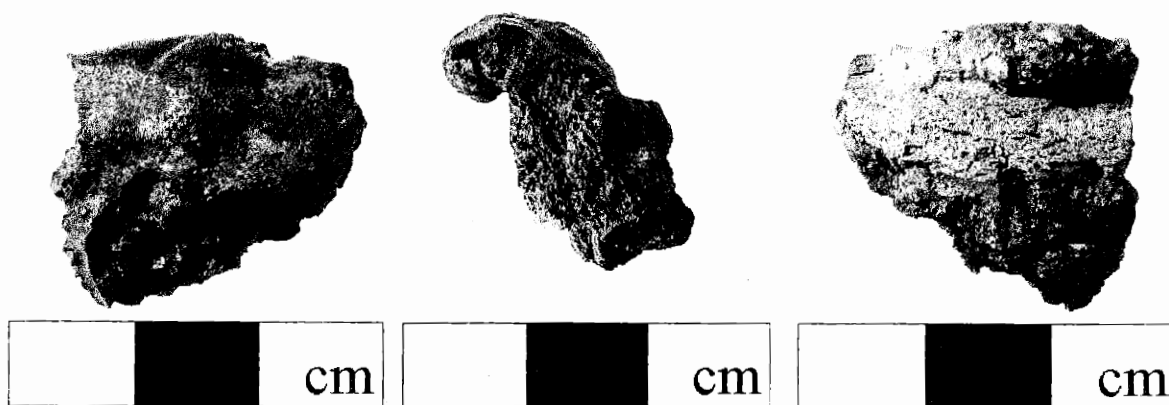


Figure 5.9. MIT No. 241γ: Tal-i Iblis crucible sherd, Level I and II profile wall. Left: view of interior heavily vitrified surface; Middle: profile view with slumped rim shown; Right: view of exterior surface.

5.1.2 Environmental Scanning Electron Microscopy (ESEM)

The zones outlined above are visible not only at a macroscopic level. We can also detect differences in the microstructure of the clay by comparing environmental scanning electron microscopic (ESEM) images of these zones. I cut complete sections through the crucible sherds to reveal the zoning in preparation for their microscopic analysis. The locations of these sections are indicated on the drawings for the relevant artifacts (Appendix A). Using ESEM I was able to document at a microscopic level the morphological changes visible in the clay fabric on the macroscopic level.

Recall from section 4.2.1 that all clays are comprised of platelets (disc-shaped features) that cause the characteristic plasticity of wet, un-fired clay. A photomicrograph of these platelets of kaolinite clay was reproduced as Figure 4.2. Upon heating to above a given temperature these platelets lose their interstitial water and then bond to each other during a process called



Figure 5.10. MIT No. 245: Tal-i Iblis crucible sherd, Level V. Left: profile view (this sherd is much larger than any of the other ones, and it is also from a much later level); Right: view of interior surface.

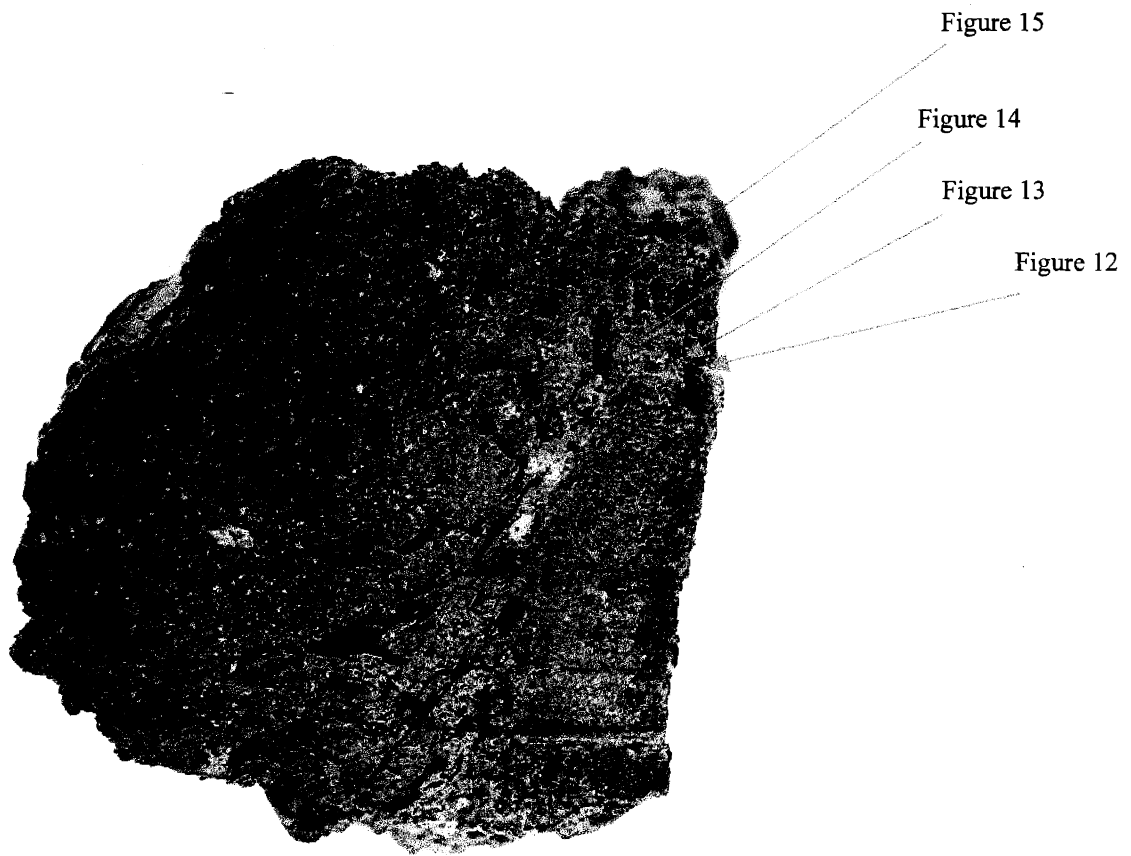


Figure 5.11. Cross-section of MIT No. 241 β with locations of ESEM images indicated with arrows.

dehydroxylation. This fusion of platelets increases the yield strength of the clay, however the temperature for fusion depends on the type of clay and heating environment (Rice 1987: 90).

In the reduced zone of the ancient sherds platelets are visible. They are fused at locations that approach the interior surface of the ceramic. Figure 5.11 shows the section cut from MIT No. 241 β and indicates the points within this section that correspond to the ESEM images shown in Figures 5.12-15. One can clearly see the fusion of platelets in Figures 5.12 and 5.13 in contrast to the unfused, distinct shape of individual platelets in Figure 5.14. Figure 5.15 completely lacks fused platelets. Figures 5.16 and 5.17 show Zone 4 of ancient sherd MIT No. 240. The microstruc-

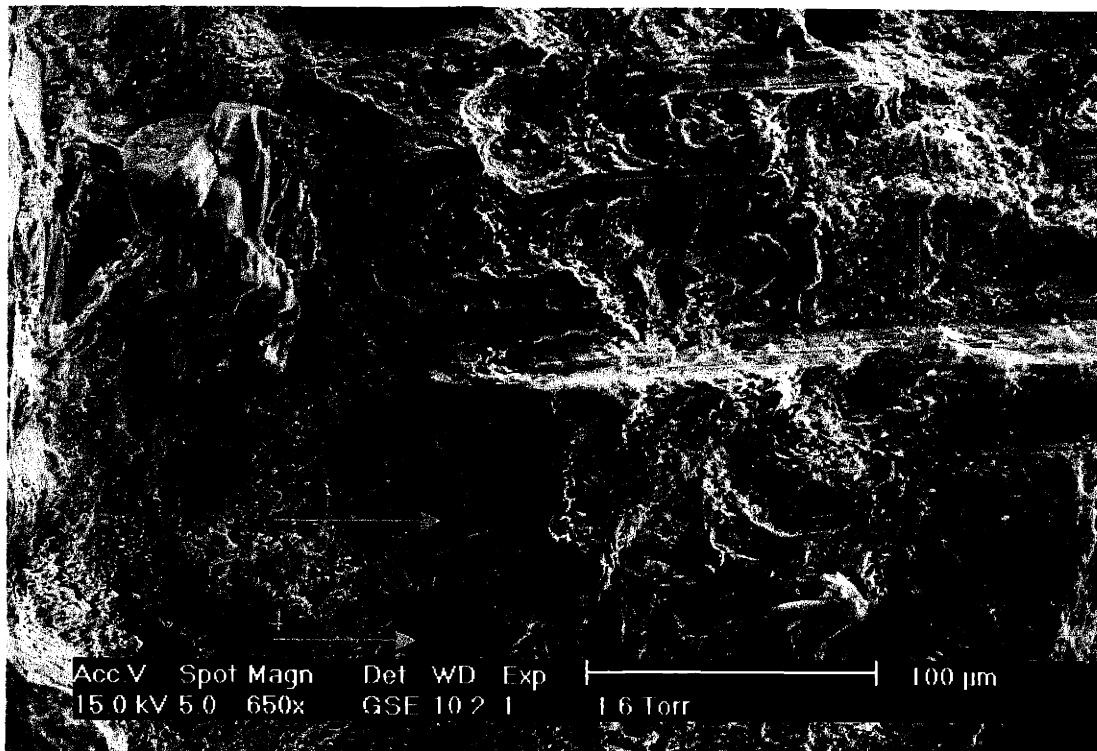


Figure 5.12. ESEM image of MIT No. 241 β at a magnification of 650, in Zone 3 near the interior surface, within the thick green accretion. (1) These streaks are artifacts of sample preparation. (2) The platelets are fused together in this area, (3) but not as much so in this area. (4) These pores are due to vitrification.

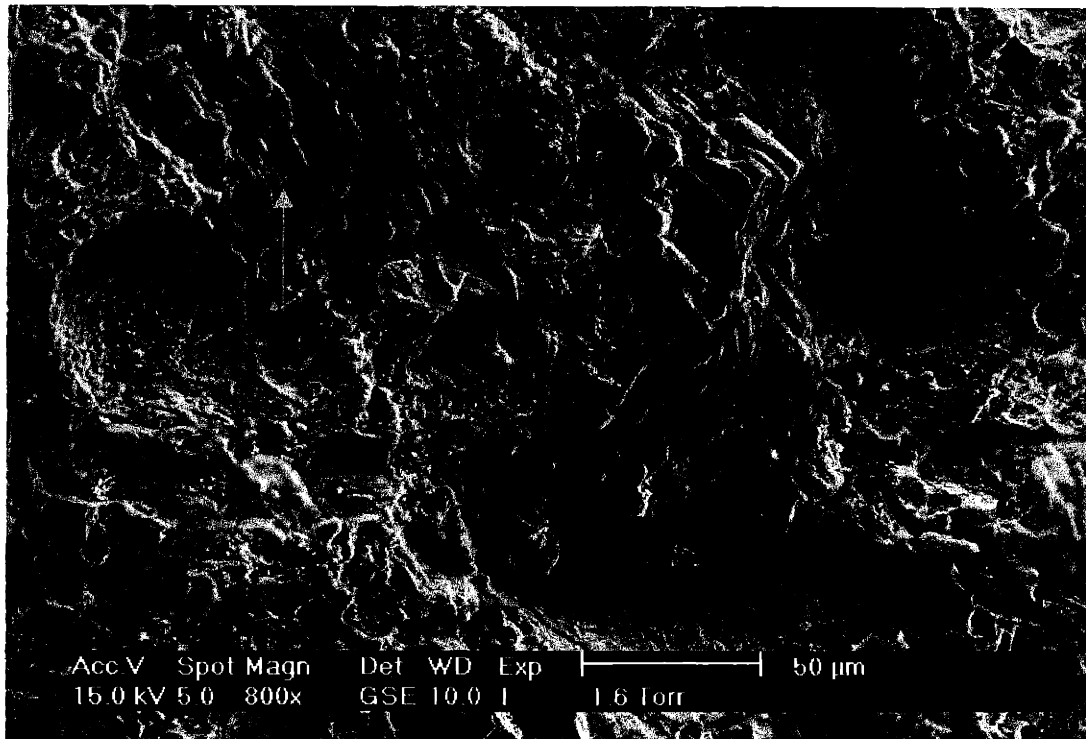


Figure 5.13. ESEM image of MIT No. 241 β at a magnification of 800, on the boundary between the green accretion zone and Zone 2, 0.8mm from the interior surface. The arrow indicates where the platelets are more distinct (less fused).

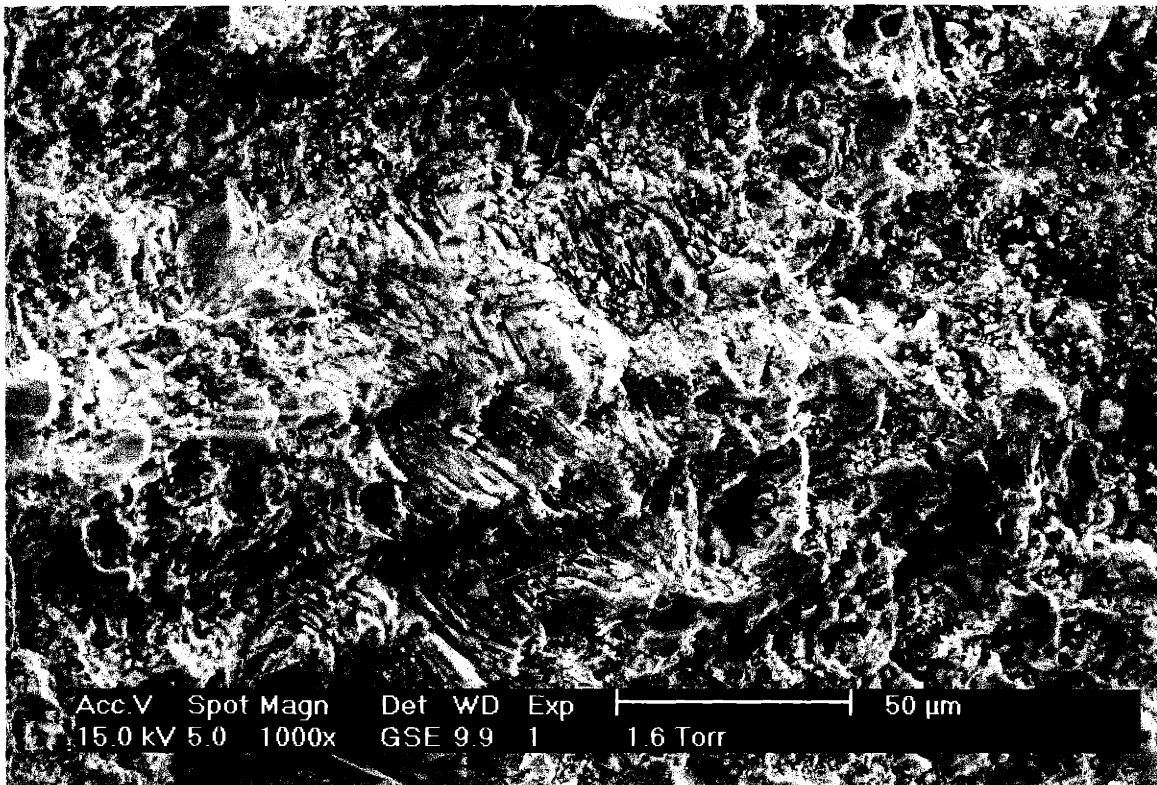


Figure 5.14. ESEM image of MIT No. 241 β at a magnification of 1000, within Zone 2 (reduced core), 2.5mm from the interior surface. The arrow indicates stacks of clearly defined platelets.

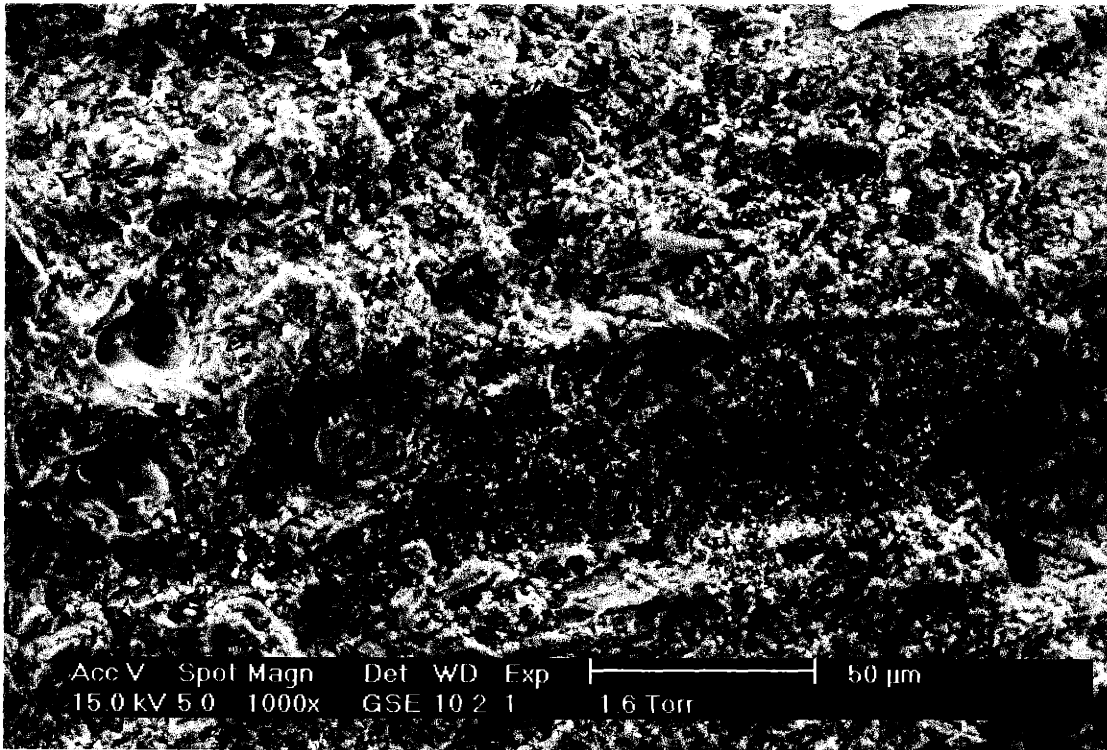


Figure 5.15. ESEM image of MIT No. 241 β at magnification of 1000, within Zone 2, 5mm from the interior surface. Notice the complete lack of fused particles.

ture is very different from that of MIT No. 241 β in that the platelets are completely fused and indistinguishable. Because Figures 5.16 and 5.17 were recorded at a lower magnification than the images shown in Figures 5.12-15, for purposes of comparison, I included Figure 5.18. Figure 5.18 captures the region shown in Figure 5.12 at a correspondingly lower magnification.

5.1.3 Summary

The sherds studied in this thesis have been characterized as exhibiting evidence of use as part of a metallurgical technology practiced during the occupation of levels I and II at Tal-i Iblis. They exhibit four discrete microstructural zones that correspond to differential heating. These descriptions of the sherds and their microstructural zones provided a framework for their subsequent analysis and for interpretation of the analytical results.

5.2 Comparison: Ancient Sherds and the Modern Replica of a Tal-i Iblis Crucible

The goal of this thesis is to determine the role of the ceramic crucibles in the metallurgical processes employed at Tal-i Iblis levels I and II. The nature of this technology can be determined through various modes of analysis. By examining the thermal properties of the crucible sherds, one can determine the temperature to which the crucibles were heated, thereby providing some clues as to their original use. By studying the composition of the heavily vitrified zone of the sherds, one can infer the nature and likely composition of the substances heated within the crucible. These two avenues of investigation are key to understanding the use of these crucibles at Tal-i Iblis, and will be addressed in section 5.3. In order to establish the level of correspondence between the archaeological sherds and the modern replica (MIT No. 5277), I had to demonstrate the compositional similarity between them. Different clay compositions can exhibit different thermal properties, and differing amounts of temper can change the refractory properties of a clay vessel. Therefore, closeness in ceramic composition indicates the likelihood that the sherds and the replica would exhibit similar thermal properties. In that case, I could use the modern replica as a proxy for the sherds in experiments designed to determine the thermal properties of the sherds. The constraints set by the

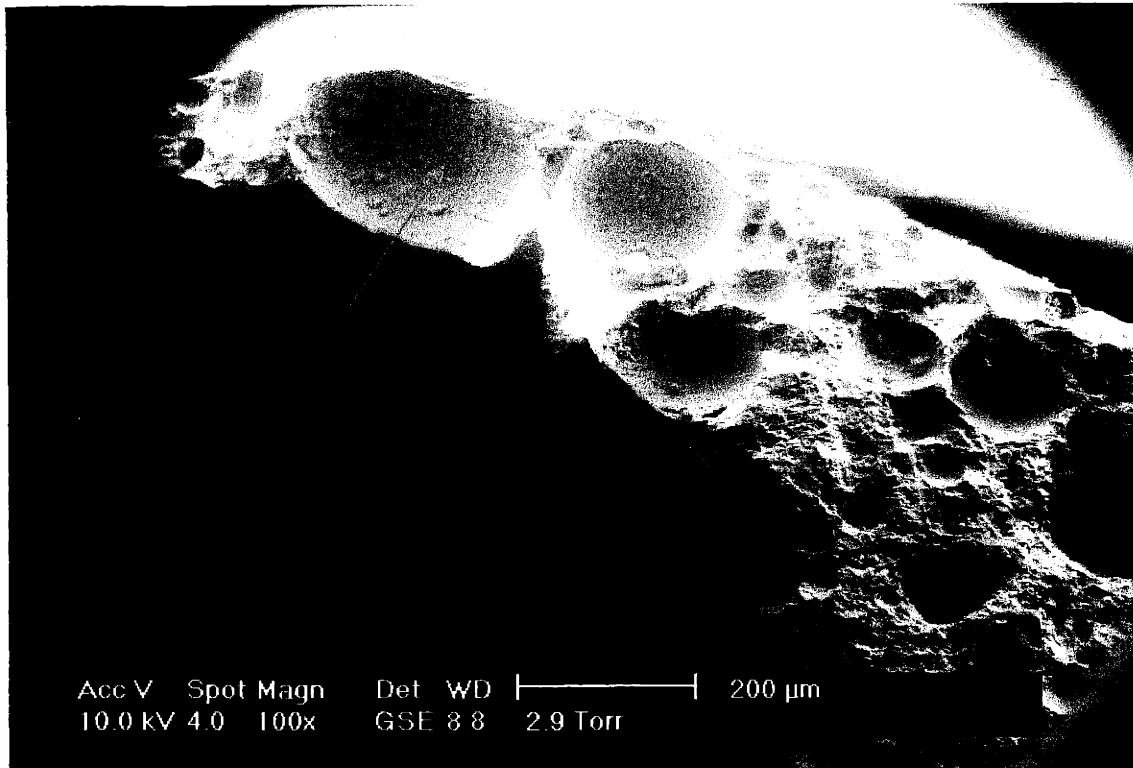


Figure 5.16. ESEM image of MIT No. 240 at a magnification of 100, Zone 4 on the interior surface. There are no discernable platelets. Notice the smooth surfaces of the void interiors and the large spherical voids.

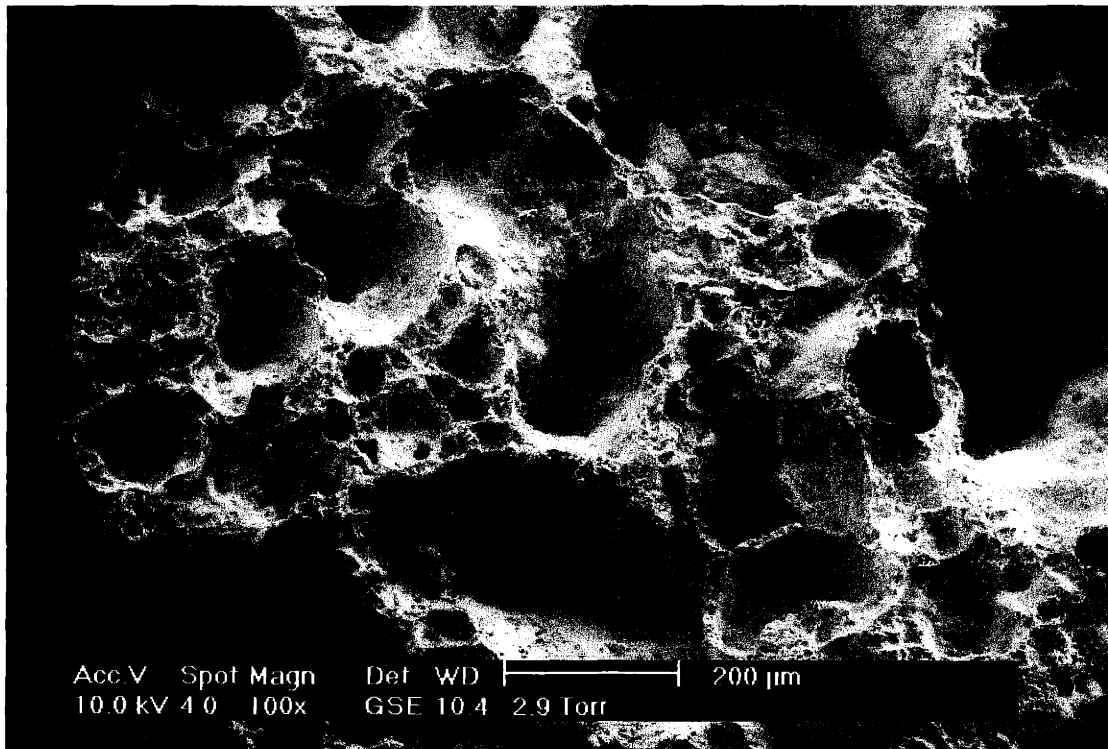


Figure 5.17. ESEM image of MIT No. 240 at a magnification of 100, Zone 4 on the interior surface. Even at broken sections through void wall, no platelets can be identified.

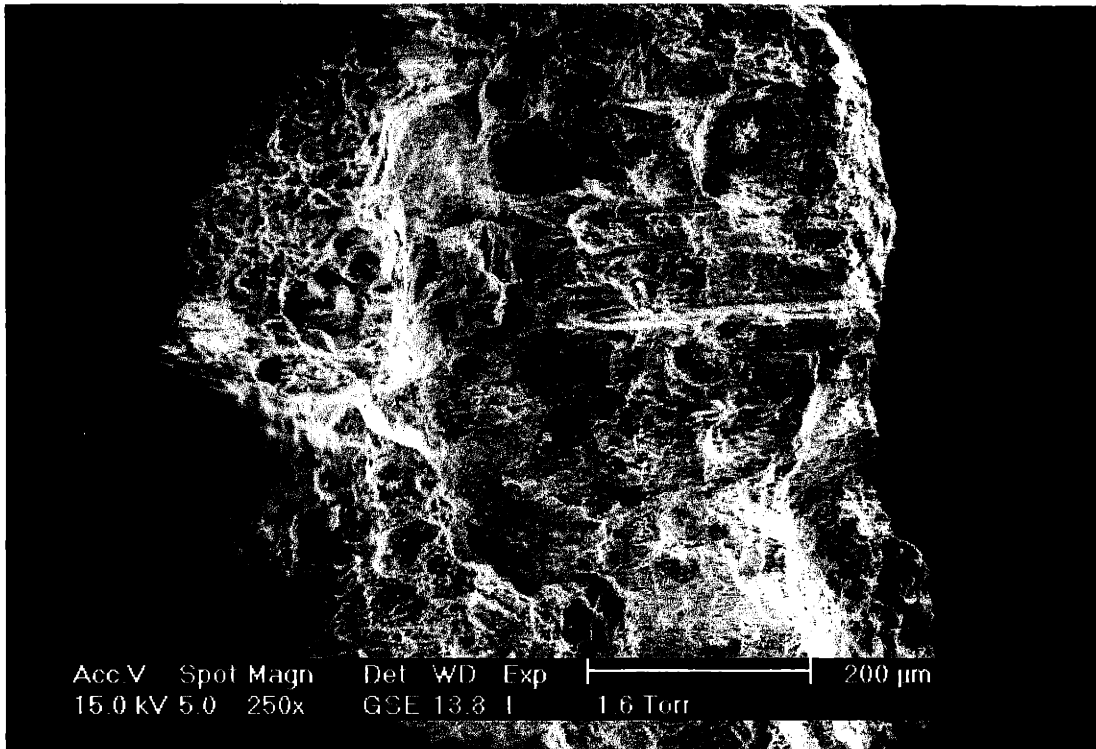


Figure 5.18. ESEM image of MIT No. 241 β at a magnification of 250. At interior surface, Figure 13 is a detail of this photomicrograph.

limited number and small size of Tal-i Iblis crucible sherds in the MIT collection required the use of this proxy.

5.2.1 Thin Section Analysis of Archaeological and Replica Crucibles

The compositional similarity between the ancient sherds and the modern replica was studied through petrographic thin section analysis. As defined here, composition similarity includes possessing a similar clay mineral type, mineral inclusion type, mineral inclusion abundance, and void abundance (porosity). Petrographic thin section analysis allowed me to address three of these points in detail, and the fourth will be addressed in sections 5.2.2 and 5.2.3. This analytical method focused on studying the minerals contained within the clay fabric and their abundance, as well as the porosity of the clay. In addition, I was able to compare the clay mineral type on a qualitative level by examining the optical activity of the clay.

Petrographic thin sections were constructed from four of the Iblis sherds (MIT Nos. 240, 241 β , 241 γ , 241 δ), the used experimental modern crucible (MIT No. 5279), and the modern replica

(MIT No. 5277), with the aim of performing point counting with a petrographic microscope. Of the four Iblis sherds, the point count data for two (MIT No. 240 and 241d) are shown in Table 5.2. The point count data for the modern replica are also shown in Table 5.2, however the data reported here are from the samples used in the re-firing experiments performed on the modern replica (these re-firing experiments are discussed in section 5.3.2). The point counts revealed that the mineral assemblages present in both the ancient and modern crucible fragments were remarkably similar.

The thin sections that underwent point counting were scrutinized at 1000 points over a regular interval as outlined in the last chapter. All thin sections contained large amounts of quartz and plagioclase feldspar. The point count data of Table 5.2 includes the minerals identified in the thin sections, their abundances, and the re-firing temperatures for the samples from the modern replica (MIT No. 5277). Samples 12D and 12+Sa were removed from ceramic briquettes constructed with clay from Patambo and Santa Cruz, Mexico. Sample S2-101 was removed from a ceramic vessel also constructed with clay from Mexico. These three thin sections were borrowed from Jennifer Meanwell, at MIT, to provide a distinctly different set of ceramic material as a control during point counting (Meanwell 2001).

Some graphical comparisons of the results of the point counts are shown in Figures 5.19 through 5.24. I have limited most of these plots to an analysis of quartz, plagioclase feldspar, clay matrix and voids. Figure 5.19 is the exception, and it shows a bivariate plot of the volume fraction of the clay matrix material versus the volume fraction of all mineral inclusions combined. The modern replica samples heated

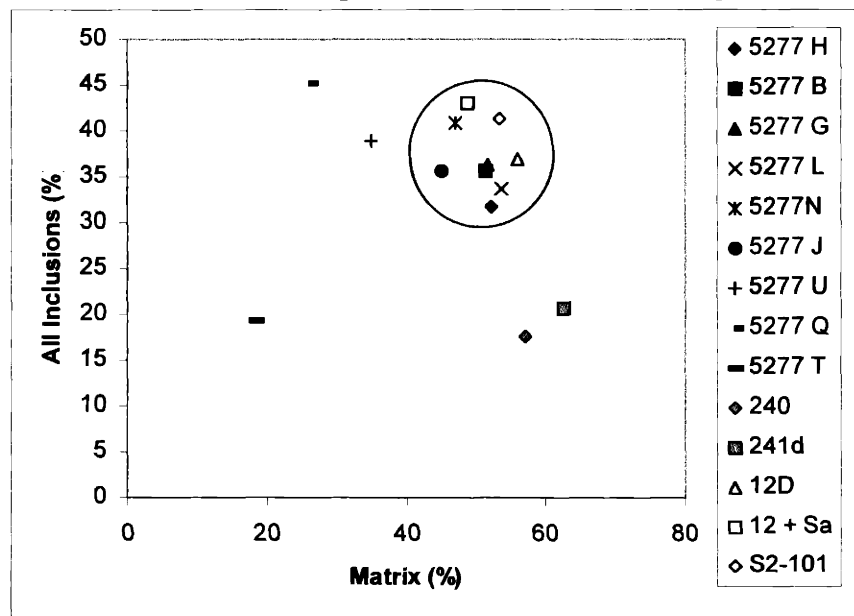


Figure 5.19. Bivariate plot of thin section mineralogy. Clay Matrix vs. All Inclusions

Table 5.2. Point count data for thin sections based on 1000 data points per sample (% Volume Fraction)

number	Temp. (°C)	Clay	Voids	Quartz	Plagioclase	Amphibole	Biotite	Opaque	Basalt	Calcite	Pyroxene	Muscovite	Fe-rich	Other	Total Inc
	No heat treatment	52.1	16.1	6.3	6.2	0.8	3	1.8	4.4	6.2	0.6	0.8	1.7	0	
	500	51.2	13.1	10	8.2	1	2.5	1	7.9	3.8	0.3	0.5	0.5	0	
	700	51.5	12.3	9.1	6.1	0.8	3.4	1.2	7.4	6.8	0.6	0	0.7	0.1	
	1000	53.7	12.5	9.3	8.3	0.7	4.5	0.8	7.3	0	0.3	0.4	2.2	0	
	1100	47	12.2	13.7	14.9	0.8	2.9	0.7	5.4	0	1.2	0.1	1.1	0	
	1125	45	19.3	11.2	16	0.1	1.3	1.1	5.2	0	0.1	0	0.7	0	
	1150	34.9	26.1	10	17.2	0.3	0	1.6	7.1	0	0.5	0	1.9	0.4	
	1175	26.1	28.7	10.5	23.2	0.9	0	3.4	5.7	0	1.5	0	0	0	
	1200	18.3	62.3	4	11.4	0.1	0	1.5	2	0	0.3	0	0.1	0	
	Tal-i Iblis	57	25.3	8.1	3.6	0.2	1.5	1.7	2	0	0	0	0.6	0	
	Tal-i Iblis	62.4	17	5.9	8.3	0.4	2.3	0.8	1.4	0	0.4	0	1.1	0	
	Mexico 950	55.9	7.1	22.9	7.1	0	0.9	0.2	0	0.5	0	0	5.4	0	
	Mexico 700	48.7	8.2	29.7	9.7	0.2	0.3	0.1	0	1.2	0	0	1.9	0	
	Mexico	53.2	5.6	21.4	7.7	0	1.1	1.1	6.7	0.7	0	0	2.2	0.3	

to 1150°C, 1175°C and 1200°C (MIT Nos. 5277U, 5277Q and 5277T respectively) have larger void sizes due to their higher re-firing temperature⁵, and therefore are not contained within the cluster. The Tal-i Iblis sherds (MIT Nos. 240 and 241d) also are not contained within the cluster

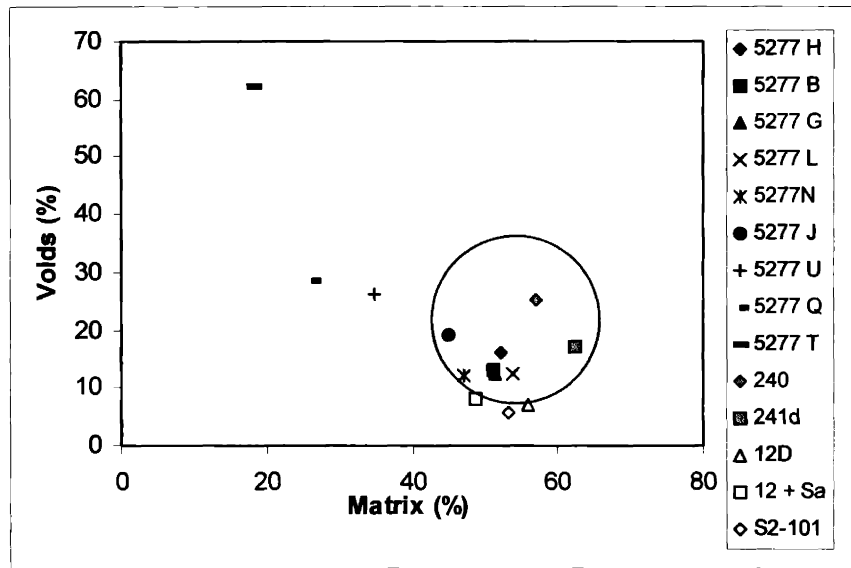


Figure 5.20. Bivariate plot of thin section mineralogy. Clay Matrix vs. Voids

because overall they have fewer mineral inclusions than the modern replica (the implications of this will be discussed in the next chapter, section 6.3). However, in all of the remaining bivariate plots, MIT Nos. 240 and 241δ fall within the main cluster of data points. In Figure 5.20 all samples cluster except for three, the modern replica samples that were exposed to the highest heat treatments.

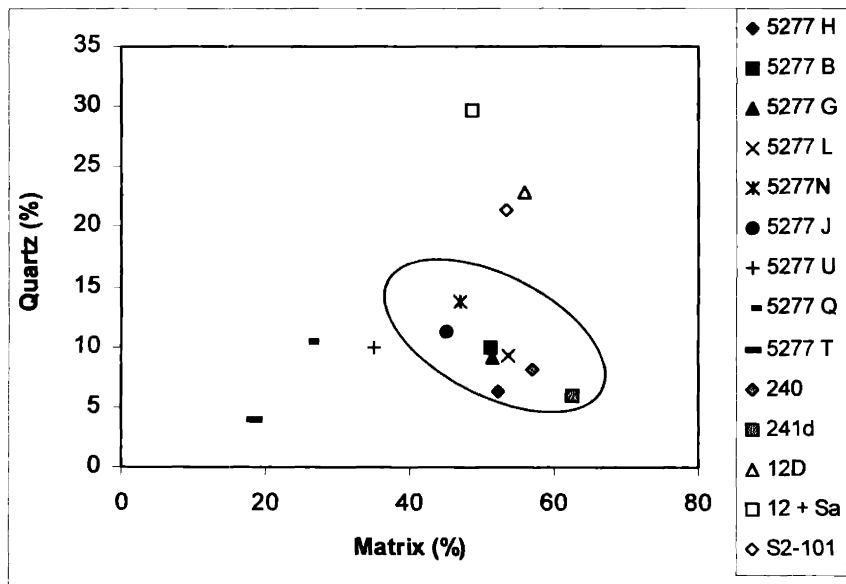


Figure 5.21. Bivariate plot of thin section mineralogy. Clay Matrix vs. Quartz

These same three samples are again separate from the main cluster in Figures 5.21 and 5.22. In addition, the samples from Mexico are distinctly different from the main clusters in Figures 5.21, 5.23, and 5.24.

The consistent outliers in these plots are the three high-fired samples (1150°C,

⁵ Heating a ceramic to higher temperatures causes densification of the material and therefore a decrease in the porosity (Kingery 1976:469; Rice 1987:351); however, these re-fired samples exhibited an apparent increase in porosity due to the densification of the matrix and an accompanying expansion of the pores.

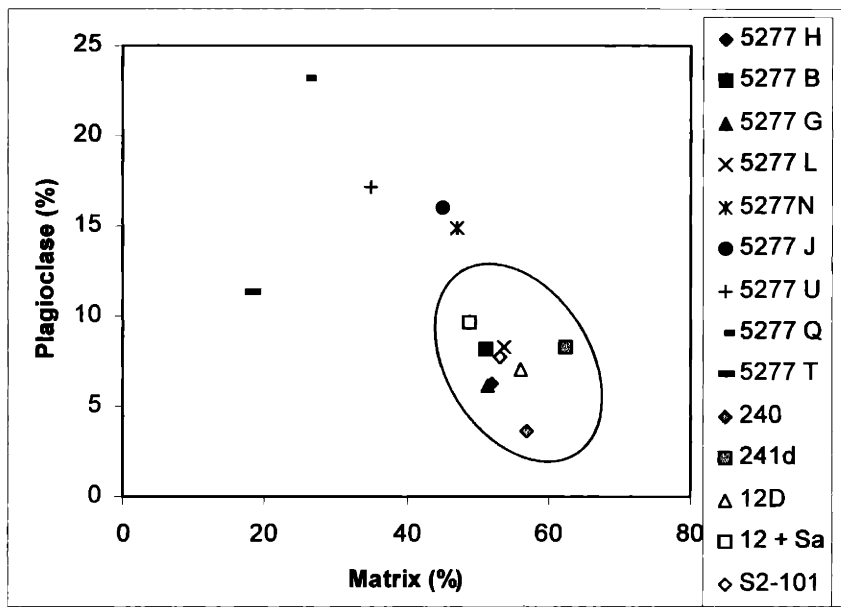


Figure 5.22. Bivariate plot of thin section mineralogy. Clay Matrix vs. Plagioclase

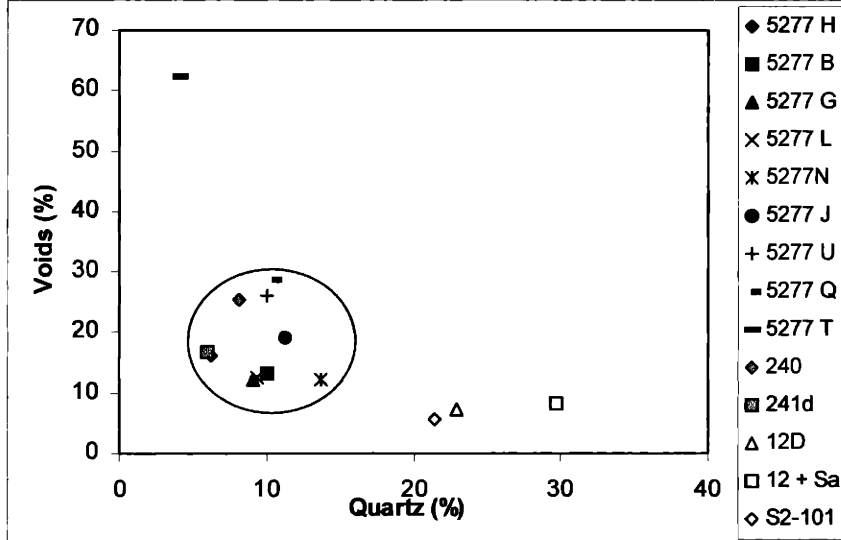


Figure 5.23. Bivariate plot of thin section mineralogy. Quartz vs Voids

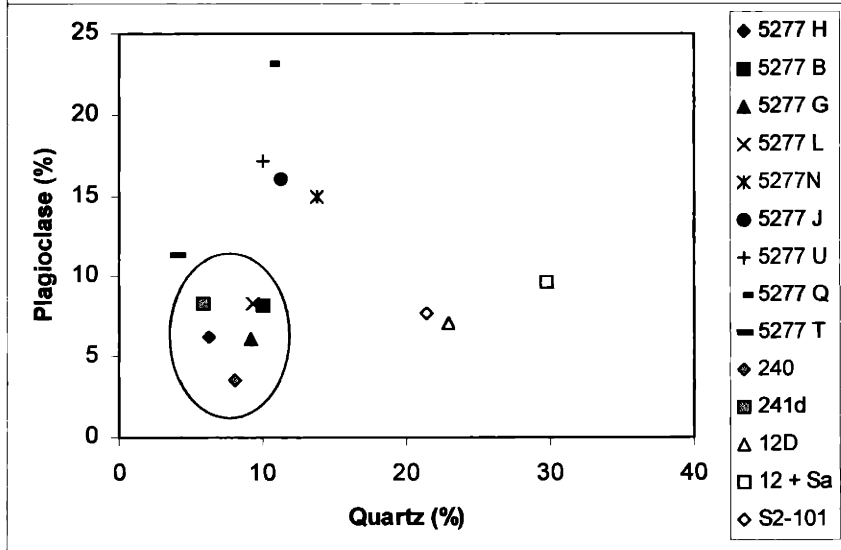


Figure 5.24. Bivariate plot of thin section mineralogy. Quartz vs. Plagioclase

1175°C and 1200°C), and the three Mexican samples. The tight clusters that are shown in Figures 5.20-23 each include the ancient sherds and the samples re-fired at lower temperatures. These data together with the data presented in Table 5.2 provide strong evidence for the similarity in type and abundance of the minerals in both the ancient and modern replica crucibles. However, this similarity in the mineralogy of the ceramic inclusions, does not translate to similarity in the clay mineral type of the ceramic materials. Therefore, additional analytical methods are necessary to establish the parallel between the thermal properties held by the ancient and modern crucibles. These methods included X-ray diffraction and bulk chemical analysis.

5.2.2 X-Ray Diffraction (XRD) of Archaeological and Replica Crucibles

X-Ray diffraction analysis was performed on one Iblis sherd (MIT No. 241β) and the modern replica (MIT No. 5277). Samples from both of these artifacts taken from the most homogenous regions (Zone 2 of MIT No. 241β; all of MIT No. 5277 consisted of similar material) were ground into a fine powder. The resulting spectra reveal remarkable similarities between the chemical compositions of these two clays. Figures 5.25 and 5.26 reproduce the spectra obtained from slow scans of MIT Nos. 241β and 5277. Many of the differences between these two spectra are likely due to different orientations of the crystals and to the different thermal histories of the artifacts (MIT No. 5277 was probably only fired once at a low temperature, whereas MIT No. 241β was used in a high-temperature metallurgical process). Most of the spectral peaks reveal the mineral constituents of the clay and have been identified as quartz, pyroxene (augite and diopside) and plagioclase feldspar (albite and anorthite); however there are some unidentified peaks (indicated as peaks A, B and C on the spectra). I believe that these peaks represent the clay phase present in the samples as distinct from the mineral inclusions in the clay. Figure 5.27 shows some spectra of common clay types. Based on the comparison of these spectra with the XRD spectrum obtained from the scan of the crucible replica sample (MIT No. 5277), I believe that the clay used for the modern sample is an illite/smectite mixture. Illite clay mixtures are commonly found in environments with high mica content and with many shales, mudstones and limestones (Deer et al. 1966:263).

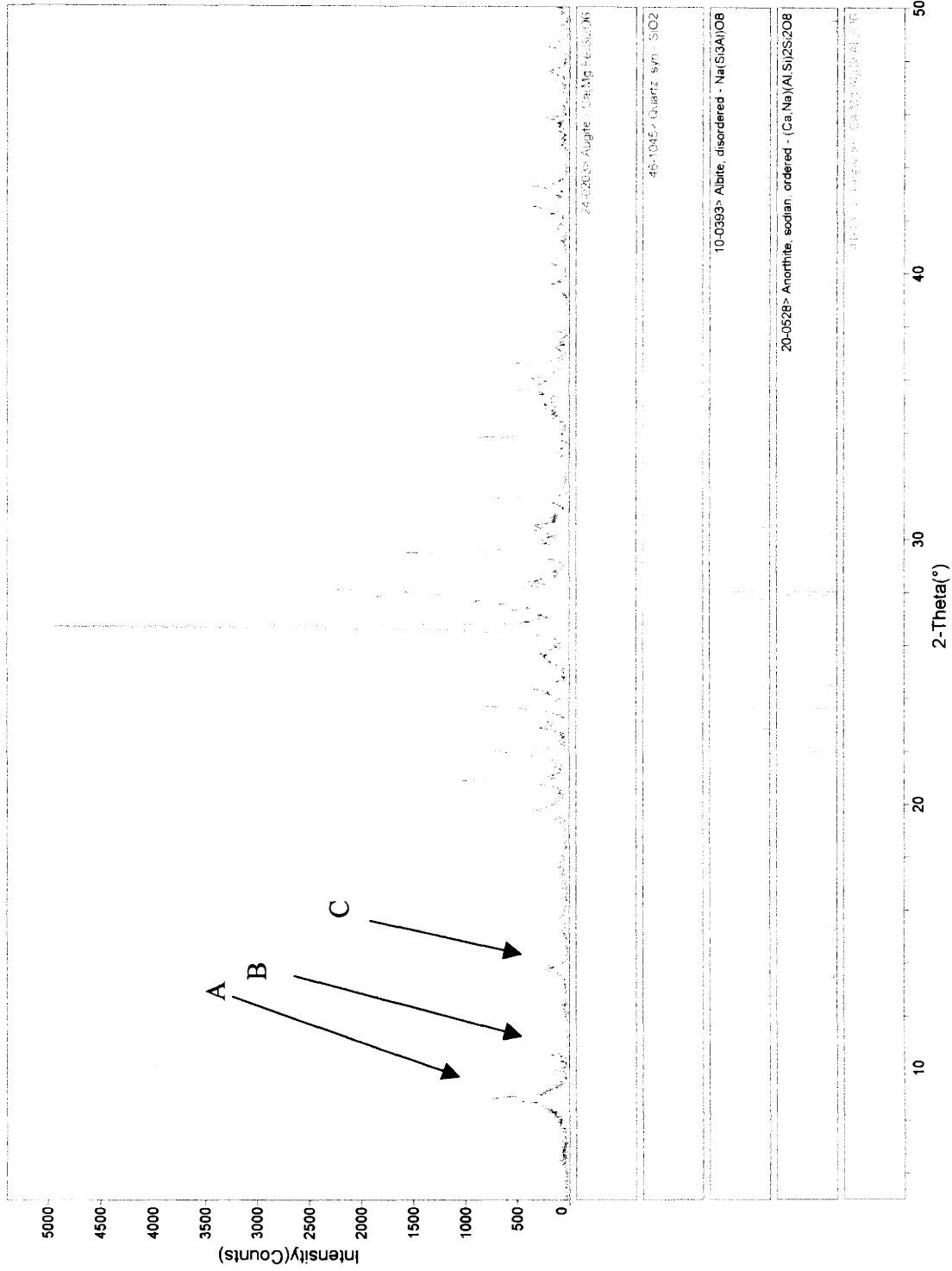


Figure 5.25. XRD spectrum of MIT No. 5277 (Modern crucible replica).

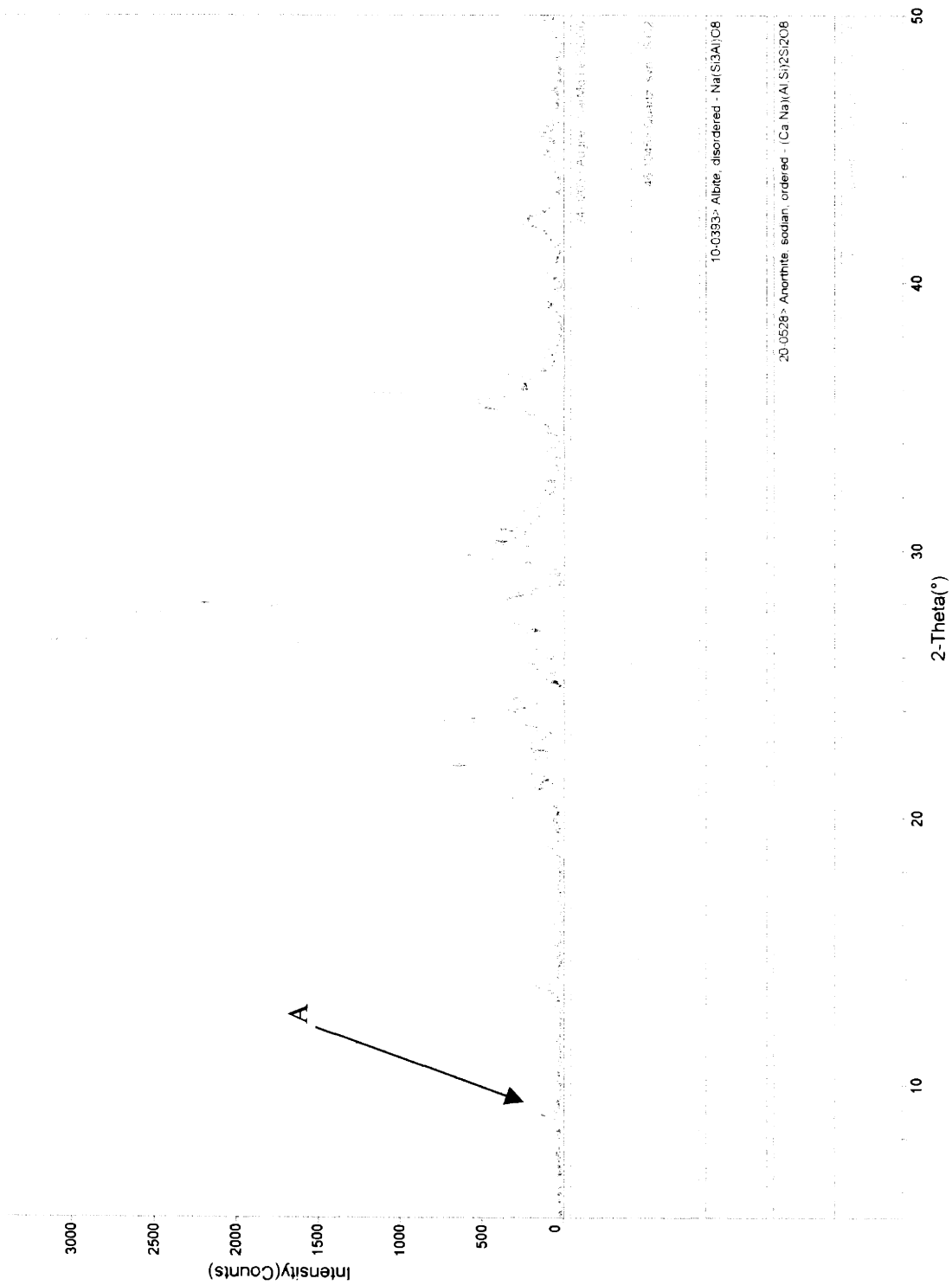


Figure 5.26. XRD spectrum of MIT No. 241 β (Tal-i Iblis crucible)

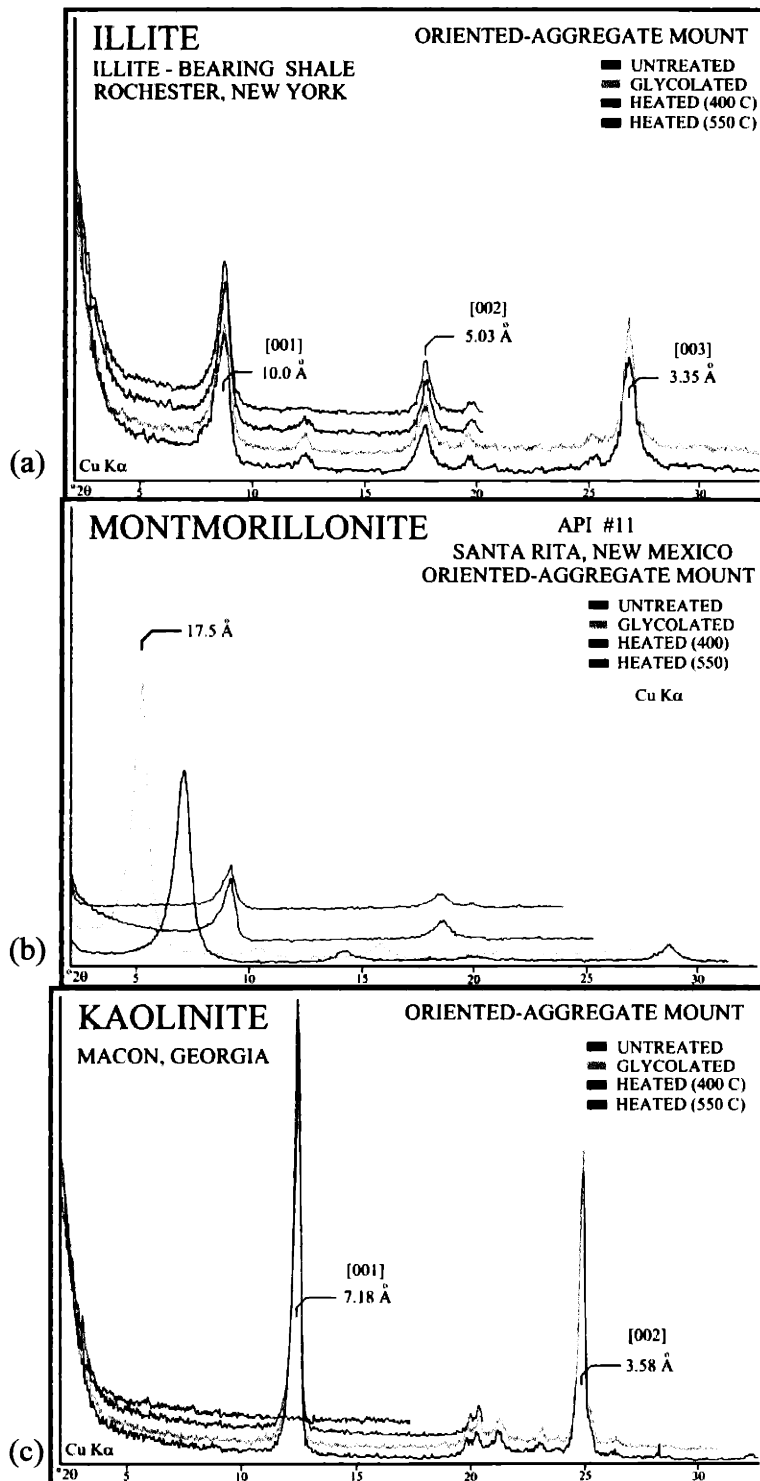


Figure 5.27. X-ray diffraction spectra for common clay types. (a) illite of the illite group; (b) monmorillonite of the smectite group. Notice the shift in the initial peak at 2θ value of 7 when the sample is heated to 400°C . This peak is also greatly diminished when the clay is heated; (c) kaolinite of the kaolinite group.

Smectites form from volcanic rocks (tuffs and ash), from calcium- or sodium-rich deposits, and are common in soils mixed with illites weathered from basic rocks in poor drainage environments (Deer et al. 1966:268).

The geological environment of the Kerman Province and that of the area immediately surrounding Tal-i Iblis is reproduced in the geological map in Figure 5.28. The area surrounding Tal-i Iblis consists of secondary sedimentary deposits of mud, clay and sand. There are neighboring outcrops of volcanic tuffs, shale, and limestone. These surroundings would provide a good environment for the paragenesis of illites and smectites.

Table 5.3. Bulk chemical analysis of Zones 1 and 2. (wt%) (Original data can be found in Appendix B, protocol can be found in Appendix C)

SAMPLE #		SiO ₂	Al ₂ O ₃	Fe ₂ O ₃	FeO	MnO	MgO	CaO	Na ₂ O	K ₂ O	TiO ₂	P ₂ O ₅	LOI	LOI2*	TOTAL2*	TOTAL
		%	%	%	%	%	%	%	%	%	%	%	%	%	%	%
MIT 5274-1	Ancient	52.54	15.78	5.04	1.08	0.123	3.21	6.54	2.07	2.92	0.609	0.31	9.10	9.22	99.43	99.43
MIT 5277-1	Replica	55.29	15.13	5.30	-0.01	0.107	3.04	8.26	2.64	2.22	0.587	0.22	5.99	5.99	98.79	98.79
MIT 5277-2	Replica	55.12	15.32	4.87	0.36	0.109	3.04	8.29	2.63	2.16	0.578	0.20	6.03	6.07	98.76	98.76
MIT 240-1	Ancient	56.08	17.97	6.33	0.83	0.150	3.76	6.97	2.16	2.78	0.657	0.25	1.95	2.04	99.96	99.97
MIT 241β-1	Ancient	58.21	17.43	4.18	2.16	0.129	3.34	7.57	2.14	2.54	0.665	0.25	0.20	0.44	99.05	99.05
MIT 241δ-1	Ancient	55.39	17.76	5.23	1.00	0.131	3.22	7.62	2.09	2.63	0.650	0.26	2.60	2.71	98.71	98.71
MIT 241ε-1	Ancient	55.81	18.03	5.32	1.44	0.141	3.51	7.66	1.88	2.47	0.643	0.26	1.39	1.55	98.71	98.71
MIT 241η-1	Ancient	57.25	17.46	4.76	2.01	0.141	3.44	6.72	2.10	2.48	0.661	0.32	0.96	1.19	98.53	98.53
MIT 245-1	Ancient	54.99	17.46	5.51	1.24	0.149	3.73	8.20	2.20	2.48	0.640	0.27	1.65	1.79	98.66	98.66

*LOI2 and Total2 correspond to Fe₂O₃.

SAMPLE #		Ba	Sr	Y	Sc	Zr	Be	V
		ppm	ppm	ppm	ppm	ppm	ppm	ppm
MIT 5274-1	Ancient	367	475	16	17	118	2	123
MIT 5277-1	Replica	427	699	14	13	116	1	105
MIT 5277-2	Replica	427	690	15	13	115	2	106
MIT 240-1	Ancient	387	429	18	20	116	2	140
MIT 241β-1	Ancient	423	507	17	18	132	2	133
MIT 241δ-1	Ancient	401	556	17	17	118	1	126
MIT 241ε-1	Ancient	398	508	17	19	118	2	137
MIT 241η-1	Ancient	407	498	17	19	137	2	137
MIT 245-1	Ancient	362	446	18	19	122	2	113

Analysis provided by Activation Laboratories Ltd.

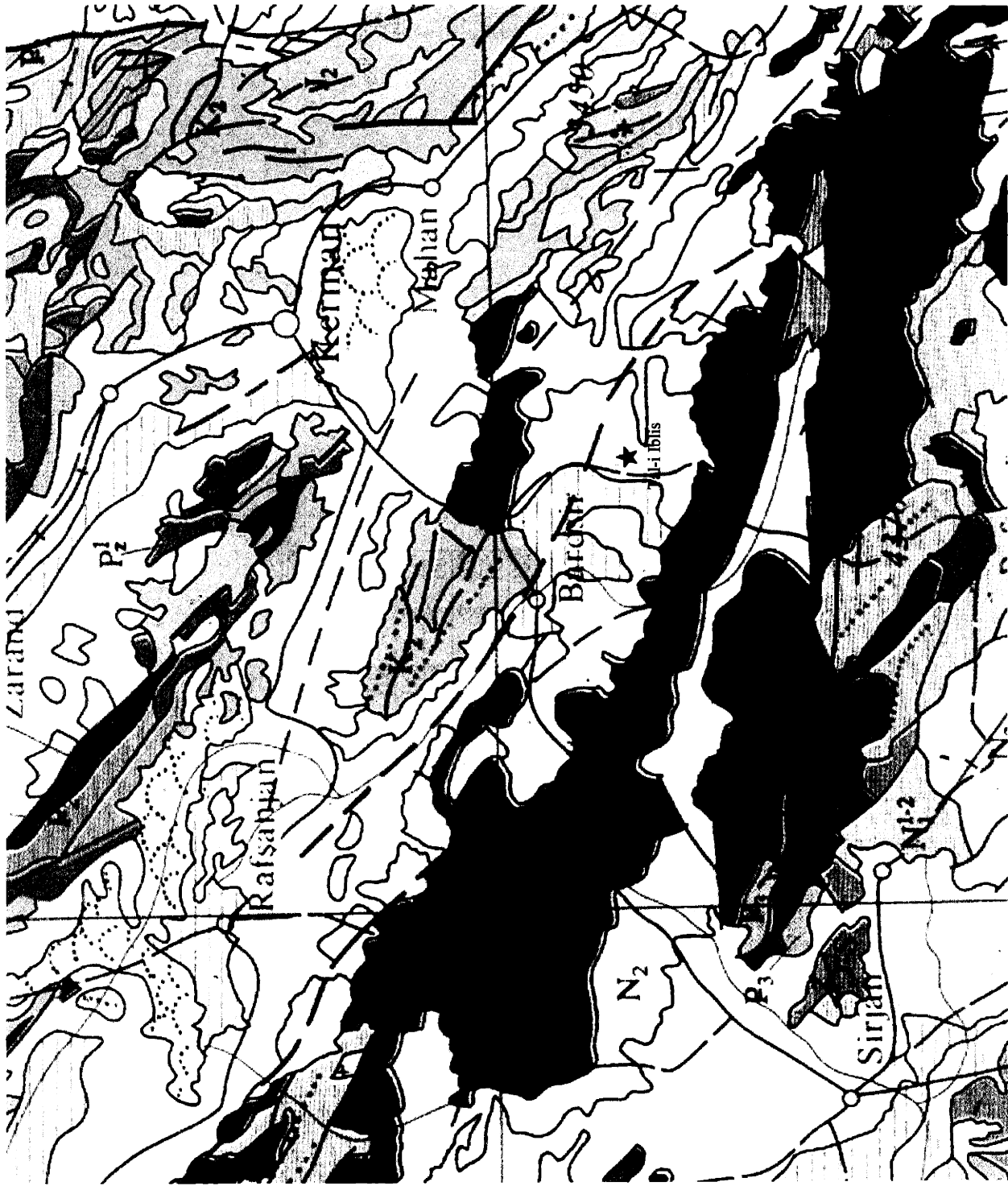

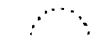


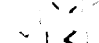

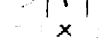
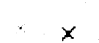
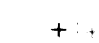



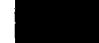









Figure 5.28. Geological map of area surrounding Tal-I Iblis. (Haghipour and Aghanabati 1985)

Key:

-  Kavir (Salt Desert)
-  Sand Dunes
-  Volcanic Tuff
-  Lava and Tuff
-  Intrusive
-  Extrusive
-  Intermediate
-  Acid
-  Ophiolitic melange
-  Kavir Deposits-Playa type: sl, m, cl, st
-  Coastal Deposits: s, m, cl, ml, cg
-  Neogene-Quaternary Red Beds: ep, ml, ss/cg/v
-  Makran F.: cl, ml, st, s, shelly ls, cg, ss, st, sh
-  Terraces and volcanics: g, v
-  Chahar Gonbad F: ls, ss, ml, cg, v,
-  Lower Red F.: sh, ml, ss, gy, cg, v
-  Alimoradi F.: v, ls, cg
-  Nummultic Series: ss, sh, ml, ls; and Volcanics, flysch
-  Marl: ls, ss, cg
-  Kerman Conglomerate: cg, ss

Orbiolina Limestone; Cretaceous red beds: cg, ss, sh, ml; Biabanak Shales

Upper Jurassic Salt F.: sl, gy, sh, ls; Red Terristic F.: ss; Pectinid Limestone and Gypsum Facies: ls, ml, gy; Garedu Red Beds: ss, sh, cg, ls

Baghamshah F.: sh, ss, ml

Abadeh Upper Triassic: ls, sh

Nakhlak Group: ls, sh, cg, ss

Abedeh Lower Triassic: ls, ss, sh

Bahram Limestone: ls, sh, dl; Padcha F.: ss, dl, gy/b, sh, cg, ls, sts; Sibzar Dolomite

Niur F.: ls, ss, sh

Gushkamar Group

Abbreviations: b-basalt, cg-conglomerate, cl-clay, dl-dolomite, ep-evaporite, g-gravel, gy-gypsum, ls-limestone, m-mud, ml-marl, s-sand, sh-shale, sl-salt, ss-sandstone, st-silt, sts-siltstone, v-volcanic

5.2.3 Bulk Chemical Analysis of Archaeological and Replica Crucibles

The Tal-i Iblis crucible clay was also compared to the clay of the modern replica through bulk chemical analysis. The method used for this analysis was ICP-OES (see Appendix B for original data and standards, see Appendix C for protocol). The results of this analysis are shown in Table 5.3. All of the sherds are similar in composition with main constituents of SiO₂, Al₂O₃, CaO, Fe₂O₃, MgO, K₂O, and Na₂O in their order of relative abundance.

5.2.4 Dissimilarities between modern replica and ancient sherds

The data presented in this section provide evidence for the similarity between the modern replica crucible (MIT No. 5277) and the ancient sherds from Tal-i Iblis. However, there are a few dissimilarities that should be addressed. These include differences in porosity, overall mineral inclusion abundance, and the XRD spectra for MIT Nos. 5277 (modern replica) and 241β.

The samples from the modern replica contain fewer voids on average (17.5%) than the average of two of the Iblis sherds (MIT No. 241δ and 240) (21.2%). This difference in porosity no doubt affects the thermal conductivity of the ceramic material (as will be discussed in section 6.2). However, the standard deviation for volume fraction of voids in both the modern replica and the ancient sherds is high (see Table 5.4). For the modern replica samples this large variation in pore density is due to the heat treatments the samples received; for the ancient sherds, it is due to the problem of point counting across zones in the section of the sherd that reached different temperatures when the crucible was used. This means that there is no one porosity that represents the

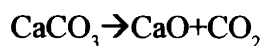
Table 5.4. Porosity of Tal-i Iblis crucible sherds and modern crucible replica.

MIT No.	Porosity (%Vol. Fraction)	Standard Deviation	Comments
5277	18.3	6.7	This is an average of all re-fired samples, with the highest and the lowest values of porosity discarded.
241β & 240	21.15	5.9	This is an average of tow ancient sherds.

characteristics of all zones of any one Iblis crucible sherd. It also means that at least some of the modern replica sherds (e.g. the samples heated to temperatures in the range of 1125-1175°C) possess the same volume fraction of voids that is present in the ancient sherds. In addition, the re-firing experiments were designed to allow inspection of the changes occurring in the ceramic fabric of the replica itself, not in the transfer of heat across the ceramic sample. Consequently, the differences in thermal conductivity that may result from different pore densities are not a concern when justifying the validity of the re-firing experiments. The presence of these pores, however, are important insofar as the changes in their *morphology* can be used to estimate the temperature reached by the crucible. Pore shapes reflect the alterations occurring in a ceramic material as a result of increases in temperature.

A second dissimilarity between the ancient sherds and the modern replica can be found when comparing the total volume fraction of mineral inclusions in each thin section. The thin sections constructed from the samples of the modern crucible replica contained slightly more mineral inclusions overall than did those from the ancient crucible sherds. For our purposes, similarity in the type of minerals is more important than similarity in the abundance of inclusions, for many reasons. First, if the same types of minerals are present in both the ancient sections and in the modern replica, morphological changes occurring in these minerals can be compared in the two sets of samples. Second, the presence of the same types of minerals in both sets of samples (modern replica samples and ancient sherds) could indicate a similarity in the paragenesis of the clays or possibly even establish that the same source of clay was used for both the ancient and replica crucibles. It should be noted, however, that clay sources are easily manipulated by the environment and could change drastically over a period of six thousand years. In addition, clays are so ubiquitous with so much variation that distinguishing between clay sources is very difficult (Neff 2000:81). Furthermore, within even a single clay source, the variation in the concentration of mineral inclusions can vary tremendously. A third reason supporting the importance of mineral type over mineral inclusion abundance in the ceramic material is that the effect of heat will alter certain minerals, causing the clay composition to change. Calcite provides an example of this. When calcite is

heated to above 850°C (this temperature varies depending on the time and atmosphere of the heating application) it decomposes to form lime and carbon dioxide:



The lime can react with both the vessel and the environment to change the chemistry of the ceramic. For these reasons, the analysis of the thin sections was focused largely on mineral inclusion type rather than on overall mineral abundance.

A final dissimilarity between the data for the ancient crucible sherds and the modern crucible replica lies in their x-ray diffraction analyses. The peaks from the spectra created through slow scans of the modern replica and one ancient crucible are slightly different. In fact, some of the peaks found in the spectrum for the modern crucible replica are missing in the spectra for the ancient sherds. This is explained by the fact that the clay undergoes crystalline transitions when heated above 600°C. These transitions are both minor (resulting in shifted peaks on an XRD spectrograph) and major (resulting in the disappearance of peaks on an XRD spectrograph). In the former case, these changes, studied by others (USGS), and are presented in Figure 5.27.

All of these dissimilarities are products of natural, expected, and inconsequential variations in the ceramic material. Although the ancient crucible sherds and the modern crucible replicas are not identical, they are adequately analogous for the purposes of this study.

5.2.5 Summary

The close similarity between the ceramic fabric of the ancient sherds and the modern replica was established through petrographic thin section analysis, x-ray diffraction, and bulk chemical analysis. Because the modern and ancient sherds are similar, it was feasible to perform re-firing experiments on samples of the modern replica crucible. The aim of these experiments was to determine changes in the chemistry and microstructure of the modern crucible replica as samples from this object were heated under a controlled regime of temperatures and environment. These changes could later be correlated with the chemistry and microstructure observed in the Tal-i Iblis crucibles to establish the temperatures to which the sherds were heated.

5.2.5 Thermal Analysis

The temperatures to which the Tal-i Iblis sherds were heated during their use were determined through Differential Thermal Analysis (DTA) as well as by a series of re-firing experiments. DTA was used to develop an estimate of the temperature at which the fabric of the ancient sherds slumped. The re-firing experiments provided samples of the modern crucible replica that were heated within that temperature range. These samples were used for both macroscopic and microscopic evaluation and to study morphological changes in the ceramic material as a function of temperature. As mentioned in section 5.2, the chemical composition of the modern crucible replica is similar enough to the chemical composition of the ancient sherds that it could be used as a proxy for the Tal-i Iblis sherds in the re-firing experiments. Because the study corpus included so few artifacts from Tal-i Iblis, I did not attempt to use the Tal-i Iblis sherds for the re-firing experiments.

5.3.1 Differential Thermal Analysis of Tal-i Iblis and Modern Replica Sherds

As mentioned in the previous chapter, a dip in the DTA curve represents an endothermic reaction and a peak in the curve represents an exothermic reaction. Figure 5.29 is a hypothetical DTA curve showing the main reactions that occur in pottery during a heating cycle of 0-1000°C (Tite 1972:296). Only those reaction temperatures will appear on an experimental DTA curve that occur above the final temperature to which the ceramic was heated. Therefore, DTA can be a

Table 5.5. Morphological changes predicted for a ceramic as a function of temperature (Tite 1972:296).

Temperature (°C)	Peak type on DTA curve	Morphological change
100-200	Endothermic	Loss of absorbed water
250-500	Exothermic	Combustion of organic material
600	Endothermic	Loss of chemically combined hydroxyl water
750	NA	Hornblende transforms from green to brown (Rice 1987:431)
825	Endothermic	Decomposition of calcite
950	Exothermic	Formation of high temperature minerals

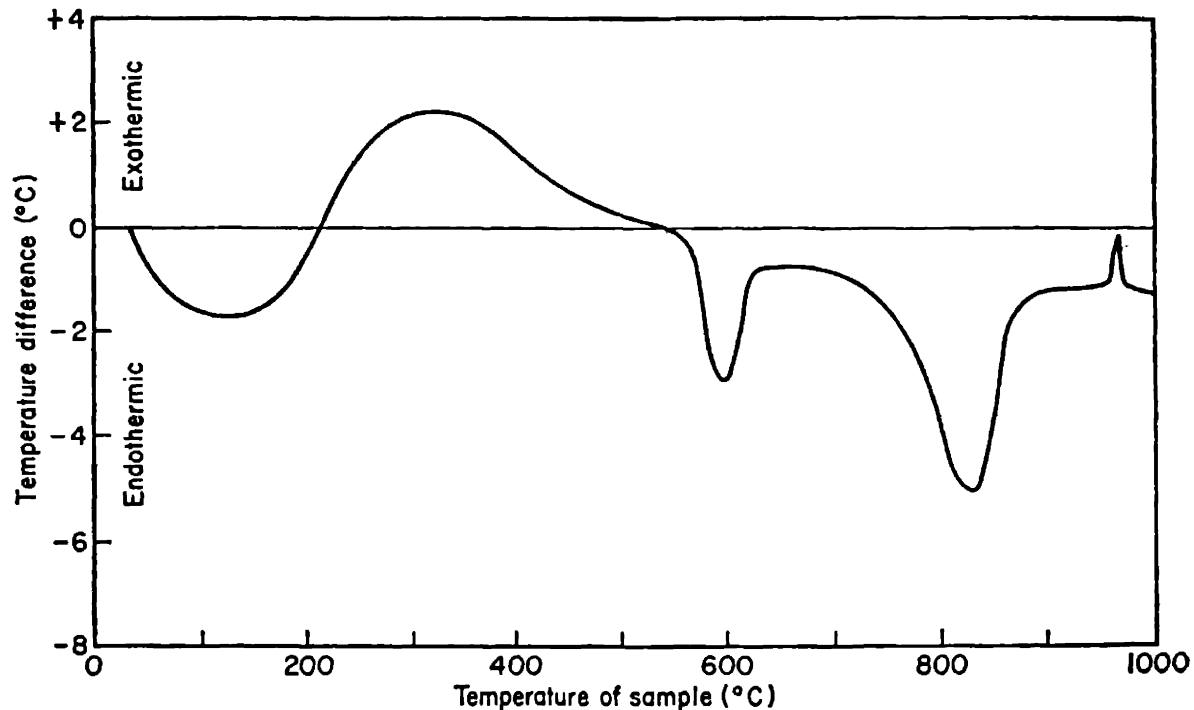


Figure 5.29. Hypothetical DTA curve for ceramic material over the range of 0-1000°C (Tite 1972:296)

useful method for determining a range of temperatures over which the ceramic was originally fired or heat-altered. These predicted temperatures are summarized in Table 5.5. However, if the ceramic reached a temperature above these reaction temperatures, the only determinants one can obtain from DTA are the slumping and melting temperatures of the material. Slumping and melting of the ceramic material appear as endothermic peaks for all ceramic materials.

I sampled Zones 1 and 4 of an Iblis sherd (MIT No. 240) and compared the results to (1) an analysis of the modern replica vessel that was later used in the re-firing experiments (MIT No. 5277) and (2) a fragment of a modern replica vessel (MIT No. 5279) used at Tal-i Iblis in an ore smelting experiment at the site (Pleiner 1967). Figures 5.30-33 present the DTA curves for these artifacts. Figure 5.30 shows that for the modern replica (MIT No. 5277), the decomposition of calcite occurred at approximately 780°C and slumping occurred at about 1180°C. One can see in Figure 5.31 that Zone 1 of the Iblis sherd (MIT No. 240) slumps at around 1150°C. The curves for Zone 4 in both Iblis (MIT No. 240; Figure 5.32) and the used experimental modern replica (MIT No. 5279; Figure 5.33) also show a slumping temperature of approximately 1150°C.

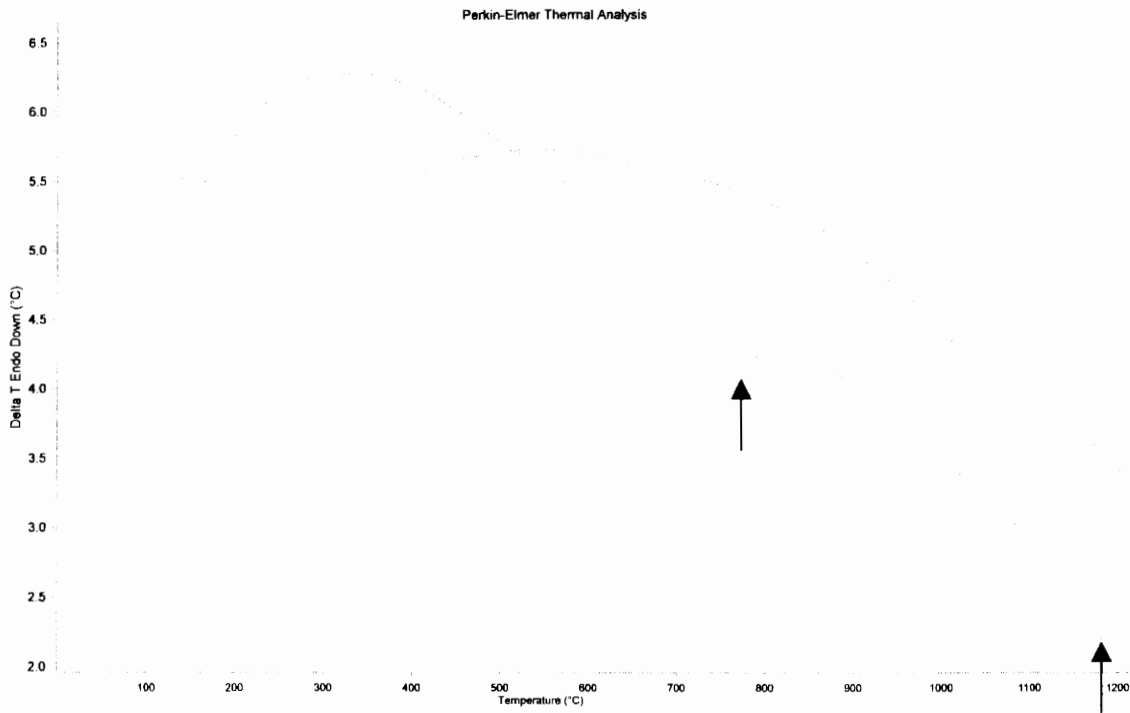


Figure 5.30. DTA curve for modern replica (MIT No. 5277); arrows indicate loss of calcite and slumping temperature.

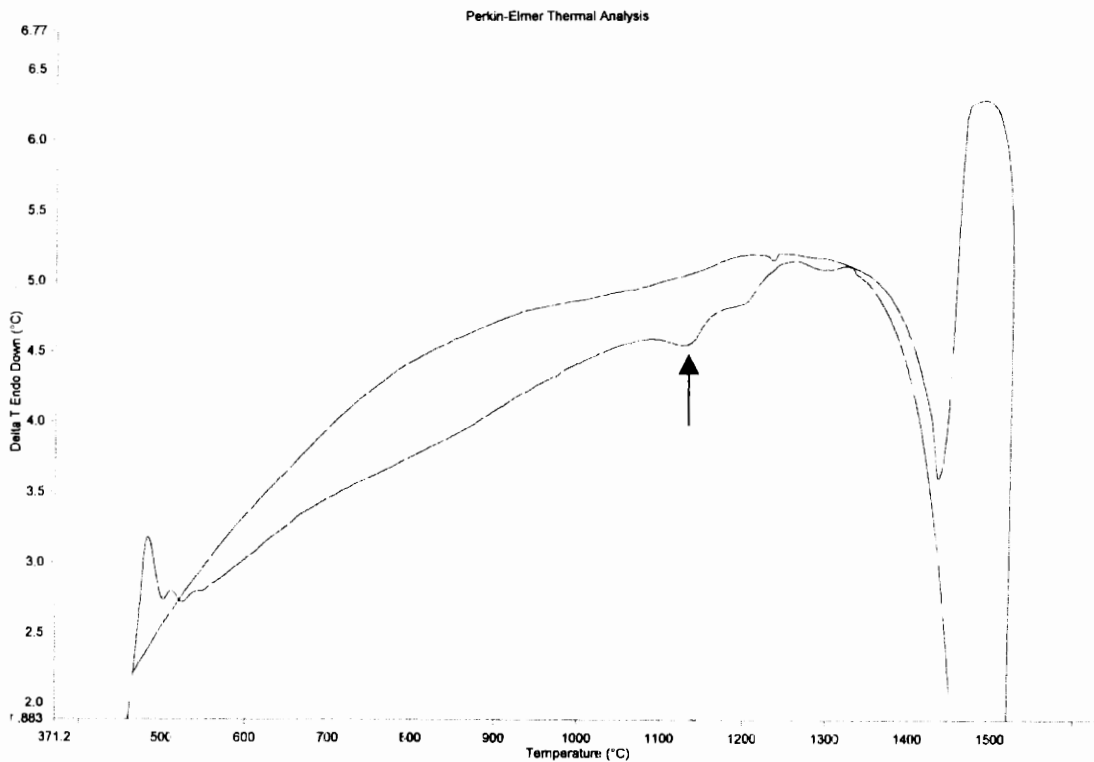


Figure 5.31. DTA curve for Zone 1 of Iblis crucible (MIT No. 240); arrow indicates slumping temperature.

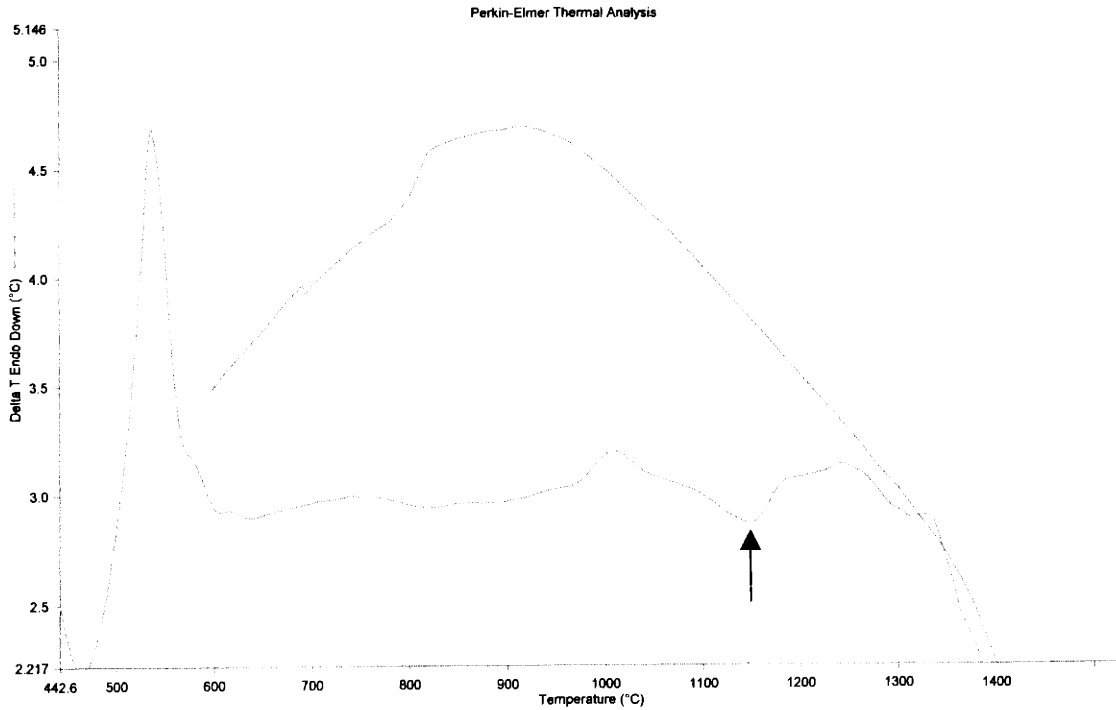


Figure 5.32. DTA curve for Zone 4 of Iblis crucible (MIT No. 240); arrow indicates slumping temperature.

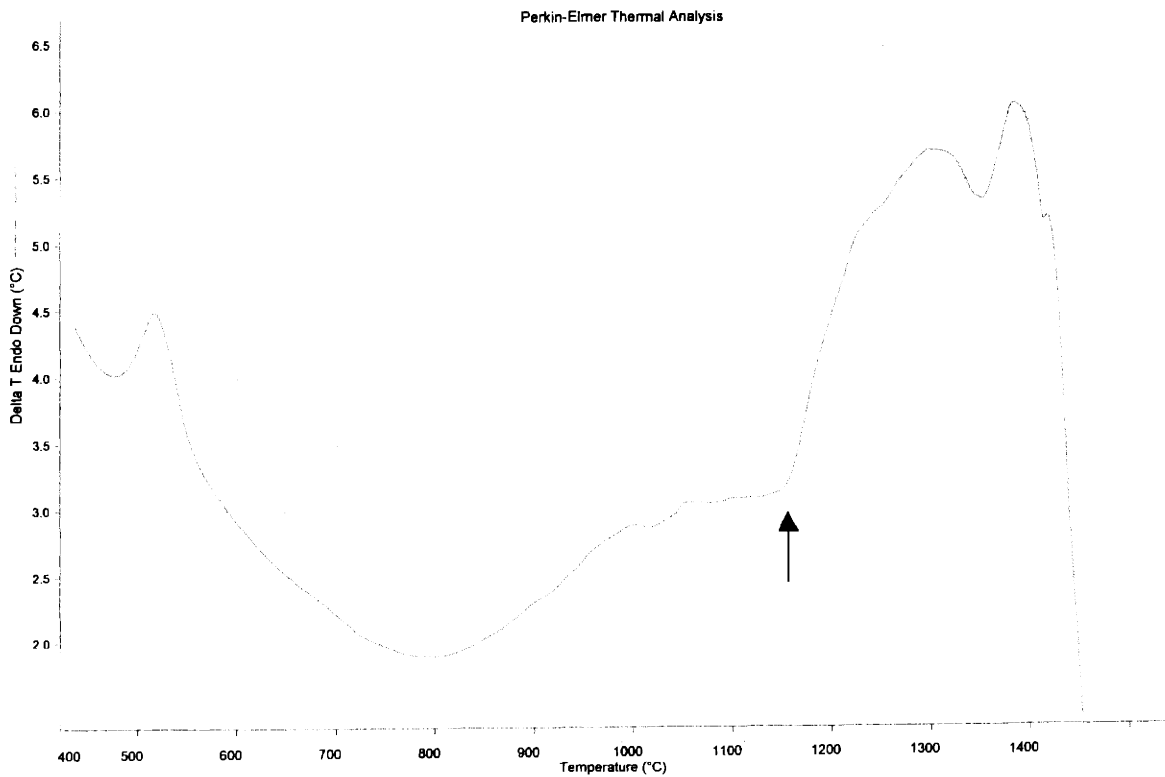


Figure 5.33. DTA curve for sherd of experimental modern crucible replica (MIT No. 5279); arrow indicates slumping temperature.

5.3.2 Re-firing Experiment using Modern Replica Crucible (MIT No. 5277)

I designed the re-firing experiments so that they would allow me to examine the morphology of the ceramic material as it was altered at different temperatures. I cut cubic pieces measuring approximately 1-2cm on a side from the modern crucible replica and re-fired the samples to 12 successively higher temperatures all of which were within the range of temperatures determined by DTA. All of these re-fired samples are shown in Appendix A. There were many macroscopic changes that occurred during heating; all of the changes noted are summarized in Table 5.6. The grey carbon-rich zone in the interior of the walls (discussed in section 5.1.1) disappeared upon firing to 700°C. At 1000°C the ceramic was significantly less powdery; above this temperature there were macroscopic changes in the color and shape of the fired samples. At 1125°C the ceramic began to darken in color, and by 1150°C it was uniformly grey. At 1175°C the ceramic began to vitrify, and at 1200°C it had fully slumped. Figure 5.34 shows these morphological changes for some of the re-fired samples. This visual verification for the slumping temperature reinforced the DTA estimate of 1180°C for a slumping temperature. Nonetheless, further investigations were necessary to document more precisely the temperatures reached at locations along the cross-section of the ancient sherds.

Thin sections were made from the modern replica samples heated to 500°C, 700°C, 1000°C, 1100°C, 1125°C, 1150°C, 1175°C, and 1200°C and including an unheated sample. With the aid of mineralogical references (Rice 1987; Tite 1972; Obstler 1996; Deer et al. 1966) I identified the mineral inclusions of these ceramic samples and performed point counts to determine the volume fraction of the minerals in each thin section. The point count data are presented in section 5.2.1. After thoroughly investigating these samples (see Figure 5.35a-n), I discovered that in addition to macroscopic morphological changes, there are microscopic morphological changes that occur as a function of temperature (presented in Table 5.6). These include the complete disappearance of calcite above 700°C. At low temperatures, the thin sections contained significant amounts of calcite (3.8-6.8 vol.%), and some of these minerals can be seen in Figure 5.37. The disappearance of

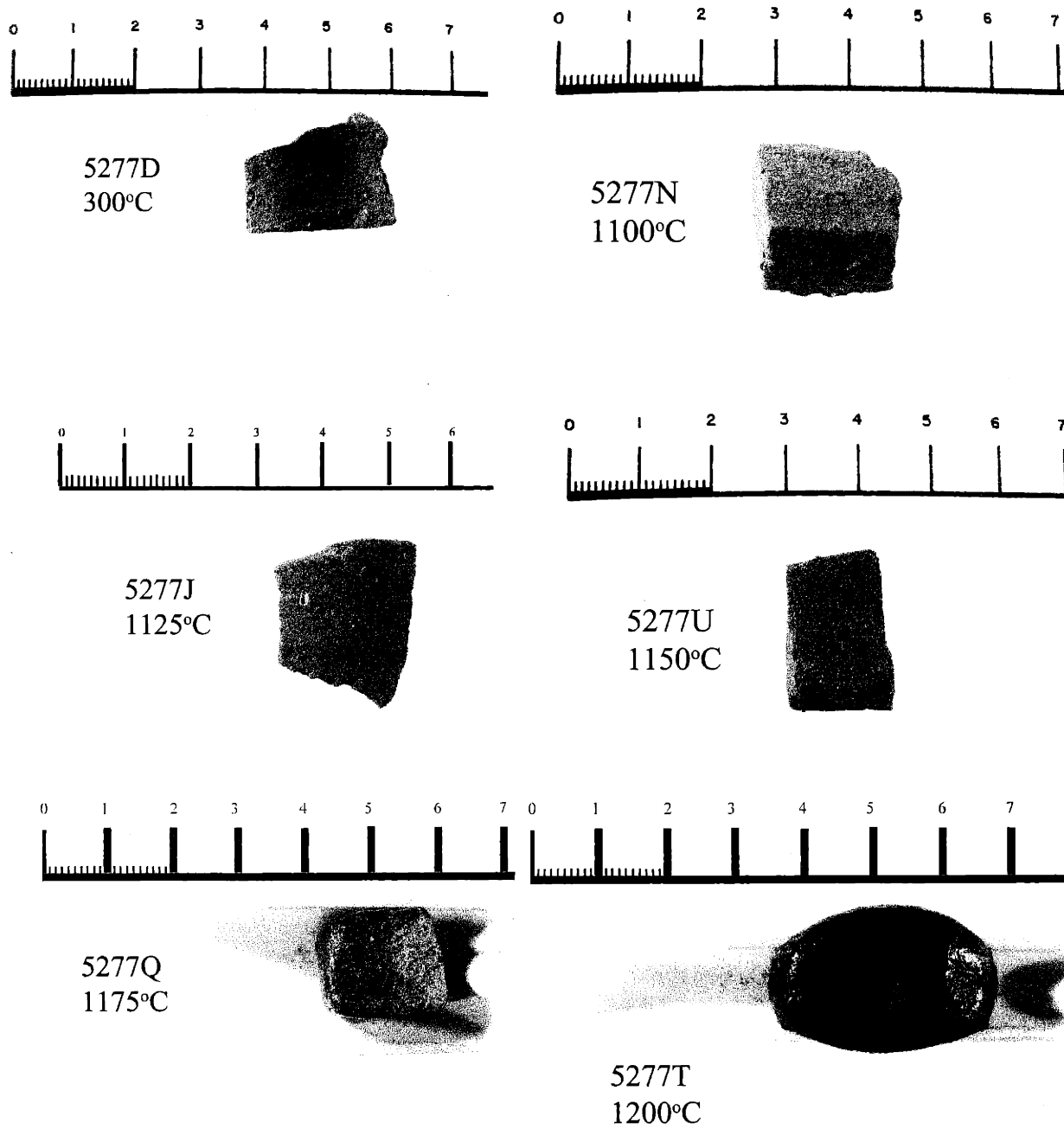


Figure 5.34. Photographs of furnace-heated samples from MIT No. 5277. MIT No. 5277D heated to 300°C in re-firing experiment; MIT No. 5277N heated to 1100°C; MIT No. 5277J heated to 1125°C; MIT No. 5277U heated to 1150°C; MIT No. 5277Q heated to 1175°C; MIT No. 5277T heated to 1200°C.

calcite above 700°C (see Figure 5.35d) agrees with the data presented by Tite (1972) in the theoretical DTA curve (Figure 5.29). Tite stated that calcite would decompose at 825°C, and Rice (1987) concurs. I also found that the optical activity⁶ of the ceramic matrix changed considerably as a function of temperature, beginning at 1000°C. When viewed in both plane and cross-polarized light, the matrix gradually made the transition from colorful (Figure 5.35a-c) to mostly red (Figure 5.35d-f), to mostly grey (Figure 5.35g-j), to yellowish-grey (Figure 5.35k-n).

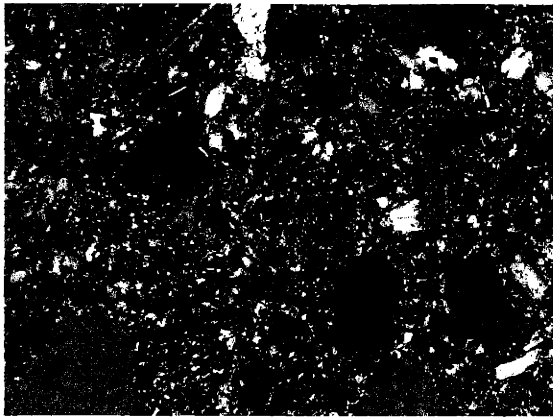
The void size and shape in the ceramic also change as a function of temperature. In the samples fired at low-temperatures, the voids are irregularly shaped, and usually resemble pieces of chaff temper (see Figures 5.36a-c). However, at approximately 1150°C (Figure 5.36d) the voids

Table 5.6. Morphological changes in ceramic of modern replica crucible (MIT No. 5277) as a function of temperature.

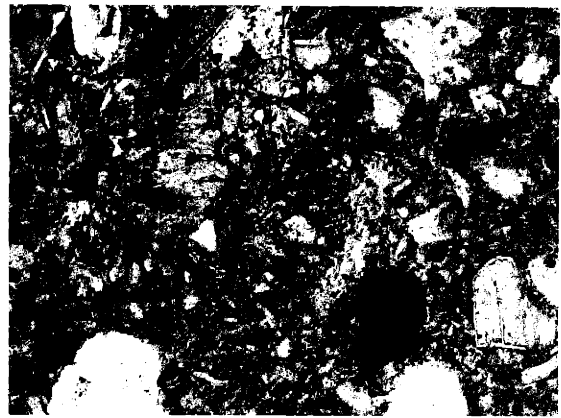
Temperature (°C)	Macroscopic Change	Microscopic Change
500	•Carbon core begins to disappear	•(Voids are irregular in shape until 1150°C)
700	•Carbon is completely gone	•No changes observed
1000	•Ceramic is more cohesive (less powdery)	•Ceramic is bright peach in color •Calcite is no longer present. •Optical activity is greatly reduced, clay looks dark reddish in xpl*
1100	•Ceramic is bright peach in color	•Optical activity is reduced, clay is grey in xpl
1125	•The color of the ceramic begins to darken	•Optical activity continues to diminish, clay looks grey in xpl
1150	•Ceramic is grey in color	•Clay is grey in xpl •Voids are more rounded.
1175	•Ceramic begins to swell and vitrify, it turns greenish-grey in color	•Most voids are rounded, but small •Clay is grey in xpl and light greenish-grey in ppl*
1200	•Ceramic has slumped and is black in color	•Voids are all large and rounded •Clay is grey in xpl, yellowish-green in ppl

*xpl: cross polarized light; ppl: plane polarized light

⁶ Here, optical activity refers to the birefringence of the clay.

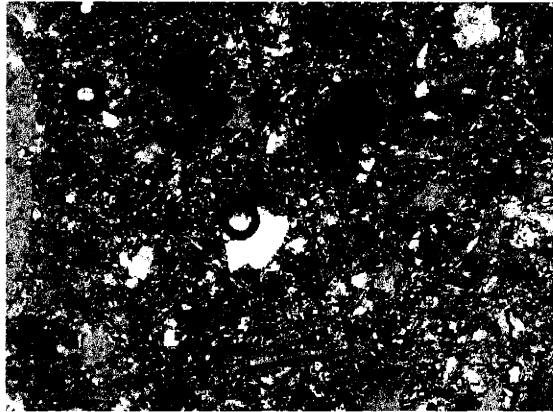


(a)



(b)

No heat applied to sample, optically active, irregular void shapes.



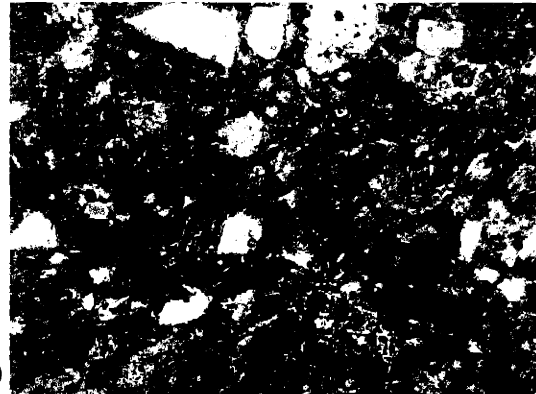
(c)

Re-fired at 700°C, optically active, irregular void shapes.

Figure 5.35a-n. Optical activity changes with temperature. All images are taken at a magnification of 100; images on the left are in cross-polarized light, images on the right are in plane-polarized light.

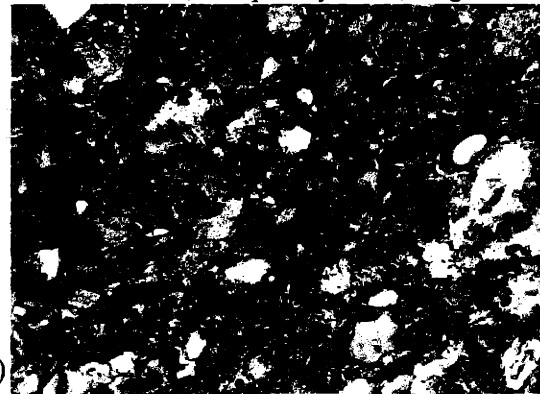


(d)



(e)

Re-fired at 1000°C, not optically active, irregular void shape, ceramic is reddish-brown, disappearance of calcite.

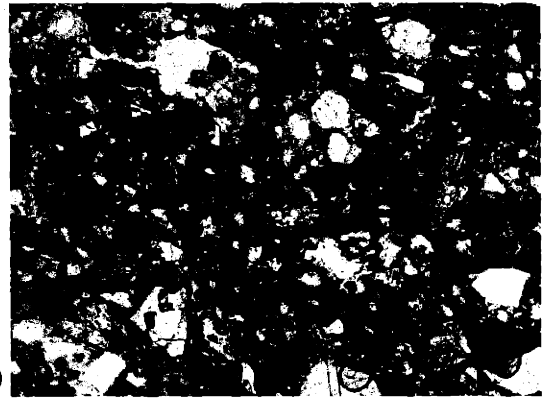


(f)

Re-fired at 1100°C, ceramic is brownish grey, irregular void shapes.

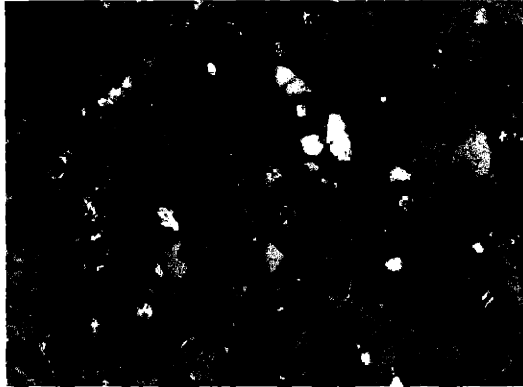


(g)

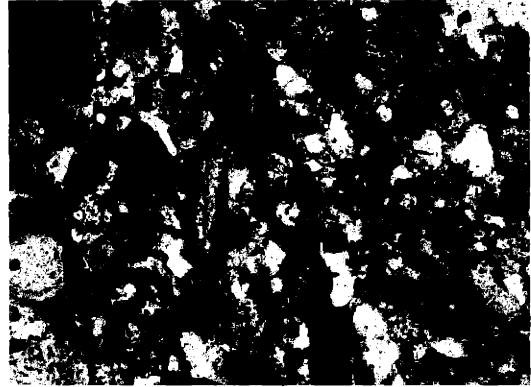


(h)

Re-fired at 1125°C, ceramic is grey, irregular void shapes.

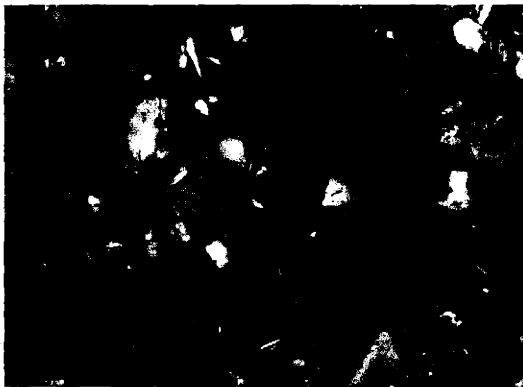


(i)

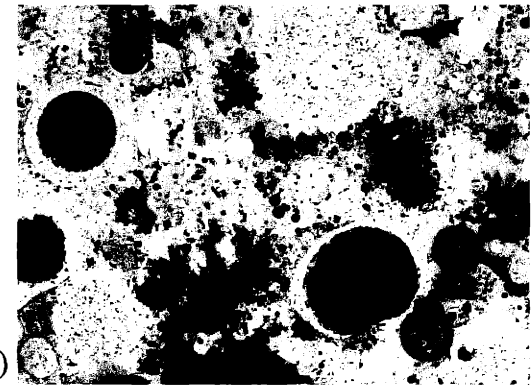


(j)

Re-fired at 1150°C, ceramic is grey, voids begin to round at edges.



(k)

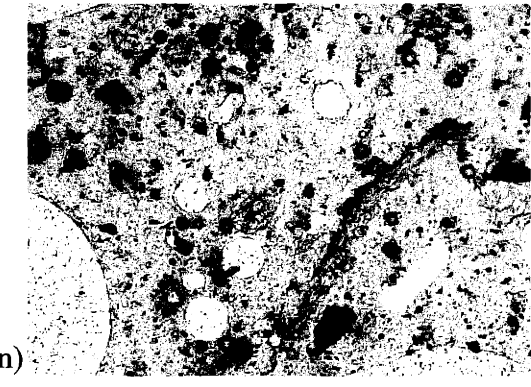


(l)

Re-fired at 1175°C, ceramic is grayish-yellow, voids are much rounder and larger

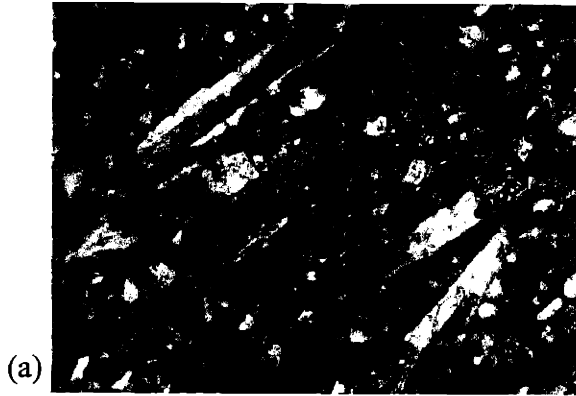


(m)



(n)

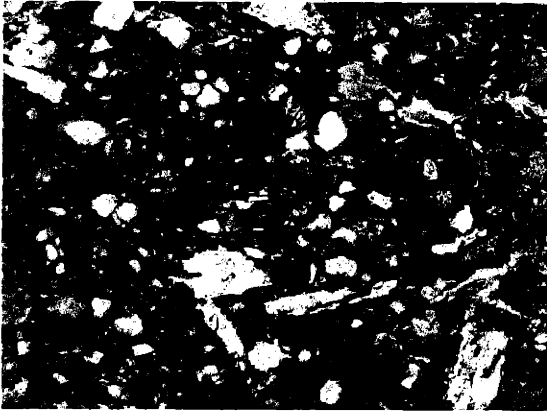
Re-fired at 1200°C, ceramic is yellowish-green, voids are very large and rounded.



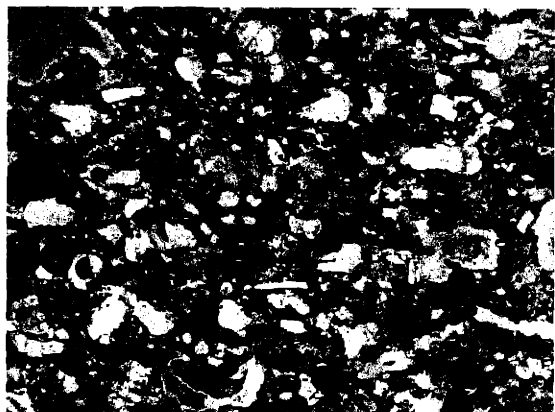
(a) no heat (irregular void shape)



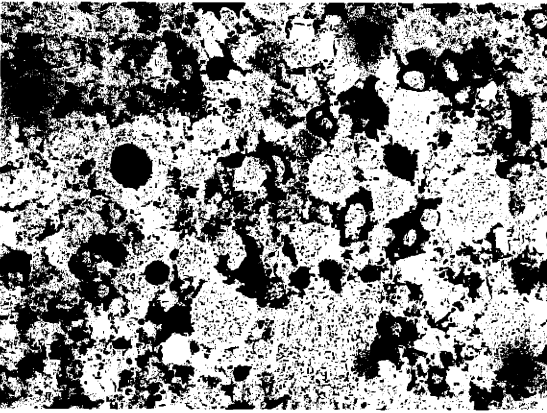
(b) 1100°C (irregular void shape)



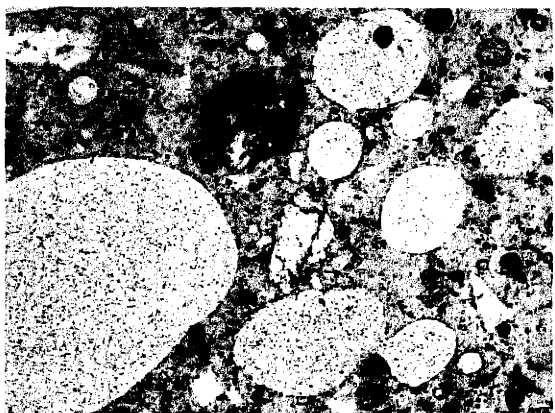
(c) 1125°C (voids begin to round, but most are irregular)



(d) 1150°C (voids slightly rounded)



(e) 1175°C (rounded voids)



(f) 1200°C (large rounded voids)

Figure 5.36. Void morphology. Plane-polarized light, taken at a magnification of 50.

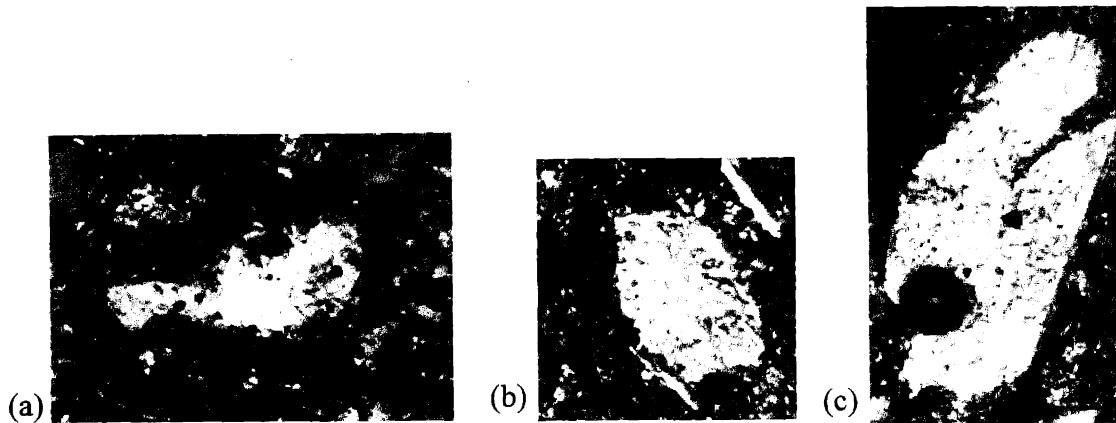


Figure 5.37. Presence of calcite in re-fired samples. (a) MIT No. 5277H (not heated); (b) MIT No. 5277B (500°C); (c) MIT No. 5277G (700°C). All images are in cross-polarized light at a magnification of 50.



Figure 5.38. Zone 1 of Iblis sherd (MIT No. 240) does not possess optical activity. Cross-polarized light, magnification of 50.

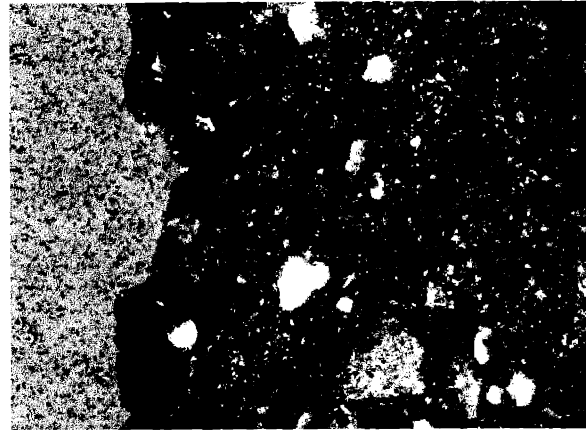


Figure 5.39. Zone 1 of Iblis sherd (MIT No. 241δ) does possess optical activity in one region. Cross-polarized light at a magnification of 50.

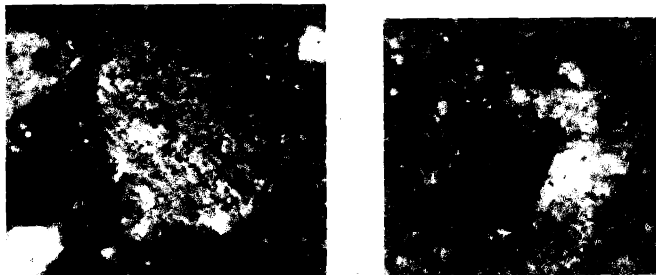


Figure 5.40. Zone 1 of Iblis sherd (MIT No. 241δ) contains calcite in one region. Cross-polarized light at a magnification of 50.

become more rounded (though some chaff-shaped voids still remain). At 1175°C (Figure 5.36e) the voids are mostly small and round, and at 1200°C (Figure 5.36f) all of the voids are round and much larger.

These microscopic morphological changes in the modern crucible replica were compared to the thin section samples of the Iblis sherds with the aim of determining the temperatures reached at points in the various zones across each sherd section. Thin sections were made of four Iblis

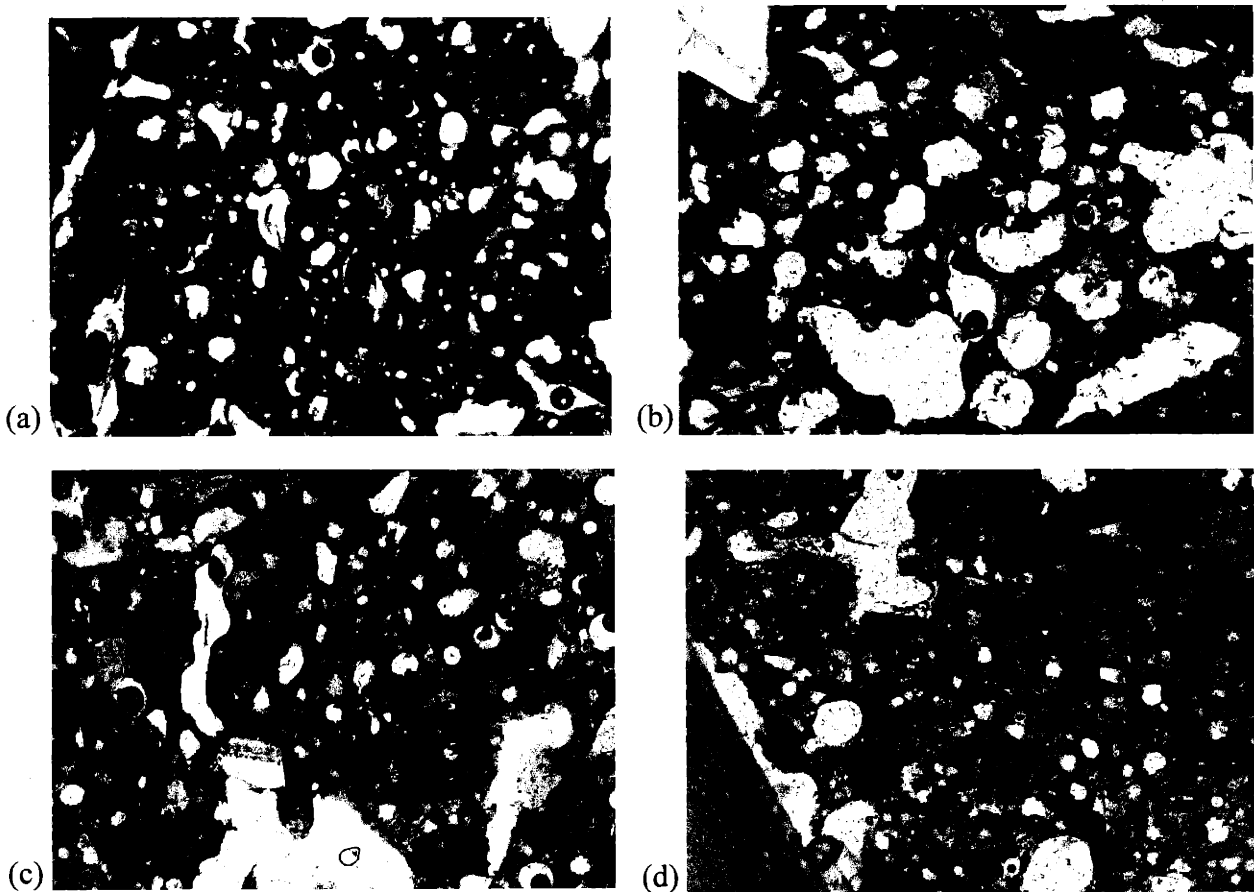


Figure 5.41. Voids present in Zone 3 of Iblis sherds. (a) MIT No. 240; (b) MIT No. 241 β ; (c) MIT No. 241 γ ; (d) MIT No. 241 δ all taken in plane-polarized light at a magnification of 50.

sherds (MIT Nos. 240, 241 β , 241 γ , and 241 δ). In Figure 5.38 (MIT No. 240) one can appreciate the lack of optical activity for Zone 1 of the sherd, as well as the distinct red color. When compared to the optical activity of the re-fired samples shown in Figure 5.35d-f, it is apparent that Zone 1 in Iblis sherd MIT No. 240 reached approximately 1000-1100°C. In contrast, sherd MIT No. 241 δ was

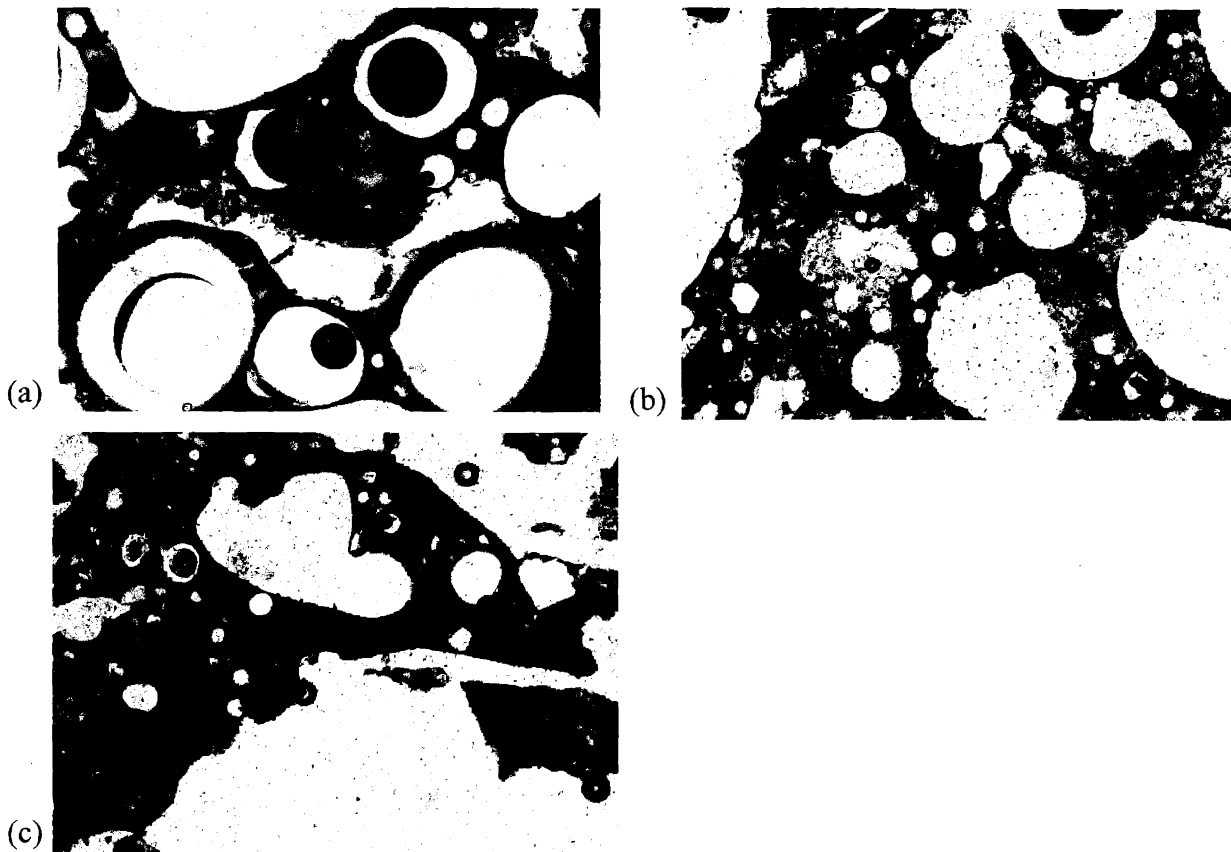


Figure 5.42. Voids present in Zone 4 of Iblis sherds. (a) MIT No. 240; (b) MIT No. 241 γ ; (c) MIT No. 241 δ all taken in plane-polarized light at a magnification of 50.

optically active in one region of Zone 1 at the lower exterior tip of the thin section. This optical activity is shown in Figure 5.39, and can be compared with the sections shown in Figure 5.35a, c. Figure 5.40 shows the presence of calcite mineral inclusions in this region as well. These two pieces of evidence allow me to suggest a firing temperature of 700°C for this region of Zone 1. Zone 2 of sherd MIT No. 241 δ is similar to the remaining major portion of Zone 1, which suggests that the predicted temperature range of 1000-1100°C also applies to this zone.

Figure 5.41 reveals the shape and size of voids present in Zone 3 of some of the ancient sherds. The small, rounded appearance of the voids in Zone 3 for all four Iblis sherds, when compared with the heated modern replica sections shown in Figure 5.35i, j, and 5.36d leads me to suspect that Zone 3 reached at least 1150°C. The voids in Zone 4 of the Iblis sherds are large and rounded (as seen in Figure 5.42). This zone was probably heated to above 1175°C and quite possibly to 1200°C (compare Figure 5.42 with Figures 5.35k-n and 5.36e,f).

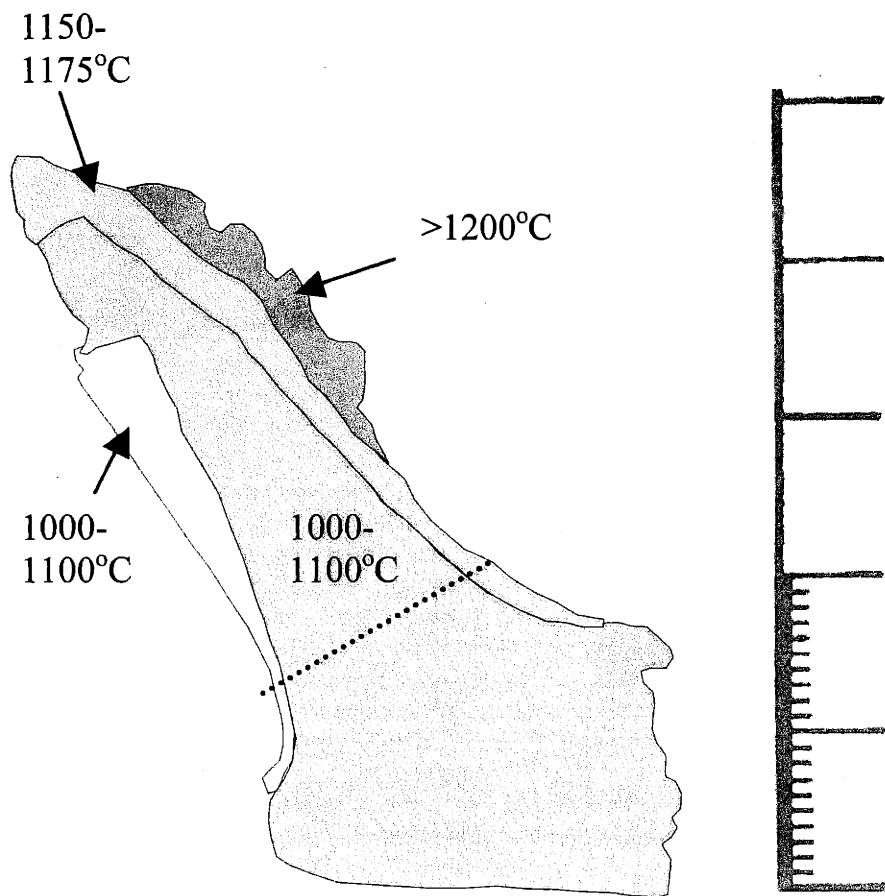


Figure 5.43. Temperature profile for Iblis crucible (MIT No. 240). Dotted line indicates the extent of the thin section sample. This sherd is also shown in Figure 5.4

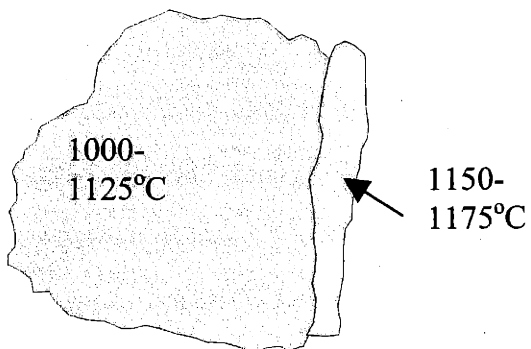


Figure 5.44. Temperature profile for Iblis crucible (MIT No. 241β). This sherd is also shown in Figure 5.7.

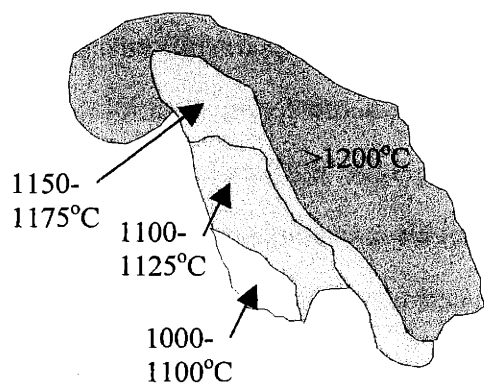


Figure 5.45. Temperature profile for Iblis crucible (MIT. No. 241 γ). This sherd is also shown in Figure 5.9.

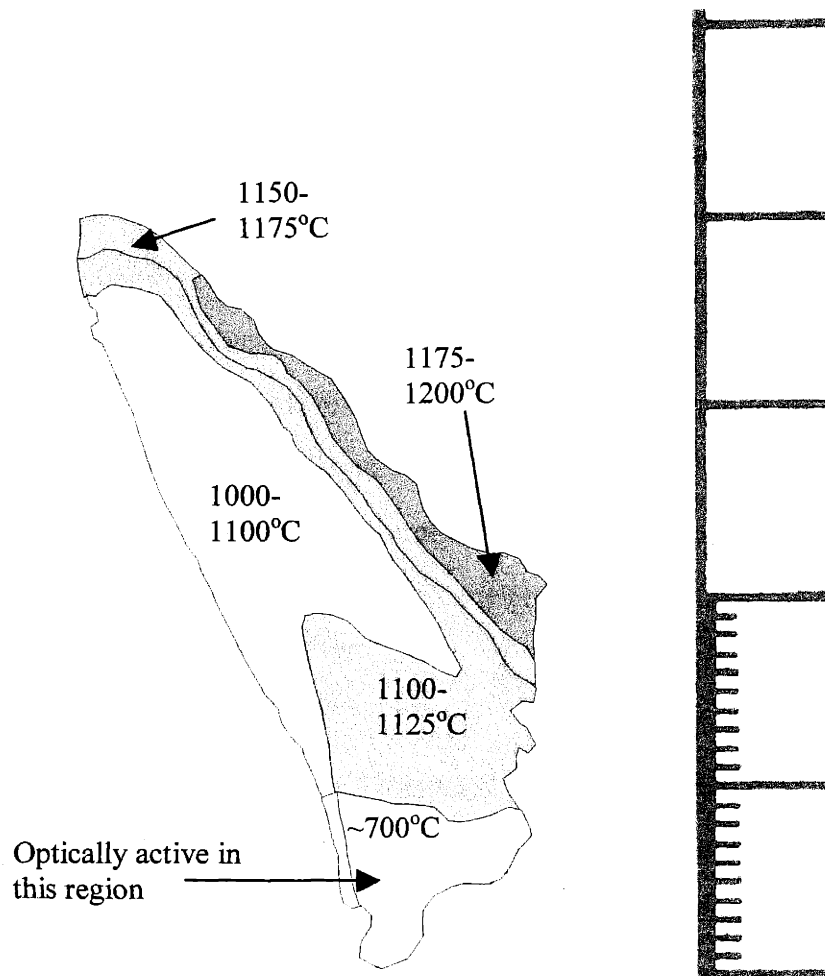


Figure 5.46. Temperature profile for Iblis crucible (MIT. No. 241 δ). This sherd is also shown in Appendix A.

5.3.3 Summary

Through DTA and re-firing experiments, I have determined the temperatures to which the Tal-i Iblis sherds were likely fired or heat-altered. The re-firing experiments have also allowed me to identify key morphological changes that occurred in the sherd ceramic fabric and in the mineral inclusions as a function of temperature. These temperature profiles help us to reconstruct the thermal history of the ancient ceramic vessels and provide some indication of the orientation of the vessels with respect to the heat source. The estimated temperatures to which these sherds were heated are shown in Figures 5.43-46, and this will be discussed in the next chapter.

5.4. Characterization of Tal-i Iblis Crucible Sherd Zones 3 and 4

Zone 4 of the Iblis crucible sherds (see Figure 5.7) is the most heavily vitrified zone and is the zone that had direct contact with the contents of the crucible during its use. Zone 3 also had contact with the contents of the crucible at the interior base and possibly at the rim. However, Zone 4 is clearly the area most affected by the processing of the contents of the vessel. For this reason, I examined the chemical composition of Zones 3 and 4 in the hope that they might provide evidence about the contents of the crucibles and about their metallurgical use. These analyses were performed by means of microscopic visual characterization, electron microprobe analysis, and by comparison of the composition of the Zone 4 material with the bulk chemical analysis of the unaltered sherd fabric discussed in section 5.2.3.

5.4.1 Scanning Electron Microscopy and Elemental X-Ray Mapping

Zone 3 of one of the Iblis sherds (MIT No. 241 β) was especially interesting because of a thick green accretion found on its interior surface (Figure 5.7). When analyzed with the X-ray mapping technique described in section 4.4.2, it was discovered that this accretion contained copper and chlorine. These X-ray maps are reproduced in Figure 5.47. Copper and chlorine concentrated in the same regions signifies the presence of copper chloride, a common copper corrosion

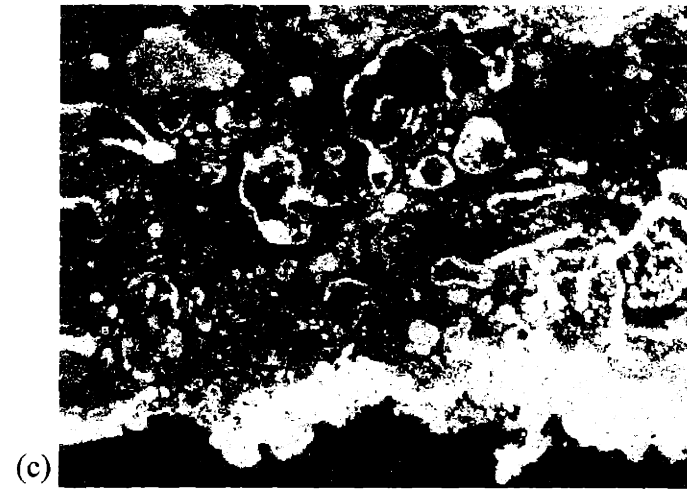
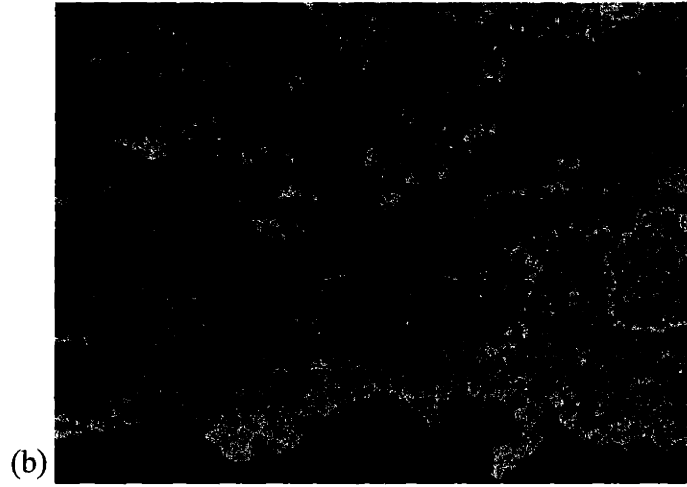
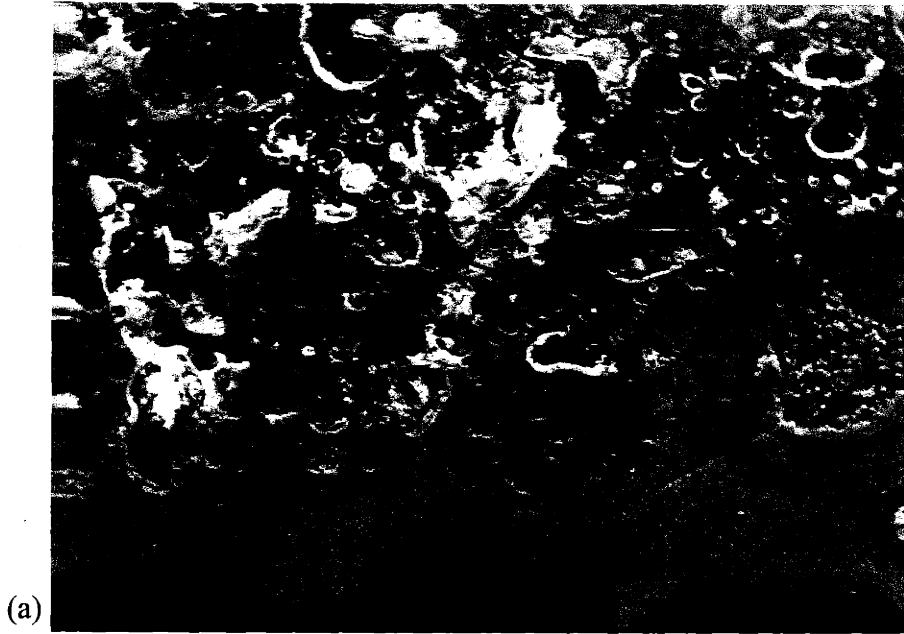


Figure 5.47. X-ray map of MIT No. 241 β in Zone 3. Copper and chlorine concentrated in the same regions of this surface zone, which I have interpreted to signify the presence of copper chloride. (a) SEM image at interior surface of MIT No. 241 β at location of green accretion (b) chlorine concentrations; (c) copper concentrations.

product. This verifies that this sherd (MIT No. 241 β) came into contact with copper metal at some point in the past.

5.4.2 Photomicrography and Electron Microprobe Analysis

During my microscopic visual investigation of Zone 4 of the Iblis sherds, I was able to identify five phases⁷. These phases include copper prills, cuprous oxide dendrites, clasts and needles, and two matrix phases. Each of these phases was photographed and studied before being analyzed on the microprobe.

Metallic prills were present in Zones 3 and 4 of the Iblis crucible sherds (MIT Nos. 241 β , 241 δ , and 241 γ). These prills can be seen in Figure 5.48. All of the prills contain over 95wt% copper metal (Tables 5.7a and 5.7b list the components of all phases identified, expressed in wt%). The largest prill, in MIT No. 241 γ , contains copper sulfide inclusions (Figure 5.49). These inclusions contain 10-15wt% sulfur and approximately 75wt% copper. One inclusion in this same prill also contains 2wt% arsenic. The prills located within MIT No. 241 β were not analyzed with the electron microprobe because they were so much smaller than those contained within the other sherds.

Dendrites (Figure 5.50) were found only within Zone 4 of MIT No. 241 δ . The quantitative analysis carried out on the microprobe revealed that these dendrites are copper oxides that grew in a silica-rich matrix. They appear to contain small amounts of silica, alumina, iron, magnesium, calcium, sodium and potassium (see calculation in Table 5.7b corrected for matrix “noise” and section 6.5 for discussion of this correction). The dendrite arm width is approximately 1 μ m in size; the diameter of the electron microprobe beam is also 1 μ m. Thus the microprobe was used at its limit of detection with respect to the dendrites, and the many of the elements recorded for the dendrites may represent contributions from the surrounding ceramic matrix material. The clasts and needles have been grouped together because they are the same composition, and in some of the

⁷ In this discussion I use the word “phase” to denote any part of Zone 4 with a discrete chemical composition.



Figure 5.48a. Copper prills found in MIT No. 241 β at a magnification of 500, Zone 3.



Figure 5.48b. MIT No. 2418 at a magnification of 100, Zone 4.

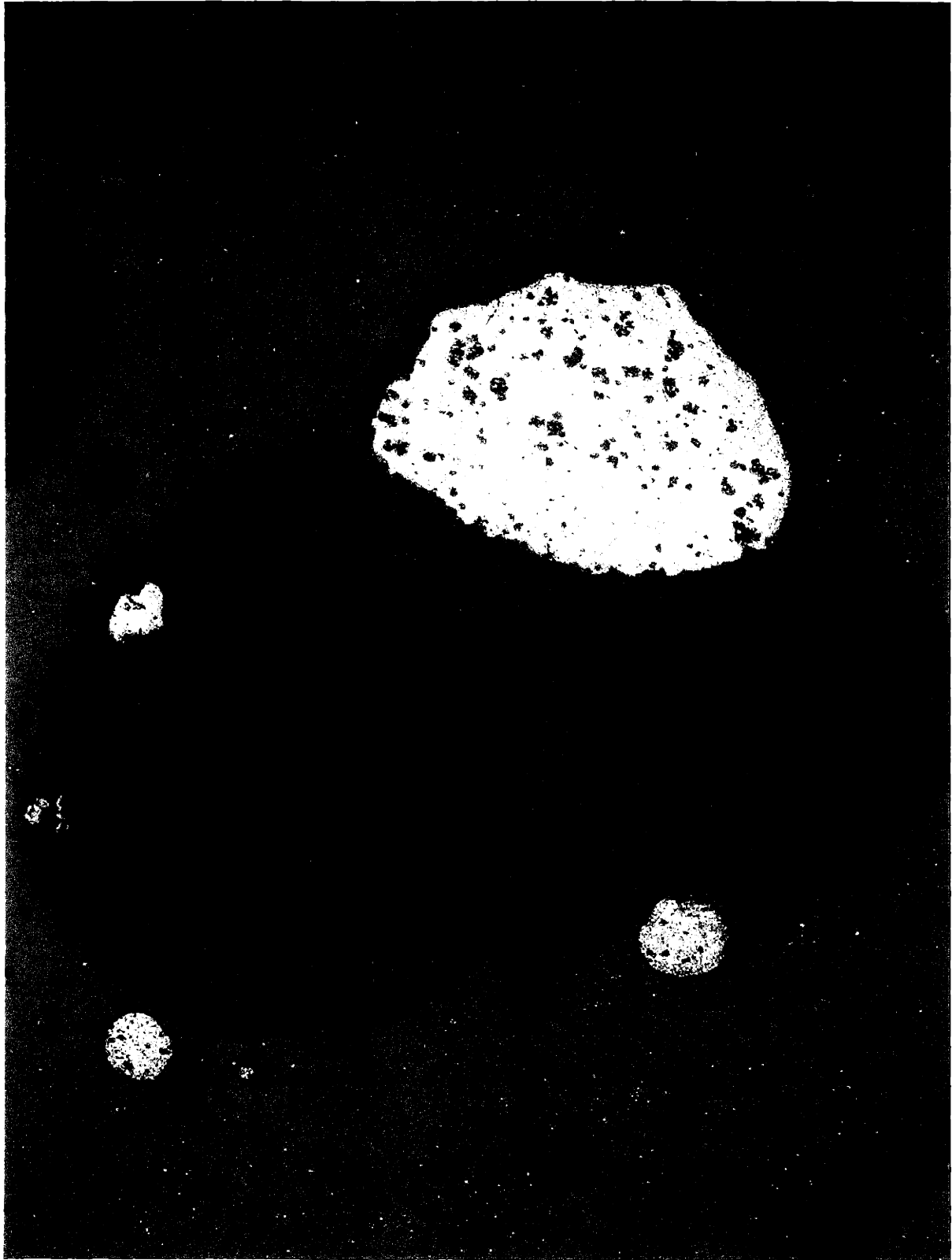


Figure 5.48c. MIT No. 241y at a magnification of 100, Zone 4.

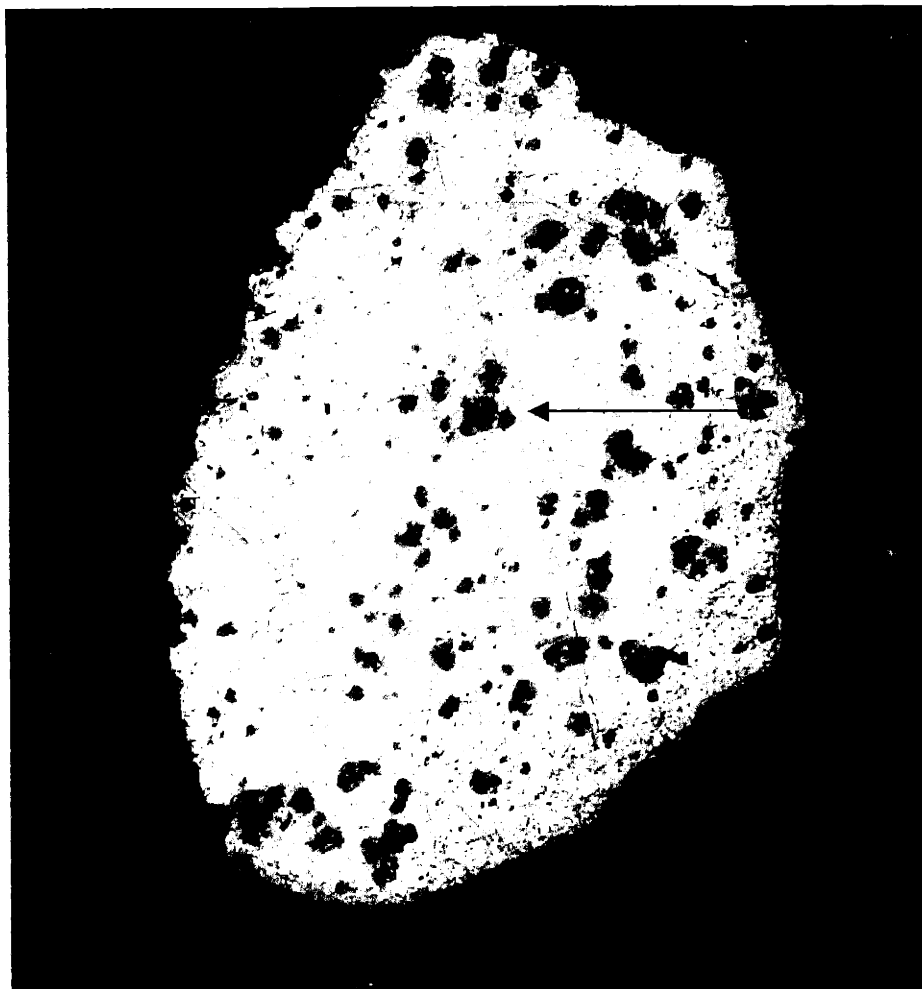


Figure 5.49. Copper sulfide inclusions in the largest prill; MIT No. 241 γ , at a magnification of 200.

photomicrographs the needles seem to be nucleating from the clasts. The composition of this phase consists primarily of iron and oxygen, although it contains about 5wt% copper in solution. The morphologies of this phase appear in Figure 5.51.

The matrix of Zone 4 is also of great interest. It is composed of two phases, however these phases are not the same for both artifacts in which they appear. Figures 5.52 and 5.53 show the matrix material for Zone 4 in the two crucible sherds, MIT No. 241 δ and 241 γ . Table 5.7a shows that the lighter phase in MIT No. 241 δ consists mostly of silicon, iron, magnesium, aluminum and calcium⁸, and the darker phase of the same artifact consists primarily of silicon, aluminum, iron,

⁸ Oxygen is indicated in Table 7b to be able to report every element as an oxide, but it was not measured with the microprobe.

Table 5.7a. Weight % of elemental composition for Iblis crucible sherds: phases in Zone 4.

MIT No.	Phase	Cu	Fe	Mg	Ca	Na	K	As	Co	Ni	Ag	S	Si	Al	O	Total
241δ	Prill	92.022	1.108	--	--	--	--	0.009	0.018	0.03	0.057	0.272	--	--	--	93.
	Dendrite	55.165	2.631	0.288	3.62	0.777	1.205	ND	ND	ND	ND	ND	8.17	2.159	19.56	93.
	Dendrite recalculated	53.48	1.49	0.21	0	0.50	0.66	ND	ND	ND	ND	ND	3.16	0.97		
	Clasts/Needles	5.437	61.777	1.473	0.302	ND	0.035	--	--	--	--	--	0.095	0.765	27.06	96.
	Clast rim	37.67	36.83	0.341	0.303	0.075	0.028	--	--	--	--	--	0.126	0.664	22.96	98.
	Lighter Matrix	0.685	16.463	3.46	15.8	0.19	0.153	--	--	--	--	--	17.177	4.1	40.47	98.
	Darker Matrix	6.9	4.67	0.31	14.833	1.154	2.223	--	--	--	--	--	20.513	4.87	41.067	96.
241γ	Large Prill	97.226	0.042	NA	--	--	--	ND	0.196	0.319	0.185	0.004	--	--	--	97.
	Prill Inclusions	76.783	0.032	NA	--	--	--	0.866	0.17	0.26	0.154	13.263	--	--	--	91.
	Lighter Matrix	4.9	7.39	1.434	14.94	0.657	0.575	--	--	--	--	--	18.857	6.253	40.423	9.
	Darker Matrix	0.444	1.937	5.013	24.63	1.885	0.016	--	--	--	--	--	19.06	3.95	41.543	98.

ND not detected; -- not sought

MIT No.	Phase	SiO ₂	Al ₂ O ₃	Fe ₂ O ₃ *	FeO*	MgO	CaO	Na ₂ O	K ₂ O	SO ₃	CuO*	Cu ₂ O*	Total (high)	Total (low)
241d	Dendrite	17.48	4.08	3.76	3.38	0.48	5.07	1.05	1.45	0	69.09	62.13	102.446	95.109
	Clasts/Needles	0.203	1.445	88.323	79.474	2.442	0.422	0	0.043	0	6.809	6.123	99.687	90.152
	Clast rim	0.27	1.255	52.657	47.381	0.566	0.424	0.101	0.034	0	47.176	42.423	102.481	92.453
	Lighter Matrix	36.746	7.747	23.538	21.18	5.738	22.107	0.256	0.185	0	0.858	0.771	97.173	94.728
	Darker Matrix	43.884	9.202	6.677	6.008	0.514	20.754	1.555	2.678	0.026	8.641	7.771	93.932	92.392
241γ	Lighter Matrix	40.34	11.815	10.566	9.507	2.379	20.904	0.886	0.693	0.038	6.137	5.518	93.756	92.079
	Darker Matrix	40.775	7.463	2.769	2.492	8.313	34.462	2.541	0.019	0	0.556	0.5	96.898	96.565

*Copper and iron are reported both in their higher oxidation states and lower oxidation states, and the totals have been calculated for each of these.



Figure 5.50. Dendrites in MIT No. 2418 Zone 4 (a) photomicrograph at a magnification of 500; and (b) SEM image with scale bar indicated.



Figure 5.51. Clast and needle phases in MIT No. 241δ. SEM image with scale bar shown.

calcium and copper. In artifact MIT No. 241γ, the lighter phase is similar to the darker phase of the previous artifact, that is, it consists mostly of silicon, aluminum, iron, calcium and copper. The darker phase of MIT No. 241γ consists mainly of silicon, aluminum, magnesium and calcium. The chemical compositions of the matrix material in Zone 4 of these two sherds are slightly different, implying that slightly different procedures or materials were involved in the use of each of these vessels. When these Zone 4 matrix analyses are compared to the bulk chemical analyses of the unaltered zones of the sherds, (section 5.2.3 and Table 5.3), one notices the drastic increase in copper and calcium in the Zone 4 matrix phases. The significance of these data is discussed in the next chapter.

5.5 Summary

The results presented here show that the modern crucible replica is close in composition to the Tal-i Iblis crucible artifacts. This similarity allowed me to design valid re-firing experiments on



Figure 5.52 Matrix phases for MIT No. 241 δ Zone 4, taken at a magnification of 500 (Matrix for MIT No. 241 δ can also be seen in Figures 5.48b, 5.50, and 5.51)



50μm

EE 241G Matrix morphology

Figure 5.53 Matrix phases for MIT No. 241γ Zone 4, SEM image with scale bar indicated.

the modern replica with the aim of comparing these re-fired samples to the Tal-i Iblis crucible fragments. Upon studying the morphological changes that occurred in the ceramic of the modern replica as a function of temperature, I was able to compare these with the microstructure of the Iblis crucible sherds. The comparison allowed me to estimate the original temperatures to which the Tal-i Iblis artifacts were fired or heat-altered. The interior surfaces of these crucibles (Zone 4) reached approximately 1200°C. I characterized Zone 4 to clarify the structure and chemical composition of the five phases found within the zone. This chemical composition was compared to the bulk chemical analysis of the ceramic matrices of Zones 1 and 2 of the Iblis sherds. In the Discussion chapter I will present explanations for and interpretations of these results, as well as the implications of such data.

Chapter VI: Discussion

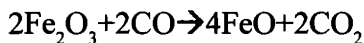
6.1 Copper at the site of Tal-i Iblis

The early inhabitants of Tal-i Iblis had their choice of ores to exploit from many nearby copper ore deposits. The site's prime location in one of the five main copper districts of Iran enabled its inhabitants to benefit from the numerous mineralized veins and contact joints between igneous intrusions and sedimentary deposits (Bazin and Hübner 1969:10). It is likely that the Iblis miners did not travel far to obtain their ore because there were so many source outcrops near to them. As mentioned in section 2.1, the majority of the ore sources immediately surrounding Tal-i Iblis include deposits of copper carbonate ore, which means that it would have been relatively easy to obtain this weathered oxidized ore for metallurgical activity. Furthermore, bits of malachite were found in level II at the site of Tal-i Iblis in many locations (Caldwell 1967). This indicates that the Tal-i Iblis inhabitants were at least obtaining some of these carbonate ores.

6.2 The use of crucibles at Tal-i Iblis

The presence of crucibles such as those discussed in this thesis is interesting in itself; however, the more crucial question remains as to their purpose. The ancient crucible sherds discussed in this thesis share many of the same qualities. Their shapes are similar enough to assume that they all came from crucibles shaped like the modern crucible replica that was fashioned on-site (Figure 5.3a) by Hildegard Wulff. They are also similar in their alterations as a result of heating. The crucible cross-section zones defined in section 5.1 (Figure 5.1) indicate that the source of heat was located above the crucible and directed to the interior of the vessel. The zoning also reveals that a reducing atmosphere was achieved within the vessel hollow. The heavy vitrification on only the upper interior surfaces of the crucible sherds provides the clearest evidence that the intense heat

that caused vitrification was concentrated within the vessel. The exterior surfaces of the sherds show no evidence of this intense heat. Previous studies (Obstler 1996; Freestone and Gamester 1997) on archaeological ceramics have established a correlation between the presence of a reducing atmosphere during the heating of pottery and a color change in the ceramic fabric, from tan to grey. This color change is largely due to the reduction reaction that occurs when iron oxide in the ceramic fabric is reduced under the influence of heat:



This reaction occurs in the temperature range of 900-1000°C. The presence of the grey color in Zone 2 of the Iblis sherds indicates that the ceramic was exposed to a reducing environment generated within the crucible. Furthermore, the characteristic tan/salmon color of Zone 1 shows that the atmosphere to which the crucible was exposed at the exterior wall was oxidizing.

This evidence, taken together, suggests that the metallurgical operations at Tal-i Iblis were carried out in a set-up similar to that shown in Figure 6.1. This figure shows a schematic section of a smelting operation uncovered archaeologically in Cyprus in which a fuel source was piled above the contents of a crucible to create a high-heat, reducing region within the crucible suitable for smelting carbonate or other copper oxide ores. Not only would this installation create a reducing atmosphere at the interior, it could also permit an oxidizing atmosphere at the exterior rim of the vessel if the fuel source were piled

only within the crucible and not around it. A set-up with features similar to those shown in Figure 6.1 was found in level II at Tal-i Iblis. Called a “hearth” by Caldwell, it was described as having been “scooped out of the ground and show[ing] neither much preparation nor evidence of repeated firing”

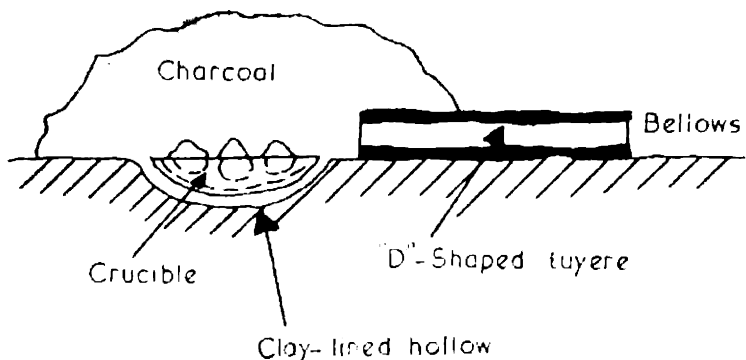


Figure 6.1. An example of a pit smelting operation in Ambelikou, Cyprus drawn by Tylecote (1982:233). No date or site information provided.

(1967:35). This pit scooped out of the ground contained metallurgical artifacts including small fragments of copper oxide mineral, one crucible sherd, and fragments of a brick. Since this was the only “hearth” found in either level I or level II at Iblis, it does not provide conclusive evidence of having been used in the metallurgical processes occurring at Tal-i Ibis. Keeping this in mind, it is necessary to look for additional evidence to support the use at Iblis of a set-up similar to that shown in Figure 6.1.

Tylecote (1982: 235) suggests that the Cypriot installation (Figure 6.1) would also optimally exploit the refractory properties of the crucible. The open shape of such crucibles may provide for easy loading of the crucible contents, but it also allows for slow heat transfer from below and rapid heat loss from above, if not covered. If a crucible were used such as in the Cypriot set-up, it could be designed to insulate rather than conduct heat, and one could avoid the problem of trying to move heat through the base and walls of the container in order to heat the contents of that container. In support of this, it seems that the crucibles at Tal-i Iblis were in fact designed to act as insulators.

Both Rice (1987) and Tylecote (1982) report that increasing the porosity of a clay fabric can reduce its thermal conductivity (increasing its insulating properties). The Tal-i Iblis crucibles were tempered with chaff, presumably to serve this purpose. Being an organic compound, chaff will burn off when the ceramic is fired above 500°C, leaving behind air-filled pores (Rice 1987:103; Tylecote 1982:235). Air has a much lower thermal conductivity ($K=0.0249$ W/mK at 26.7°C) (Weast 1981:E-2) than the ceramic material ($K=0.472$ W/mK at 70°C) (Touloukian 1970:806), which means that with every additional pore, the vessel becomes a better heat insulator. Figure 6.2 provides supporting evidence for this argument with data taken from a standard reference book (Touloukian 1970).

However, Rice (1987) and Tylecote (1982) also note that increasing the porosity of clay with chaff temper can also greatly weaken the fabric by reducing its yield strength⁹, since the pores act as stress concentrators within the fabric of the ceramic vessel. This weakening is not a concern,

⁹ Yield strength is the stress at which a material makes the transition from elastic to plastic deformation.

however, if the vessel is stationary and does not have to support its own weight or the weight of its contents. This is the case when the vessel is placed in a shallow pit similar to that shown in Figure 6.1; the surrounding earth supports the crucible during use.

Additional evidence for the use of the Iblis crucibles in a metallurgical activity comes from the residues and vitrification found on their interior surfaces. Many of the crucible sherds exhibit a green residue and contain green nodules on their interior surfaces. These are

copper corrosion products commonly caused during burial when metallic copper is in contact with corrosive ground water. In section 5.4.1 I have identified this residue as a copper chloride. In addition, many sherds contain copper prills in Zone 4. These features all constitute direct evidence for the use of these crucibles as part of a metallurgical technology at Tal-i Iblis, regardless of whether that activity involved melting copper metal or smelting copper ores. The vitrification on the interior of these sherds provides further evidence of this metallurgical technology.

With a fuel source piled inside and above the crucible, as shown in Figure 6.3, the concentration of heat and slag formation should occur along the upper interior walls and rim of the crucible, not at the interior of its base. In the case where metal is being melted inside the crucible, slag formation might occur as a result of the interaction between the alkali fuel ash and the silicate material in the crucible. When metallic ores are being smelted within the crucible, slag may form

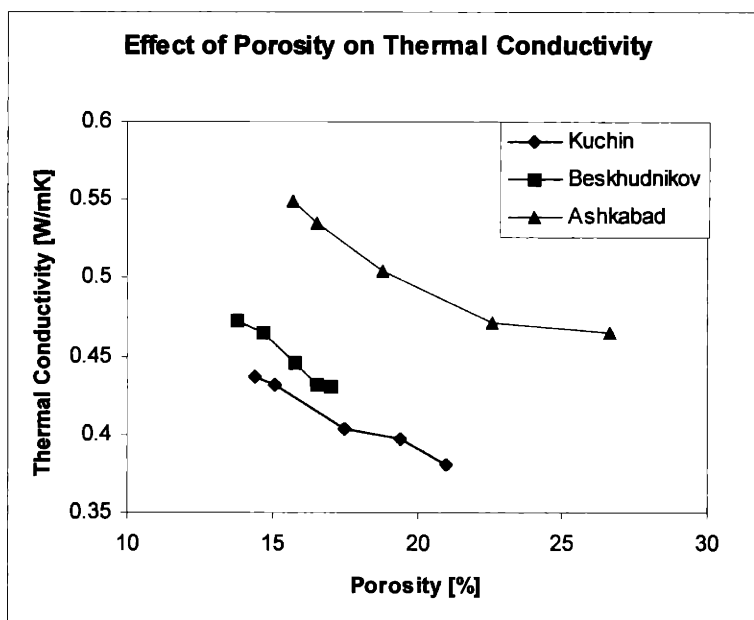


Figure 6.2. Plot of the effect of porosity on the thermal conductivity of clay at temperatures of 70.5-120.5°C. Clay samples were taken from three source areas (Kuchin, Singapore; Beskhudnikov (location unknown); and Ashkabad, Turkmenistan). Five samples were taken from each source area with different degrees of porosity. Data are taken from standards presented in Touloukian (1970:806).

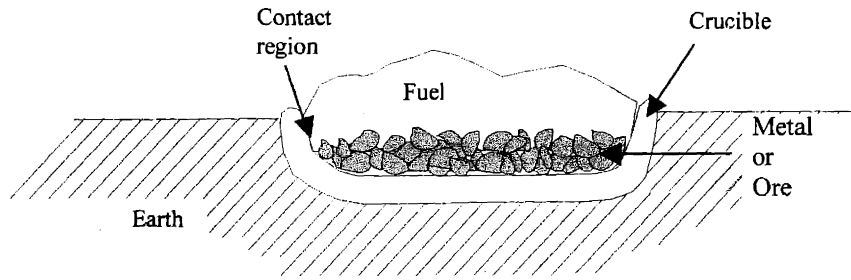


Figure 6.3. Schematic drawing for crucible smelting or melting operations. The region indicated by the arrow on the crucible wall would experience contact between the contents of the crucible and the fuel source piled on top.

as a result of the interaction among the gangue of the ore, the alkali fuel ash, and the silicates of the ceramic material (Tylecote 1976). In either case, slag would form where the contents of the crucible came in contact with the fuel at the upper wall of the ceramic (see Figure 6.3). Therefore, we would expect to see heavy vitrification there, but not at the interior base of the crucible.

Two sherds (MIT No. 241 β and 241 ϵ) appear to be from the bases of their respective crucibles (section 5.1.1; Figures 5.7 and 5.8). Their complete lack of vitrification in comparison with the heavy vitrification present on the interior walls of other crucible sherds (MIT Nos. 240, 241 γ , 241 δ , 241 η , 5274) indicates that the temperatures affecting the interior *base* of the crucibles were far lower than those that affected the *upper interior wall*.

There is little doubt that the Tal-i Iblis crucibles were used for a metallurgical technology in an arrangement similar to those shown in Figures 6.1 and 6.3. It should be noted, however, that no evidence of tuyeres (shown in Tylecote's reconstruction of the Cypriot smelting operation) or of refractory ceramic blow-tube tips was found by the archaeologists at Tal-i Iblis. We are still in the dark about the methods used to raise the temperature within the crucibles to direct the heat to the interior of the vessels.

6.3 The temperatures reached in the crucible fabric during crucible use

The comparative data presented in section 5.3 reveal the temperatures reached in each of the zones of the ancient crucible fragments. The interior of every crucible fragment reached at least 1150°C indicating that each crucible could have withstood the temperatures necessary for smelting

copper carbonate ore (600-700°C for sponge copper; 1083°C for prills: Thompson 1958; Charles 1979) and for melting native copper ($T_m=1083^\circ\text{C}$). This evidence is strikingly different from the evidence reported by Dougherty (Dougherty and Caldwell 1966) that the crucible material he tested melted at a temperature of $990\pm 50^\circ\text{C}$. It also differs from the temperature measurement made by Pleiner (1967) during the on-site experiment performed at Tal-i Iblis. Pleiner reported that

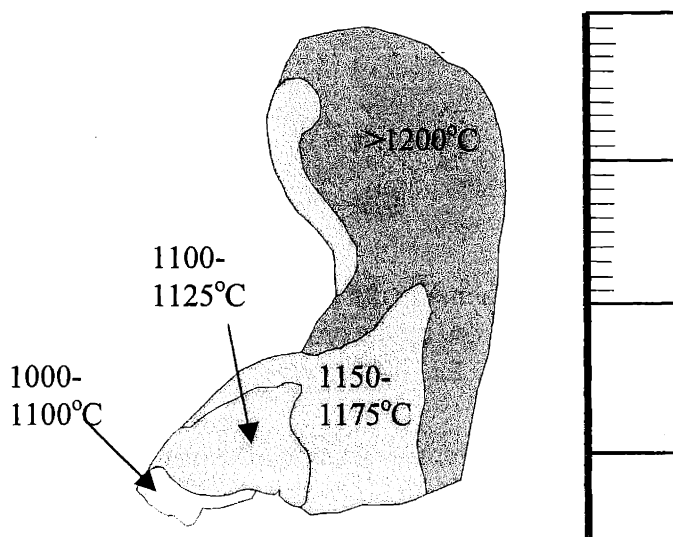


Figure 6.4. Temperature profile for fragment of modern crucible (MIT No. 5279) used in the on-site experiment at Tal-i Iblis.

the temperature measured with a thermocouple at the tip of a tuyere during the smelting experiment reached 1100°C . My analysis of a fragment of that experimental crucible (MIT No. 5279) shows that the interior surface must have reached at least 1200°C (Figure 6.4). Given the variety of laboratory analytical and experimental procedures I used in this research and the close agreement of the determinations of all my temperature measurements, I am confident in my results.

6.4 The significance of Zone 4 in the ancient crucibles

The five phases present in Zone 4 of the crucible sherds can be used to determine the thermal history and changes in composition of the fabric of the crucible. Here I will discuss the significance of the copper prills contained within this zone, and attempt to reconstruct a solidification sequence for the phases in Zone 4 of Iblis sherd MIT No. 241 β . In addition, it is interesting to consider the differences between the bulk chemical analysis of the sherd and the chemical analysis of the matrix phases of Zone 4.

The largest copper prill found in any of the ancient crucible sherds also contains inclusions. These inclusions consist of copper sulfide containing small amounts of arsenic, nickel, cobalt, iron

and silver. Such inclusions are expected to be present in copper smelting slags (Craddock 1985), but native copper usually has much greater purity than this. In a study done by Tylecote (1976) on less pure native coppers from Western Asia, it was shown that some of the same elements occur in those coppers as are found in the Iblis crucible prills (MIT No. 241 γ). However, in the case of the Iblis prills, the presence of this suite of elements within discrete sulfide inclusions provides strong evidence for the prill as a product of a smelting operation. Such multi-element inclusions are not characteristic of native coppers (Rapp 1988; Maddin et al. 1980).

The matrices of Zone 4, in which the copper prills occur, were analyzed to fully understand how each constituent phase could have formed (see Figures 5.51 and 5.52). The wt% of the three main constituents for each of these phases has been recalculated¹⁰ and plotted on their respective phase diagrams (see Figures 6.5, 6.6, 6.7, 6.8, 6.9) to determine approximate melting temperatures for each phase. Table 6.1 reports these temperatures. The melting point temperatures given in Table 6.1 correspond to each discrete phase. However, when all the phases occur together as a vitrified melt, the temperatures at which these phases solidify will be lowered according to the concentration of each phase in the melt. The information in Table 6.1 provides the basis for an estimate for the solidification sequence of the constituent phases. For Iblis sherd MIT No. 241 δ , the solidification sequence was: light phase (SiO₂-FeO-CaO) → dark phase (SiO₂-Al₂O₃-CaO) in-

Table 6.1. Melting temperatures for phases present in Zone .

MIT No.	Phase	Corresponding phase diagram	Melting temperature (°C)
241 δ	Prills	Cu	1083
	Dendrites	Cu-Si-Fe	1227
	Dark	SiO ₂ -Al ₂ O ₃ -CaO	1250
	Light	SiO ₂ -FeO-CaO	1300
241 γ	Prills	Cu	1083
	Dark	SiO ₂ -MgO-CaO	1400
	Light	SiO ₂ -Al ₂ O ₃ -CaO	1300

¹⁰ The wt% of the three main oxides present in the phase were normalized to correct for the fact that they alone did not add to 100% of the phase.

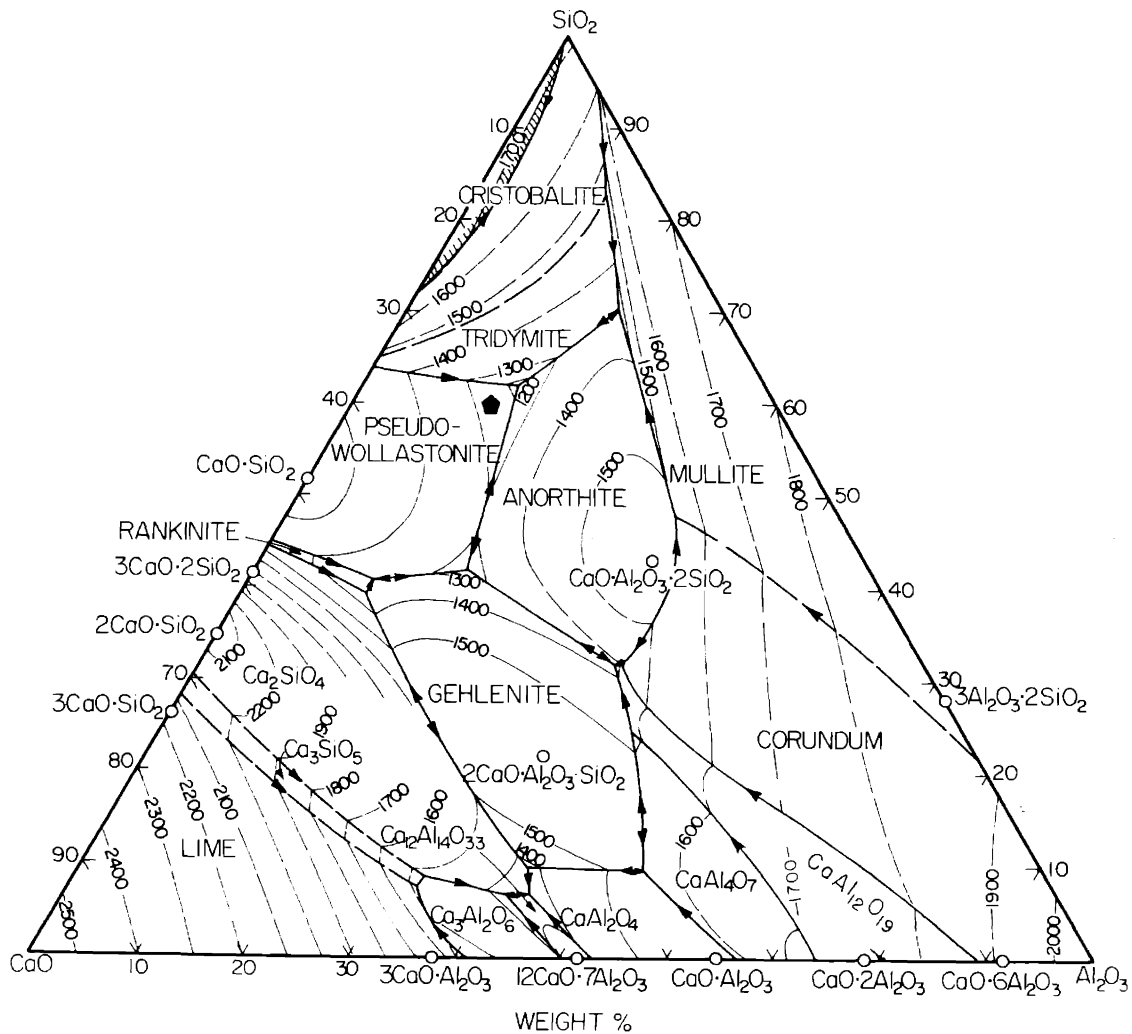


Figure 6.5. MIT No. 241 δ : Normalized composition of dark phase of Zone 4, plotted on SiO₂-Al₂O₃-CaO phase diagram.

cluding cuprous oxide dendrites → prill. For MIT No. 241 γ the sequence follows: dark phase (SiO₂-MgO-CaO) → light phase (SiO₂-Al₂O₃-CaO) → prill. The solidification sequences determined by this method correspond to my analysis of the matrix microstructures shown in Figures 5.51 and 5.52. The light phase (crystalline) solidifies first; the dark phase (glassy/amorphous) solidifies next with the formation of copper oxide dendrites; and the metallic prills solidify as the final phase.

The solidification of the dendrite phase in sherd MIT No. 241 δ is especially interesting because these dendrites exhibit such a small interdendritic spacing and dendrite arm width (1 μ m).

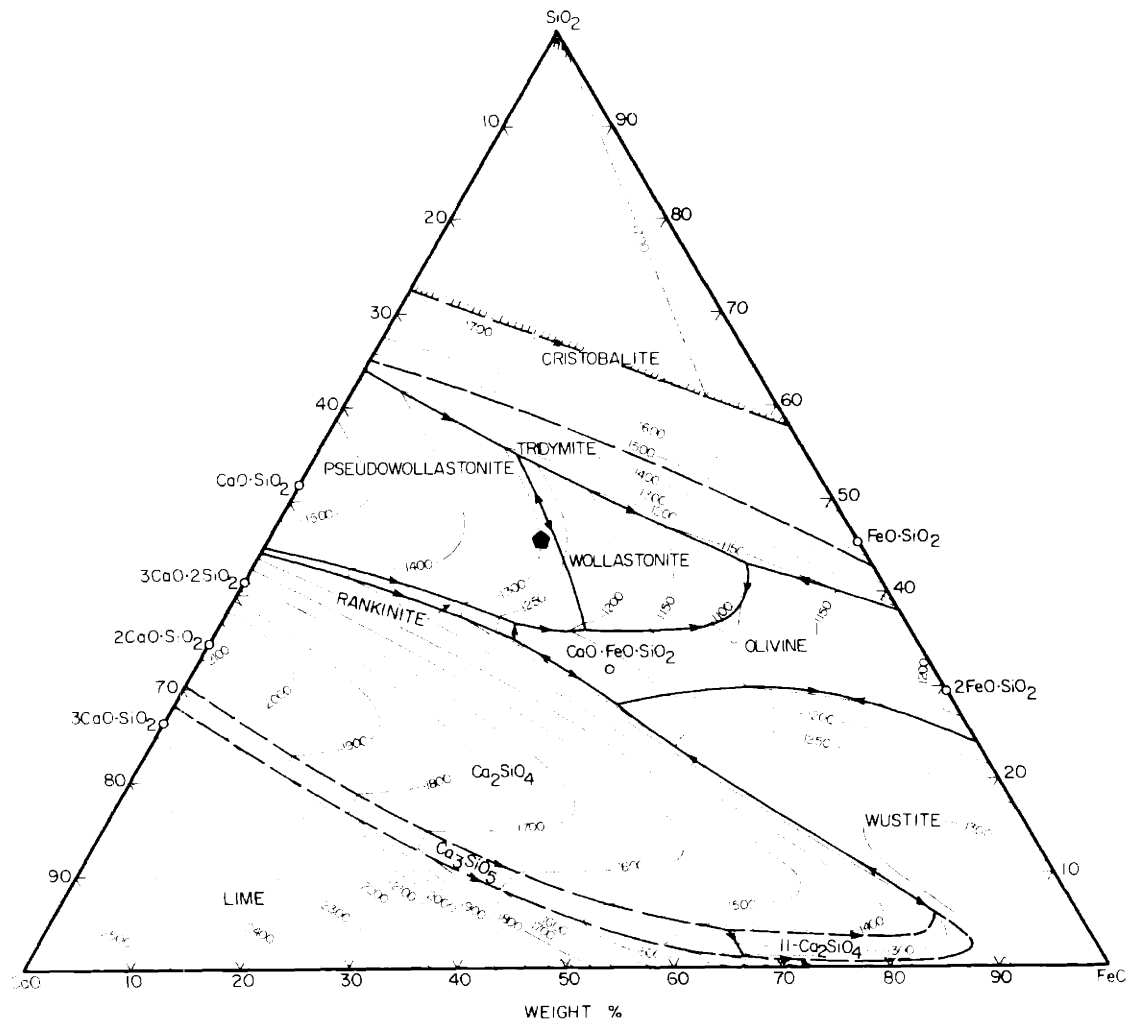


Figure 6.6. MIT No. 241δ: Normalized composition of light phase of Zone 4, plotted on SiO₂-FeO-CaO phase diagram.

The fineness of the dendrite morphology indicates that dendrite growth was constrained. It is likely that these dendrites formed as an exsolution of the Al₂O₃-rich phase over time, and the high viscosity of the matrix phase inhibited their further development. Table 6.2 reports the microprobe analysis of several of these dendrites. Because the probe beam size was approximately the same dimension as the dendrite arm width, it seems clear from the analysis that some of the elements reported likely represent the composition of the surrounding material. In an effort to eliminate these matrix effects I recalculated the dendrite element determinations. These recalculations were carried out

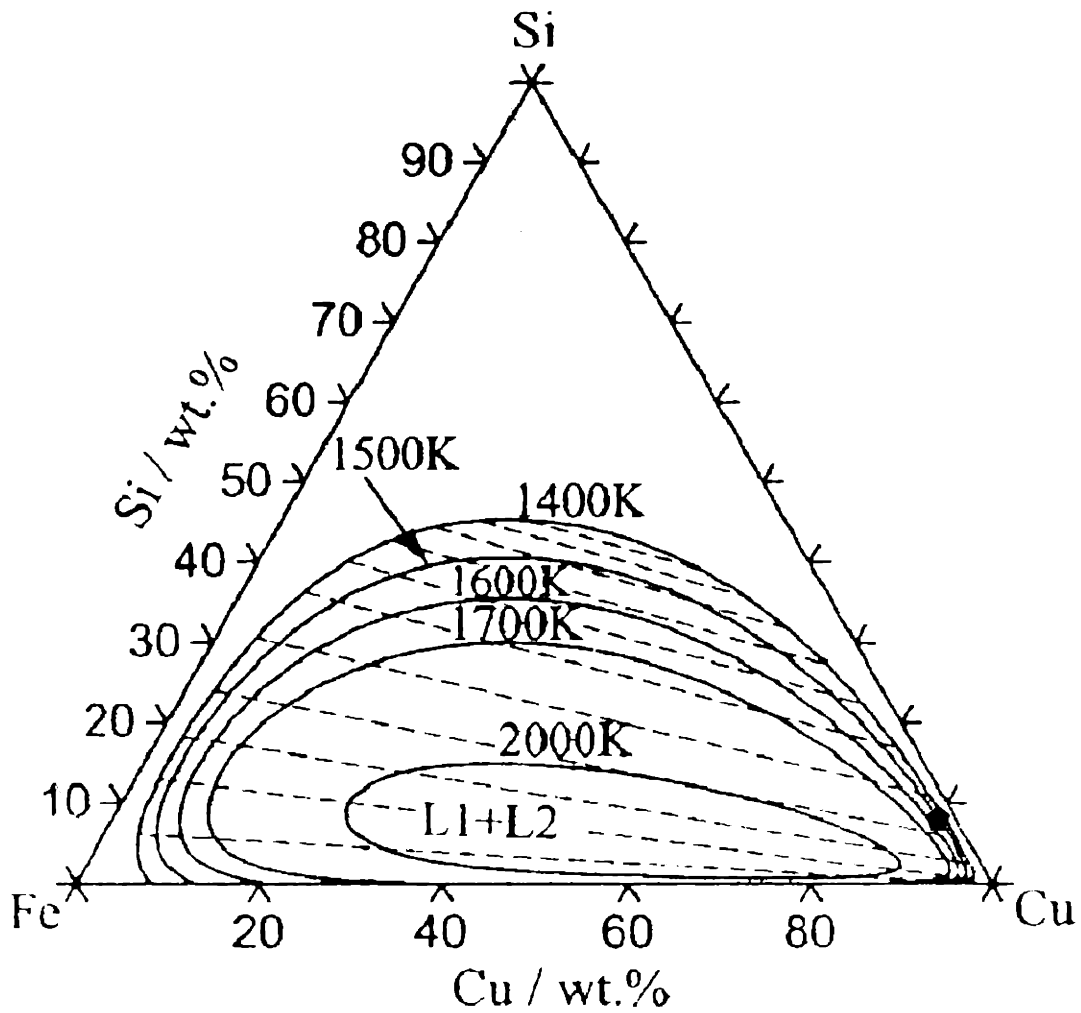


Figure 6.7. MIT No. 241δ: Normalized composition of dark phase of Zone 4 dendrite phase of Zone 4, plotted on Fe-Cu-Si phase diagram (Temperatures given in degrees Kelvin).

Table 6.2. MIT No. 241δ: Recalculation of dendrite composition

Dendrite	Cu	Fe	Mg	Ca	Na	K	Si	Al
Probe analyses	55.165	2.631	0.288	3.62	0.777	1.205	8.17	2.159
Recalculated analyses	53.481	1.491	0.212	0	0.495	0.662	3.163	0.970
Normalized	91.993	2.565					5.442	

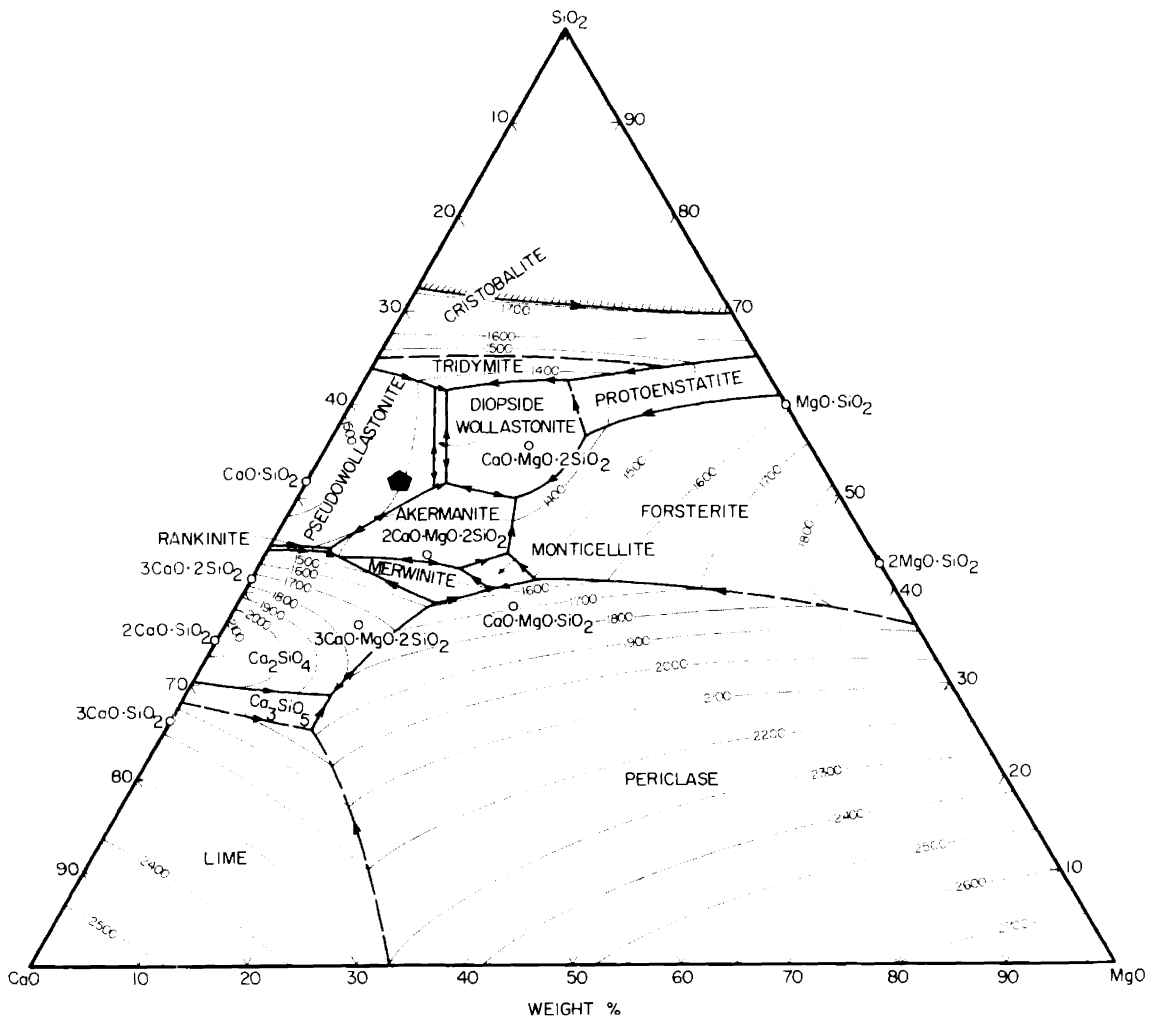


Figure 6.8. MIT No. 241 γ : Normalized composition of dark phase of Zone 4, plotted on SiO₂-MgO-CaO phase diagram.

assuming the absence of CaO (zero wt%). CaO was chosen because of its high concentration in the surrounding matrix and low concentration in the measured dendrite composition. The location of the recalculated dendrite composition has been plotted on the Cu-Fe-Si ternary phase diagram illustrated in Figure 6.7.

The bulk analysis of Zone 4 was calculated based on the volume fraction of the major phases present and the composition of each as determined with microprobe analysis. These estimated values of bulk composition (for MIT Nos. 241 γ and 241 δ) are shown in Table 6.3. Comparing these values with the bulk chemical composition determined for the rest of the crucible, one can

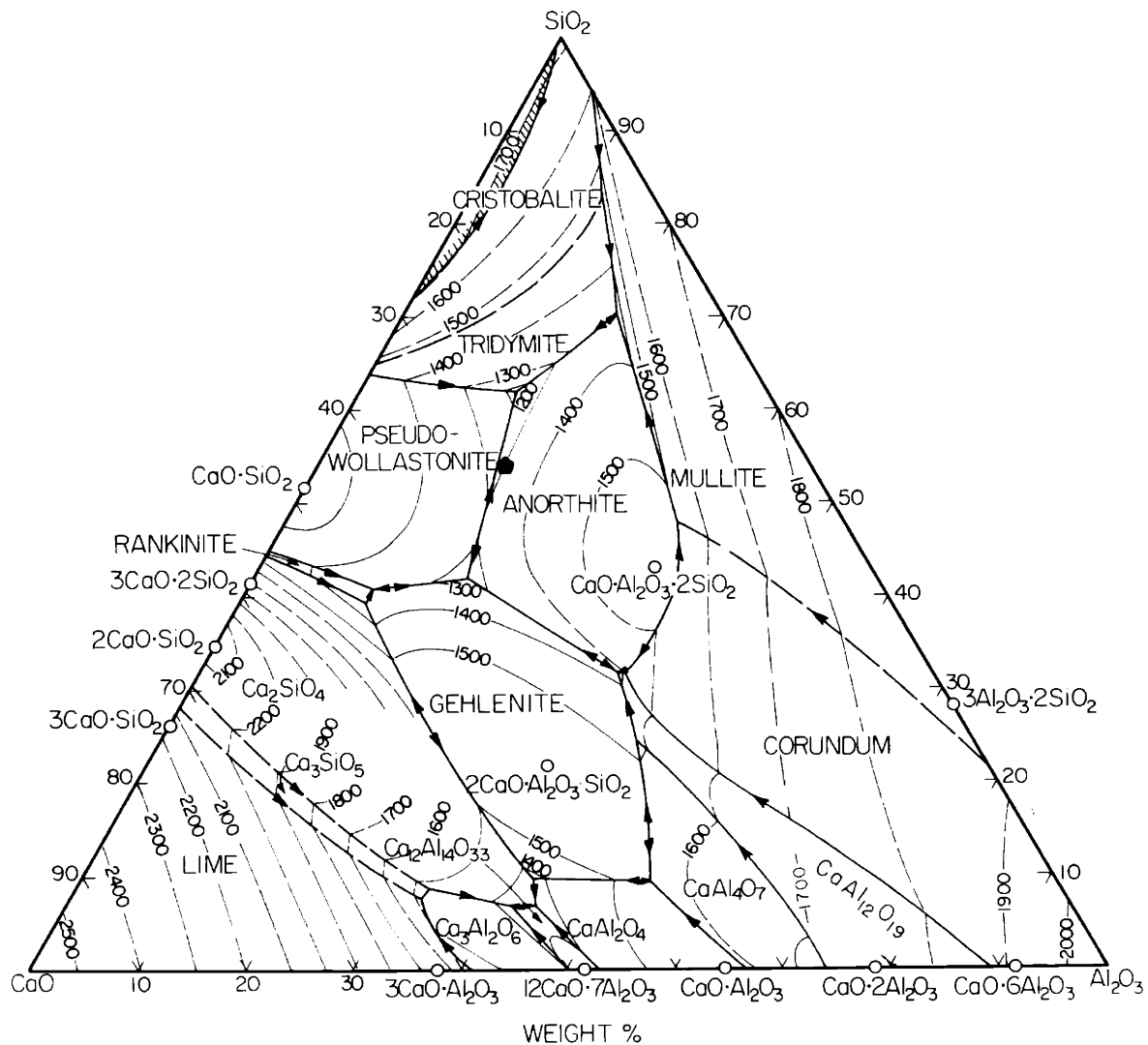


Figure 6.9. MIT No. 241γ: Normalized composition of light phase of Zone 4, plotted on SiO₂-Al₂O₃-CaO phase diagram.

evaluate the overall change in composition in Zone 4 as a result of the metallurgical process taking place within the crucible. Zone 4 exhibits a dramatic increase in the amount of calcium and iron in comparison with the concentration of those elements in the remainder of the sherd, while other constituents either remain the same or decrease in concentration.

The increase in iron is expected for a smelting slag but not for a melting slag (section 1.2 and Tylecote 1976). The increase in calcium is not so easily explained. It could have been contributed to Zone 4 via three sources: the use of a flux, the use of a calcium-rich fuel such as wood ash,

Table 6.3. Estimated composition for Zone 4 of 241 δ and 241 γ based on volume fraction of phases.

MIT No.	SiO ₂	Al ₂ O ₃	Fe ₂ O ₃ *	FeO*	MgO	CaO	Na ₂ O	K ₂ O	SO ₃	CuO*	Cu ₂ O*
241 δ	39.764	8.362	16.408	15.764	3.529	21.535	0.805	1.239	0.011	5.149	3.731
(matrix+ dendrites)	37.047	8.165	32.394	29.148	3.524	19.589	0.848	1.275	0.010	18.963	17.052
241 γ	40.528	9.929	7.188	6.467	4.950	26.779	1.603	0.401	0.022	3.719	3.344

*Copper and iron are reported both in their higher oxidation states and lower oxidation states.

or the gangue associated with the copper ore. Given the 6th millennium date of these Tal-i Iblis metallurgical activities, it is highly unlikely that the inhabitants of Tal-i Iblis levels I and II knew the effects of adding CaO (or other oxides) as a flux to a smelting charge of ore and fuel. The other sources are both likely candidates. It has been shown (Lechtman and Klein 1999) that wood ash can be a major contributor of calcium to a smelting slag. However, we do not see a corresponding increase in the amounts of Na₂O or K₂O in Zone 4, although minerals of both of these elements are also associated with wood ash. As a result of adding wood ash to a crucible, it is possible, but not likely, to find a substantial *increase* in CaO accompanied by a *decrease* in Na₂O and K₂O, as is the case in Zone 4 of MIT No. 241 δ . However, it is most likely that calcium was introduced to the vessel as the limestone (CaCO₃) gangue associated with the copper ore, which converted to CaO under the influence of heat. There are deposits of copper carbonate ore in the veins of a limestone outcrop located less than 10km from Tal-i Iblis. Assuming that Iblis inhabitants mined these ores, residual limestone in the crucible charge is the most likely supplier of calcium to the upper crucible walls.

Chapter VII: Conclusion

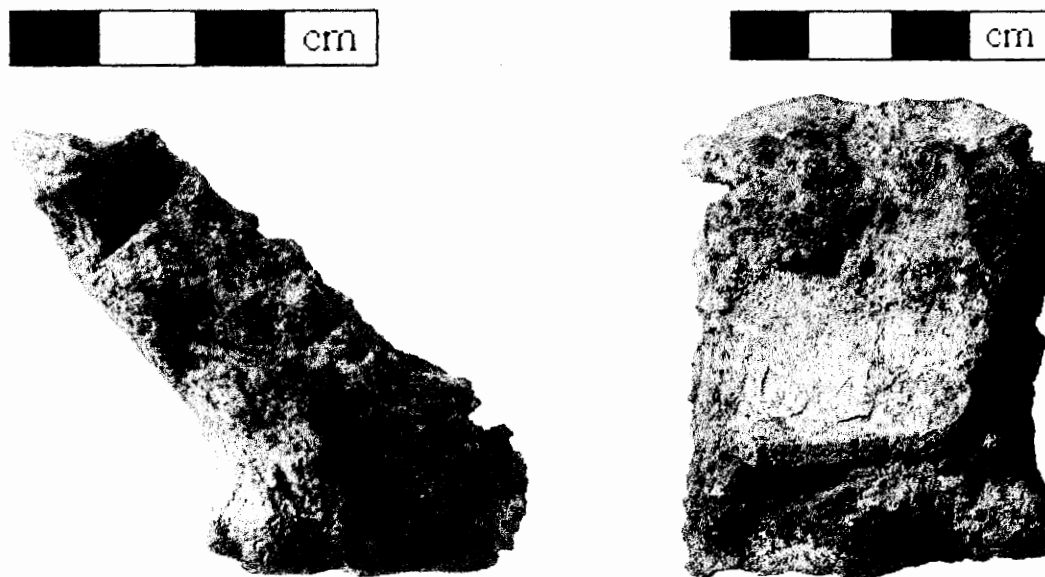
The data reported in this thesis provide strong evidence that the early inhabitants of Tal-i Iblis had developed a crucible-based extractive metallurgical process for reducing local copper carbonate ores to metallic copper. The primary evidence includes: (1) the presence of spherical copper prills in the highly vitrified, upper interior walls of the crucibles; (2) the presence of copper sulfide inclusions containing the suite of elements Ag, As, Ni, Co, and Fe in the copper prills; (3) the increase in iron and the dramatic increase in calcium, likely derived from limestone gangue, in the highly vitrified interior walls of the crucibles.

This conclusion cannot be definitive until further research can be undertaken on a larger corpus of crucible fragments from the site. Perhaps this investigation can continue with the Tal-i Iblis material curated at the University of Georgia at Athens. Nevertheless, the results are internally consistent, compelling, and I report them with a high degree of confidence.

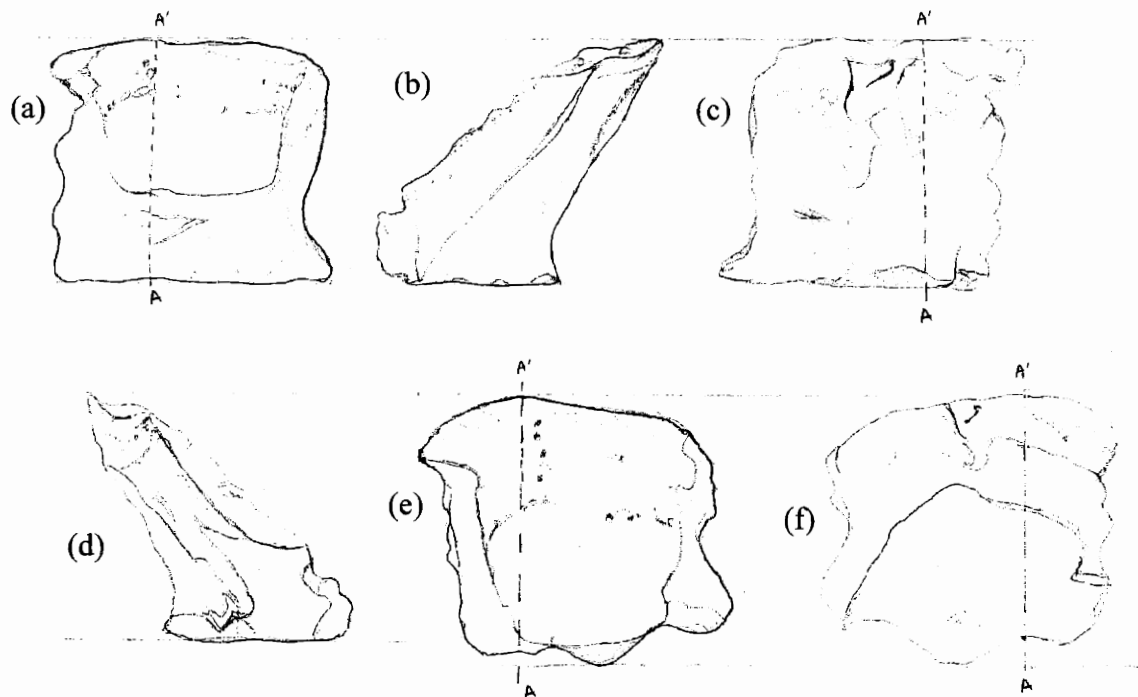
With dates falling unequivocally within the 6th millennium BCE, these laboratory analytical and experimental results make Tal-i Iblis the earliest site in Western Asia and in the world whose archaeological remains indicate the development of a copper extractive metallurgy. I hope that this analysis will enable archaeologists to understand more clearly, the early development and spread of this technology throughout the Old World.

Appendix A

Photographs and drawings of artifacts studied during the thesis research.



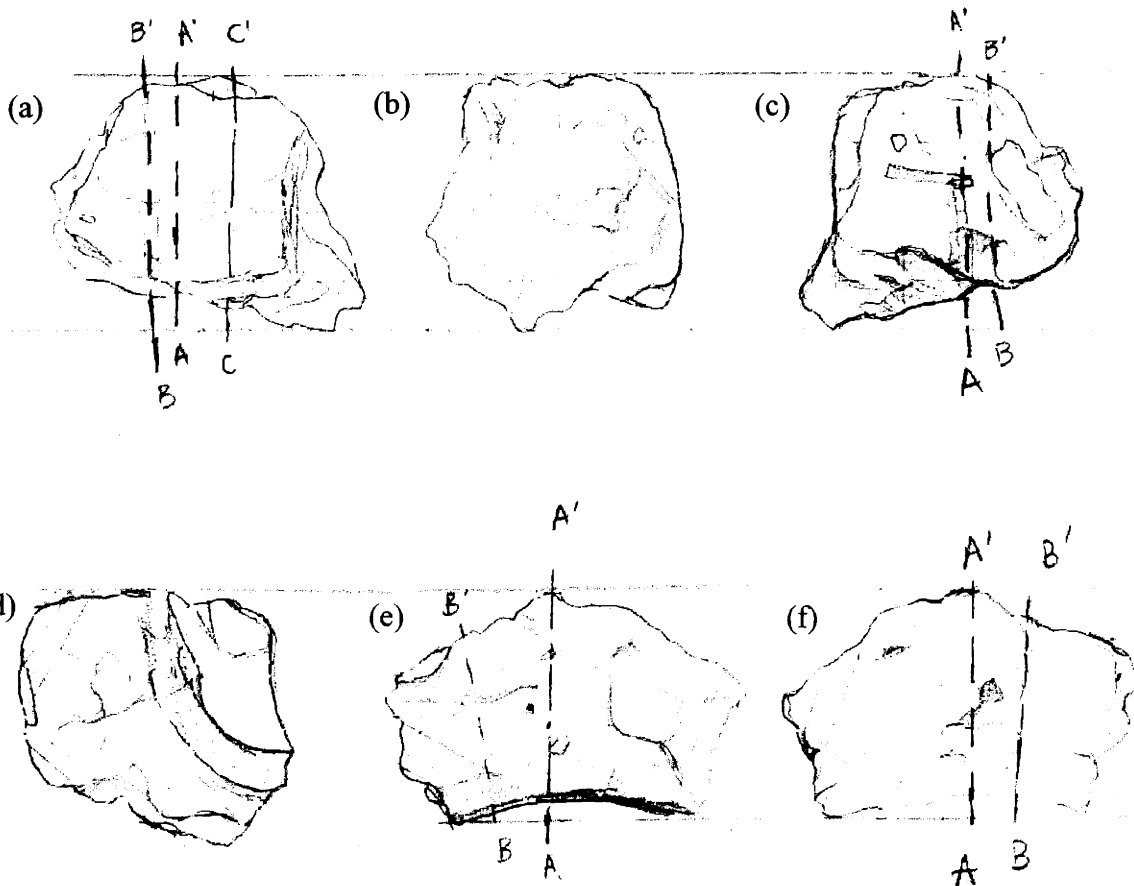
MIT No. 240: Tal-i Iblis Crucible sherd, Level I. Left: profile view; Right: view of interior wall and portion of base.



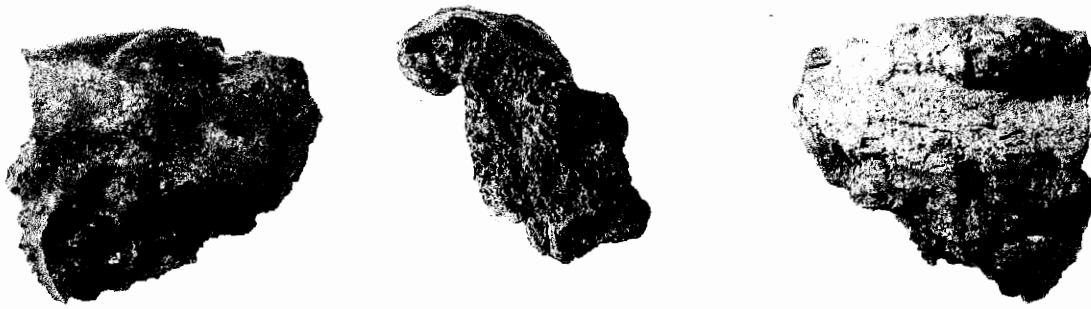
MIT No. 240: Drawings. (a) front; (b) proper left; (c) back; (d) proper right; (e) top; (f) bottom. A-A' line represents the cut made through the sherd prior to analysis.



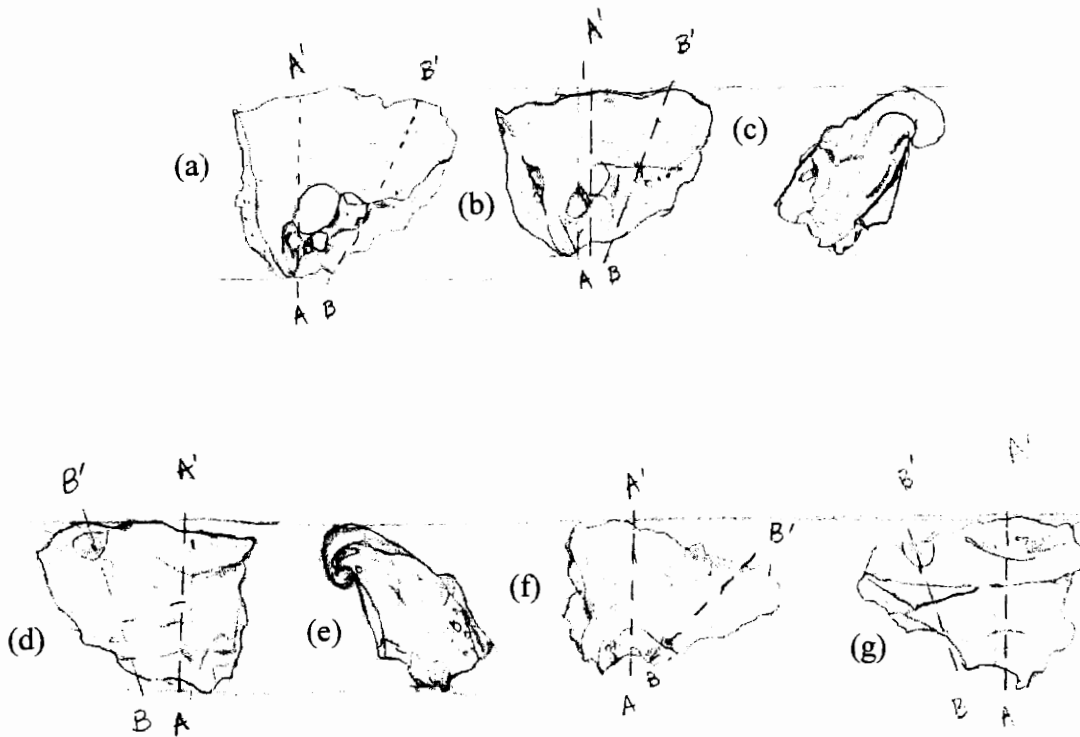
MIT No. 241 β : Tal-i Iblis crucible sherd, Level I and II profile wall. Left: profile view; Right: view of interior surface exhibiting a thick green accretion.



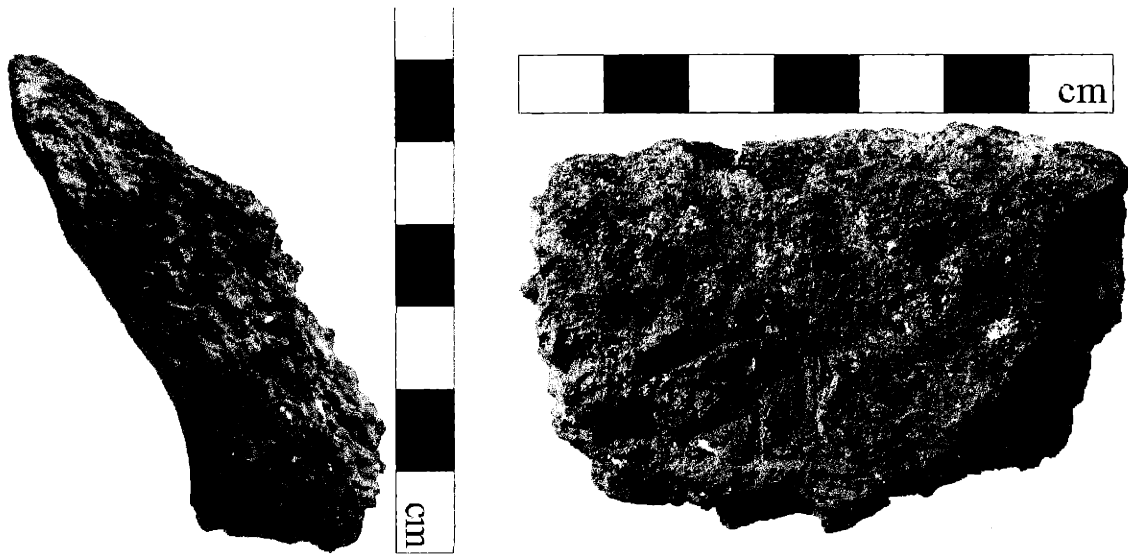
MIT No. 241 β : Drawn. (a) front; (b) proper left; (c) back; (d) proper right; (e) top; (f) bottom. A-A', B-B' and C-C' lines represent the cuts made prior to analysis.



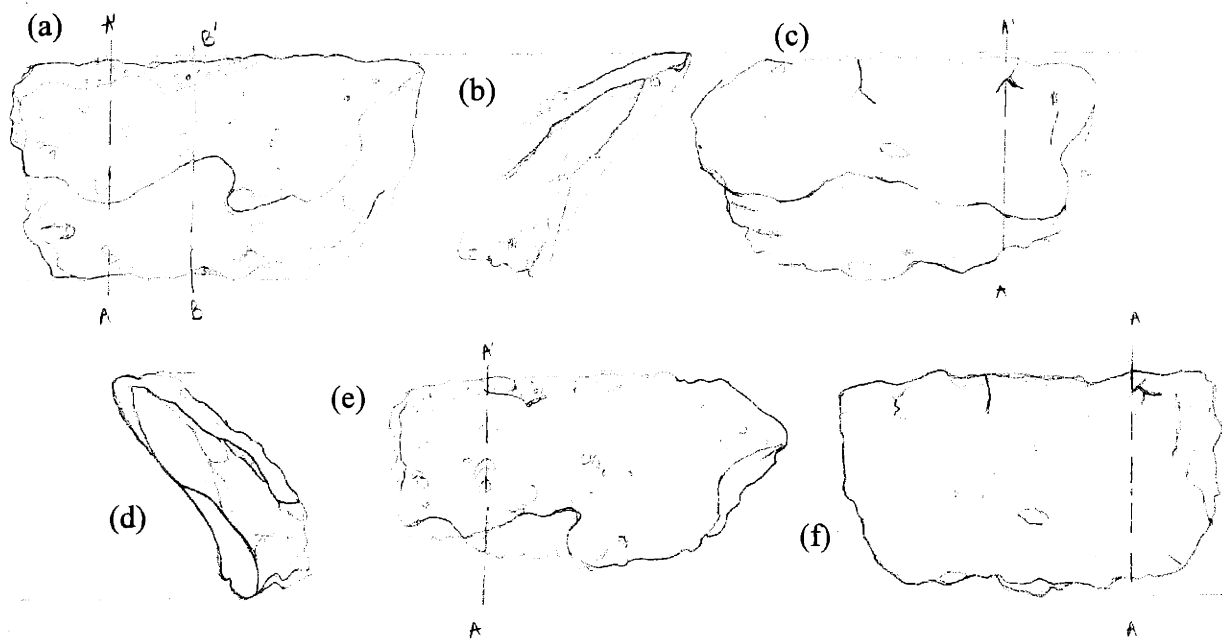
MIT No. 241γ: Tal-i Iblis crucible sherd, Level I and II profile wall. Left: view of interior heavily vitrified surface; Middle: profile view with slumped rim shown; Right: view of exterior surface.



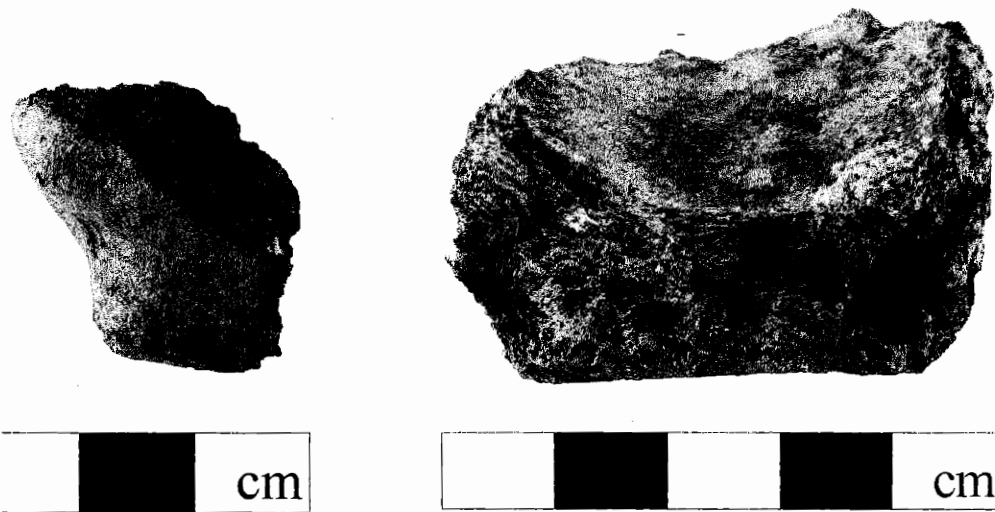
MIT No. 241γ: Drawn. (a) interior; (b) front; (c) proper left; (d) back; (e) proper right; (f) top; (g) bottom. A-A' and B-B' lines represent the cuts made prior to analysis.



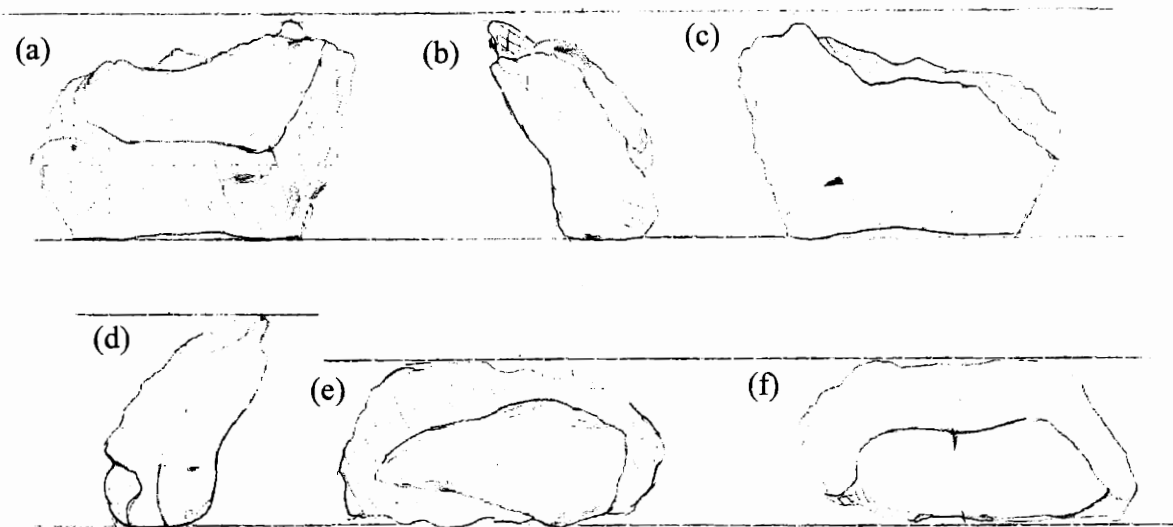
MIT No. 241δ: Tal-i Iblis crucible sherd, Level I and II profile wall. Left: profile view; Right: view of interior surface.



MIT No 241δ: Drawn. (a) front; (b) proper left; (c) back; (d)proper right; (e) top; (f) bottom. A-A' and B-B' represent the cuts made prior to analysis.



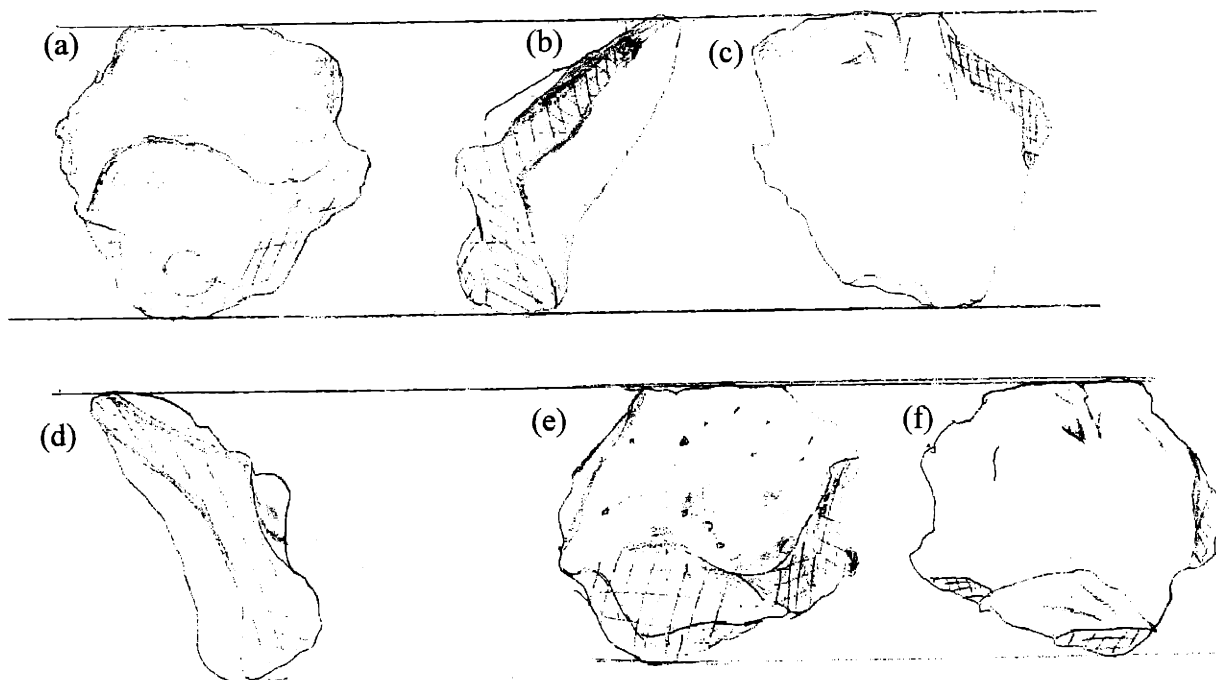
MIT No. 241ε: Tal-i Iblis crucible sherd, Level I and II profile wall. Left: profile view; Right: view of interior surface showing green residue.



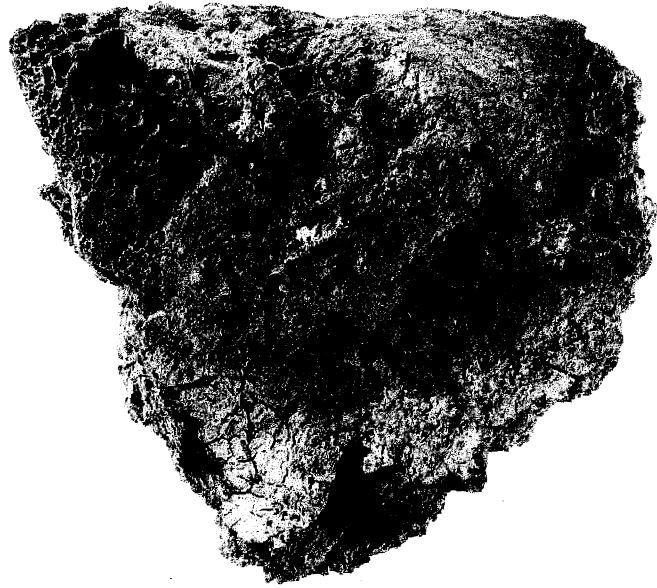
MIT No. 241ε: Drawn. (a) front; (b) proper right; (c) back; (d) proper left; (e) top; (f) bottom.



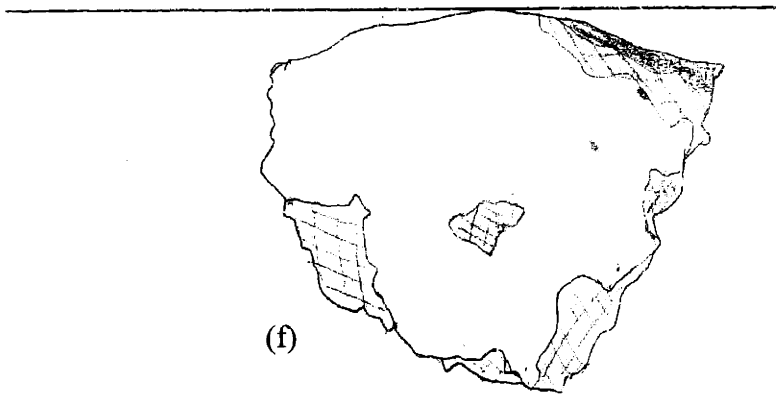
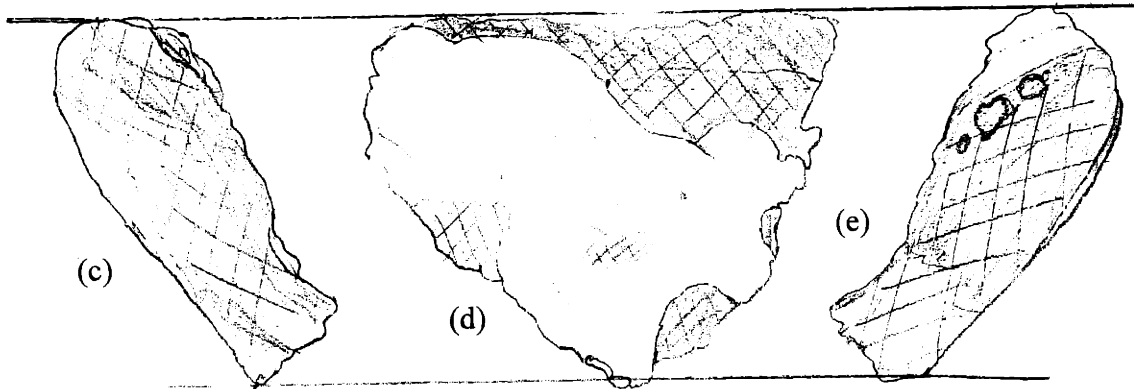
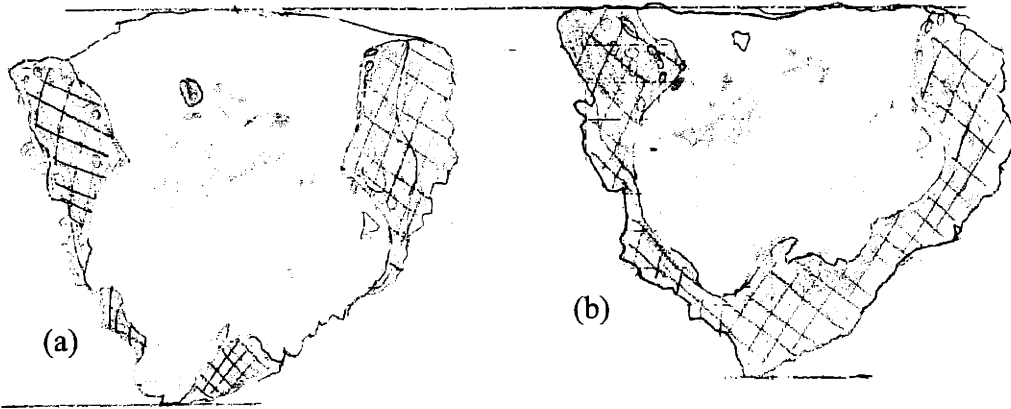
MIT No. 241η: Tal-i Iblis crucible sherd, Level I and II profile wall. Left: profile view; Right: view of interior surface.



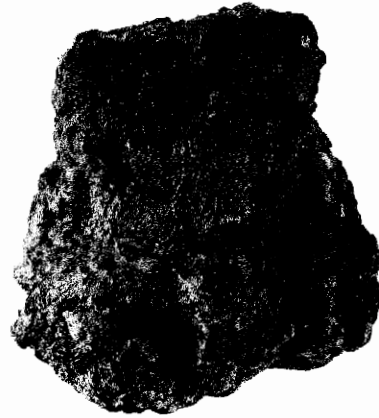
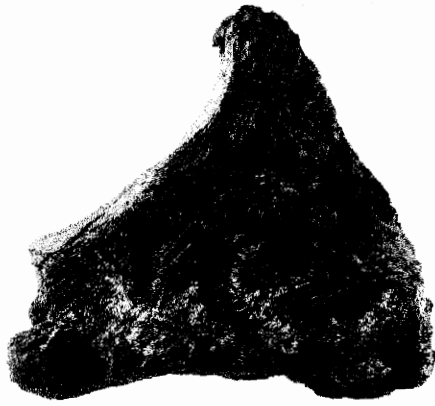
MIT No. 241η: Drawn. (a) front; (b) proper left; (c) back; (d) proper right; (e) top; (f) bottom.



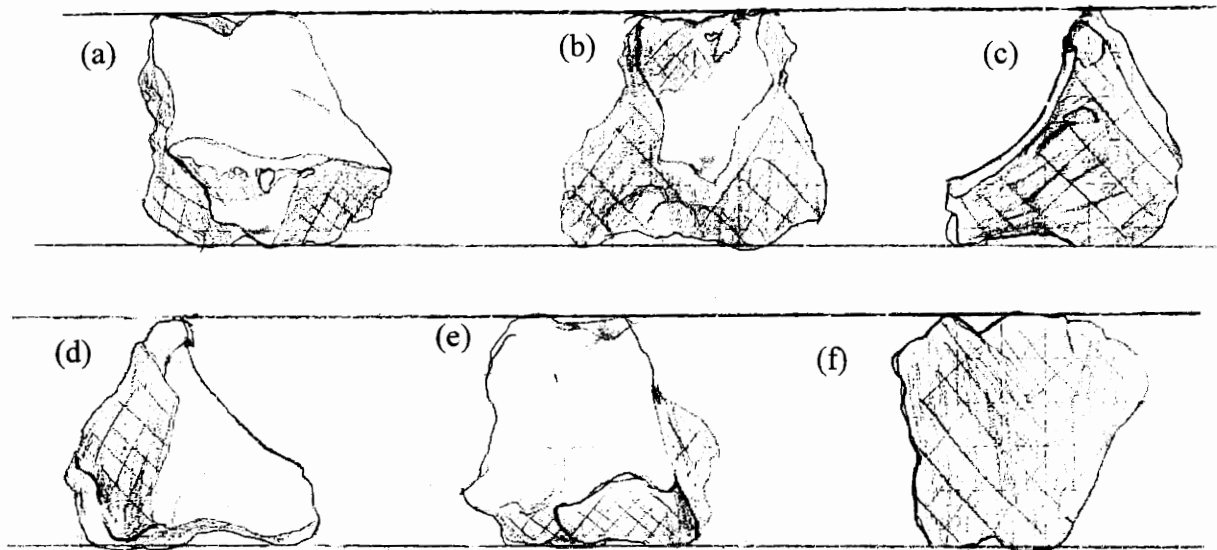
MIT No. 245: Tal-i Iblis crucible sherd, Level V. Left: profile view (this sherd is much larger than any of the other ones, and it is also from a much later level); Right: view of interior surface.



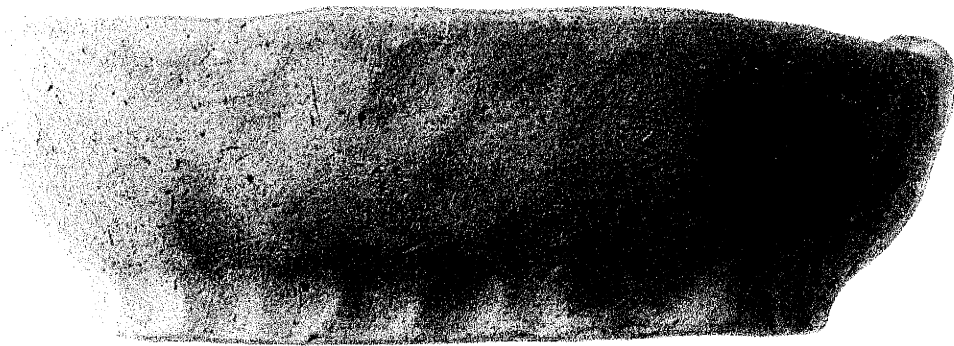
MIT No. 245: Drawn. (a) front; (b)top ; (c)proper right; (d)back; (e)proper left; (f) bottom.



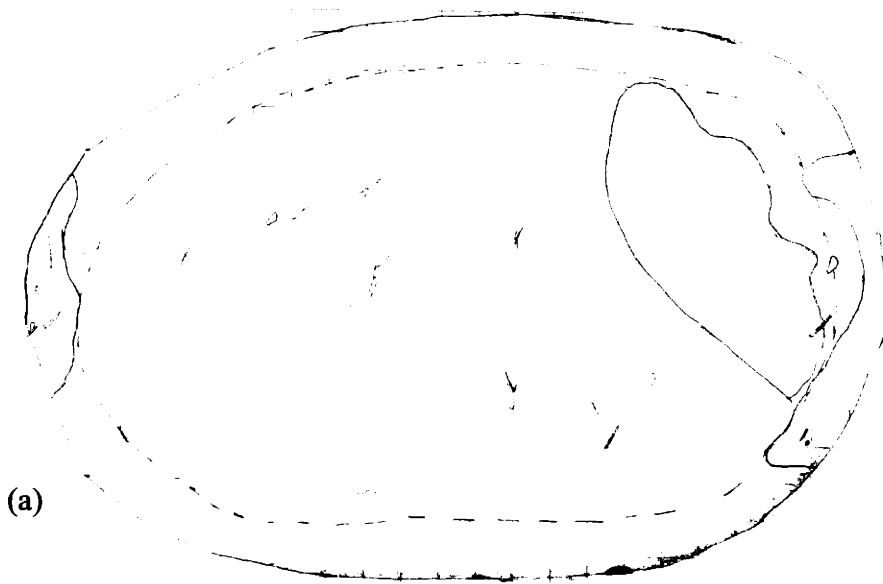
MIT No. 5274: Tal-i Iblis crucible sherd, collected by Prof. Smith. Left: profile view; Right: view of interior surface.



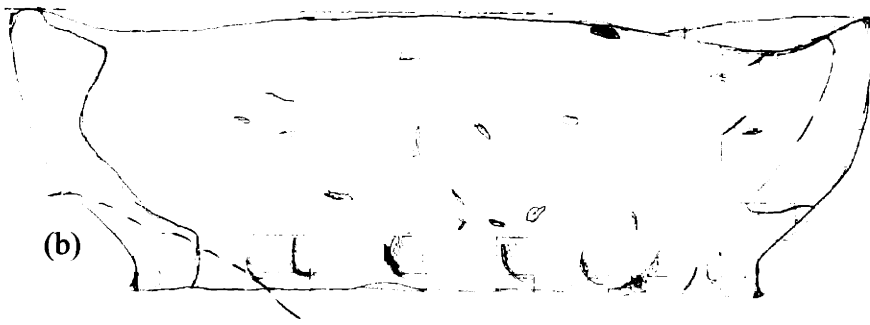
MIT No. 5274: Drawn. (a) back; (b) front; (c) proper right; (d) proper left; (e) top; (f) bottom.



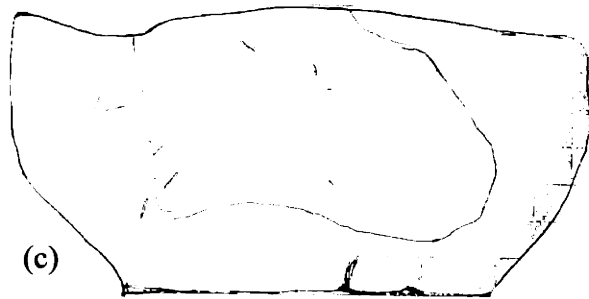
MIT No. 5277: Modern crucible replica; Top: view of interior from above; Bottom: profile view



(a)

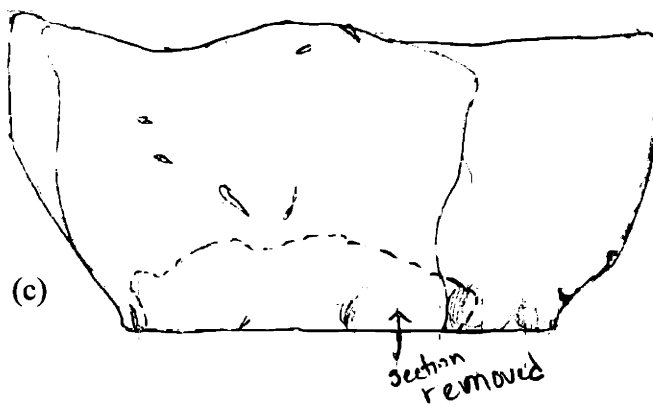
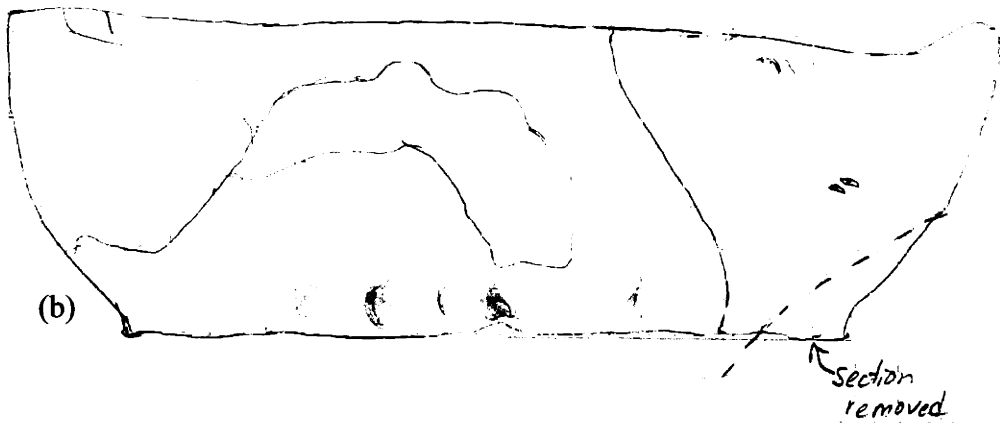
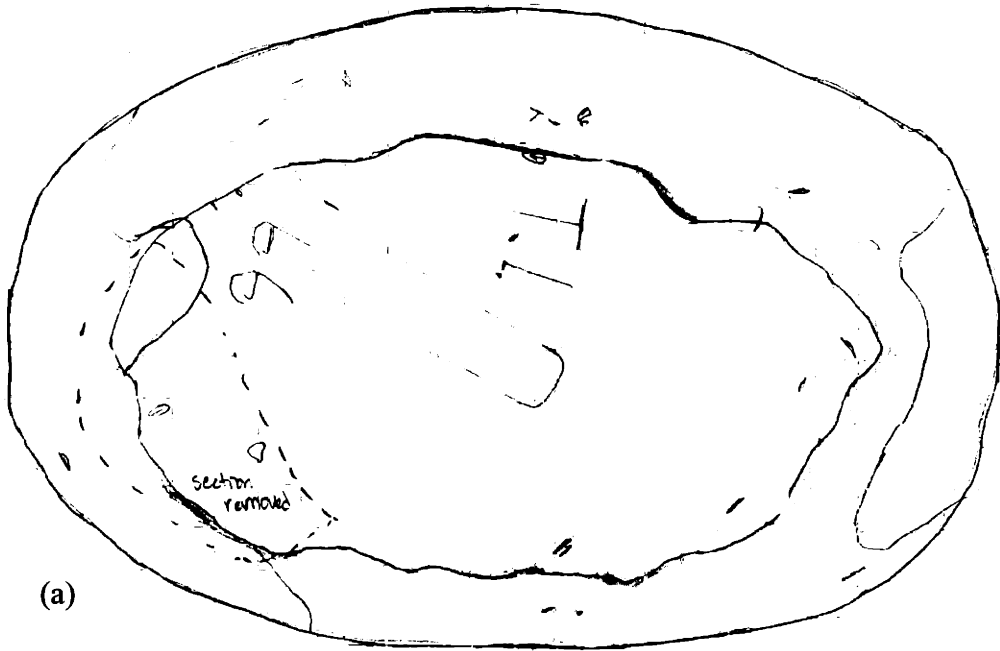


(b)



(c)

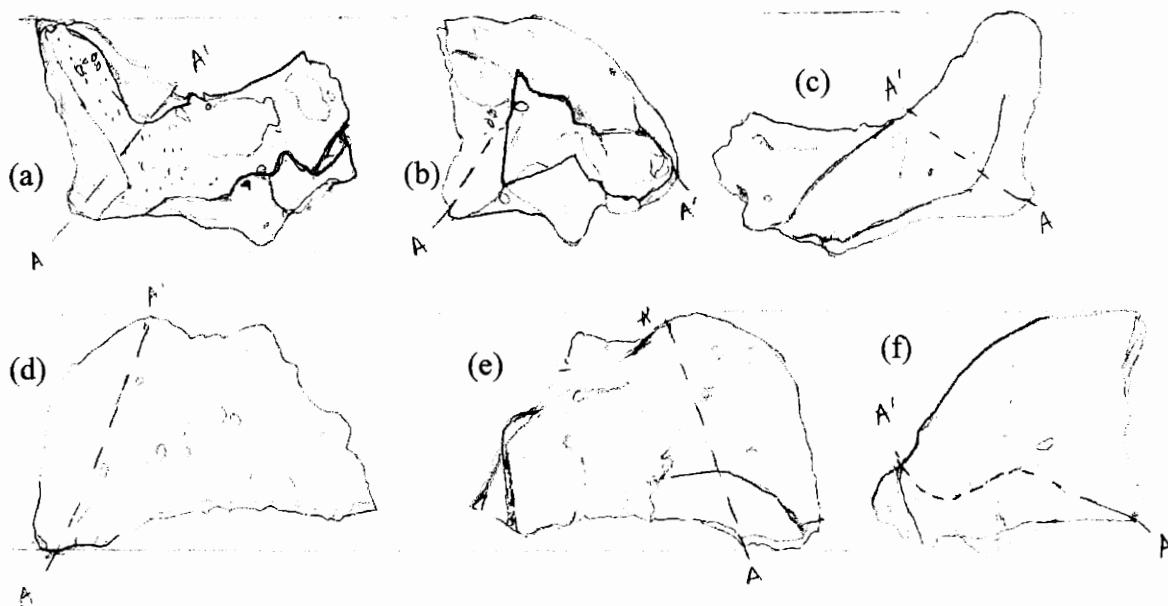
MIT No. 5277: Drawn. (a) top view; (b) long profile view; (c) short profile view. Dotted line indicates section removed for analysis.



MIT No. 5277: Drawn. (a) bottom view; (b) long profile view; (c) short profile view. Dotted line indicates section removed for analysis.

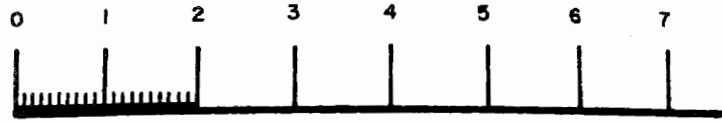


MIT No. 5279: Modern replica crucible sherd used in experiment at Tal-i Iblis in 1967. Left: top view; Right: profile view showing slumped rim.

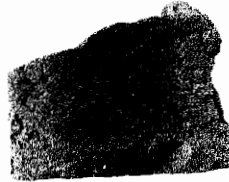


MIT No. 5279: Drawn. (a) front; (b) proper left; (c) back; (d) top; (e) bottom; (f) proper right. Line A-A' indicates cut made for analysis.

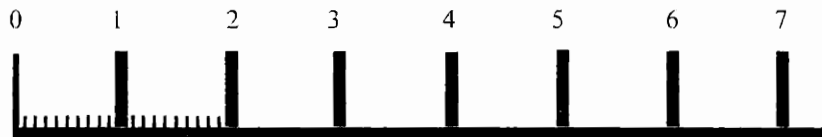
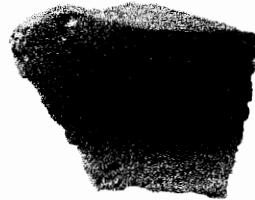
Re-fired samples from MIT No. 5277



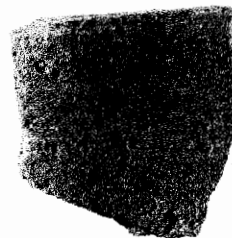
5277D
300°C

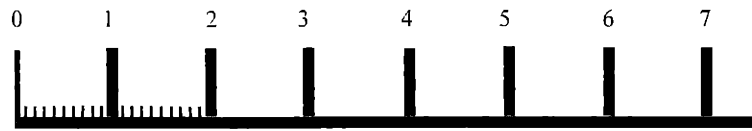


5277C
400°C

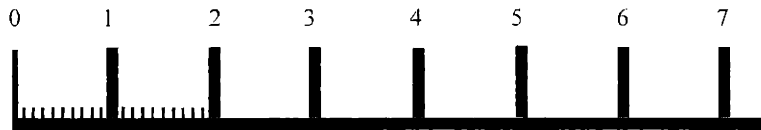
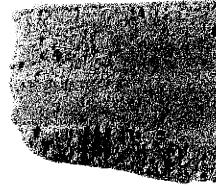


5277B
500°C

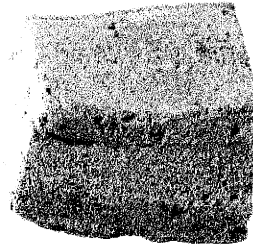




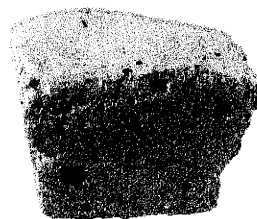
5277E
600°C

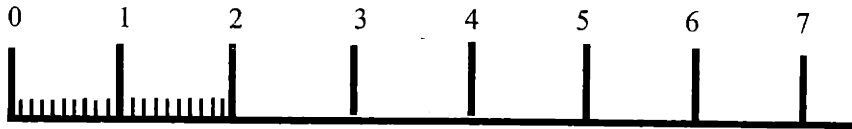


5277G
700°C

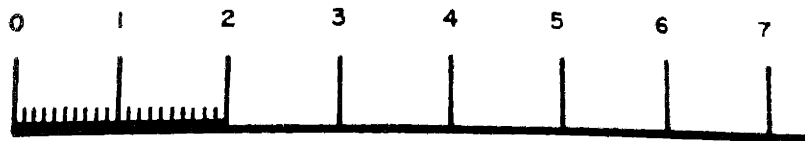
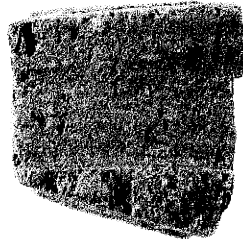


5277I
800°C

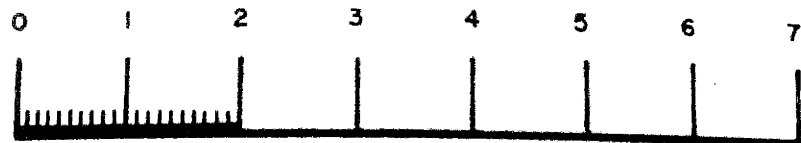




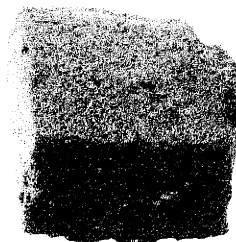
5277F
900°C

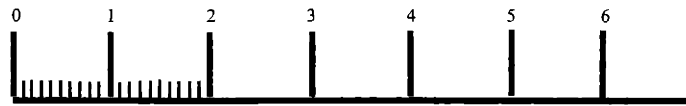


5277L
1000°C

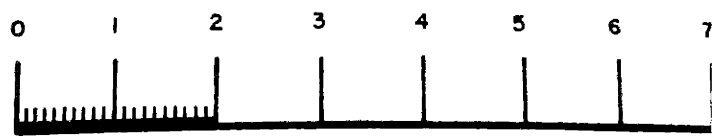
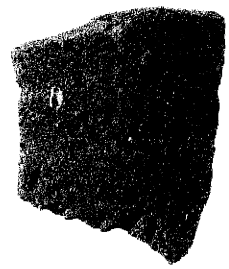


5277N
1100°C

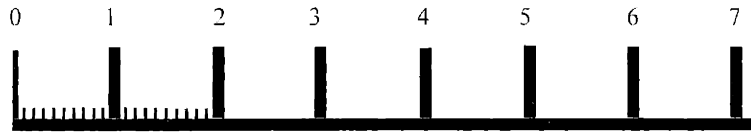
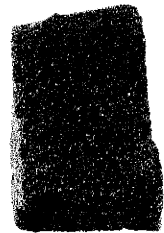




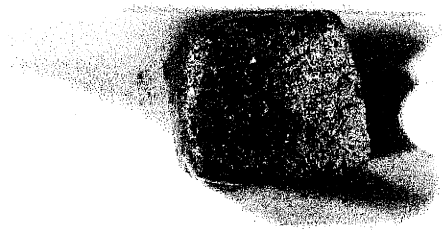
5277J
1125°C

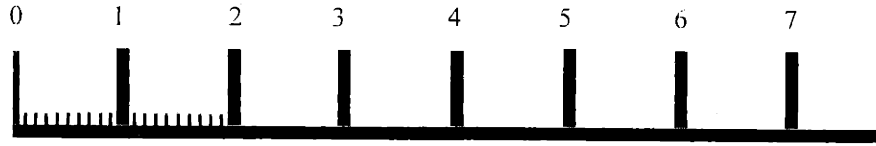


5277U
1150°C



5277Q
1175°C





5277T
1200°C

Ele Wt%										
Quant#	Label	Cu	Fe	As	Co	Ni	Ag	S	Total	
1	Tal-i Iblis mit241D Prill1	97.96	0.7102	0	0.0189	0.0258	0.0478	0.6898	99.45	
2	Tal-i Iblis mit241D Prill2	96.61	1.5292	0	0.0055	0	0.0332	0.1932	98.38	
3	Tal-i Iblis mit241D Prill3	79.15	1.2549	0	0	0	0.0738	0.2914	80.77	
4	Tal-i Iblis mit241D Prill4	100.67	1.0862	0.0434	0.0135	0.103	0.1285	0.187	102.23	
5	Tal-i Iblis mit241D Prill5	51.02	0.593	0	0	0	0	0	51.62	
6	Tal-i Iblis mit241D Prill6	85.72	0.9575	0	0.0515	0.0225	0	0	86.75	
7	Tal-i Iblis mit241D Dendrite1	49.27	2.0818	0	0	0	0	0	51.35	
		Ele Wt%								
Quant#	Label	Cu	Fe	As	Co	Ni	Ag	S	Total	
1	Tal-i Iblis mit241G Large Prill	96.42	0.0319	0	0.2028	0.3257	0.19	0	97.17	
2	Tal-i Iblis mit241G Large Prill	97.38	0.0458	0	0.2053	0.2879	0.167	0	98.09	
3	Tal-i Iblis mit241G Large Prill	98.68	0.0599	0	0.2002	0.3229	0.1864	0	99.45	
4	Tal-i Iblis mit241G Large Prill	96.79	0.0384	0	0.1981	0.3053	0.2283	0.0088	97.57	
5	Tal-i Iblis mit241G Large Prill	96.86	0.034	0	0.1759	0.3548	0.1515	0.0088	97.58	
6	Tal-i Iblis mit241G Large Prill inclusion	78.05	0.024	0.7085	0.1768	0.2934	0.1419	13.49	92.88	
7	Tal-i Iblis mit241G Large Prill inclusion	73.76	0.0059	2.3624	0.1759	0.2507	0.1554	10.14	86.85	
8	Tal-i Iblis mit241G Large Prill inclusion	76.82	0.0553	0.1528	0.1308	0.2655	0.1803	14.6	92.2	
9	Tal-i Iblis mit241G Large Prill inclusion	78.5	0.0428	0.2418	0.1969	0.2309	0.14	14.82	94.17	

NormEI%

ant#	Label	Cu	Fe	As	Co	Ni	Ag	S
1	Tal-i Iblis mit241D Prill1	98.5	0.7141	0	0.019	0.0259	0.0481	0.6936
2	Tal-i Iblis mit241D Prill2	98.21	1.5544	0	0.0056	0	0.0337	0.1964
3	Tal-i Iblis mit241D Prill3	97.99	1.5536	0	0	0	0.0913	0.3608
4	Tal-i Iblis mit241D Prill4	98.47	1.0626	0.0424	0.0132	0.1007	0.1257	0.183
5	Tal-i Iblis mit241D Prill5	98.85	1.1488	0	0	0	0	0
6	Tal-i Iblis mit241D Prill6	98.81	1.1037	0	0.0594	0.026	0	0
7	Tal-i Iblis mit241D Dendrite1	95.95	4.05	0	0	0	0	0
		NormEI%						
ant#	Label	Cu	Fe	As	Co	Ni	Ag	S
1	Tal-i Iblis mit241G Large Prill	99.23	0.0328	0	0.2087	0.3352	0.1956	0
2	Tal-i Iblis mit241G Large Prill	99.28	0.0467	0	0.2093	0.2935	0.1703	0
3	Tal-i Iblis mit241G Large Prill	99.23	0.0603	0	0.2013	0.3247	0.1874	0
4	Tal-i Iblis mit241G Large Prill	99.2	0.0394	0	0.203	0.3129	0.234	0.009
5	Tal-i Iblis mit241G Large Prill	99.26	0.0348	0	0.1803	0.3636	0.1553	0.009
6	Tal-i Iblis mit241G Large Prill inclusion	84.03	0.0258	0.7629	0.1904	0.3159	0.1528	14.52
7	Tal-i Iblis mit241G Large Prill inclusion	84.93	0.0068	2.72	0.2025	0.2887	0.1789	11.67
8	Tal-i Iblis mit241G Large Prill inclusion	83.32	0.06	0.1658	0.1419	0.2879	0.1955	15.83
9	Tal-i Iblis mit241G Large Prill inclusion	83.36	0.0455	0.2568	0.209	0.2452	0.1487	15.73

Atomic

Quant#	Label	Cu	Fe	As	Co	Ni	Ag	S	CatTot
1	Tal-i Iblis mit241D Prill1	97.753	0.8063	0	0.0203	0.0278	0.0281	1.364	100
2	Tal-i Iblis mit241D Prill2	97.825	1.7616	0	0.006	0	0.0198	0.3877	100
3	Tal-i Iblis mit241D Prill3	97.477	1.7583	0	0	0	0.0535	0.7112	100
4	Tal-i Iblis mit241D Prill4	98.2	1.2056	0.0359	0.0142	0.1087	0.0738	0.3616	100
5	Tal-i Iblis mit241D Prill5	98.695	1.305	0	0	0	0	0	100
6	Tal-i Iblis mit241D Prill6	98.654	1.2537	0	0.0639	0.0281	0	0	100
7	Tal-i Iblis mit241D Dendrite1	95.413	4.587	0	0	0	0	0	100
		Atomic							
Quant#	Label	Cu	Fe	As	Co	Ni	Ag	S	CatTot
1	Tal-i Iblis mit241G Large Prill	99.259	0.0373	0	0.2251	0.3628	0.1152	0	100
2	Tal-i Iblis mit241G Large Prill	99.303	0.0531	0	0.2257	0.3177	0.1003	0	100
3	Tal-i Iblis mit241G Large Prill	99.252	0.0686	0	0.2171	0.3515	0.1104	0	100
4	Tal-i Iblis mit241G Large Prill	99.242	0.0448	0	0.219	0.3388	0.1379	0.0179	100
5	Tal-i Iblis mit241G Large Prill	99.263	0.0396	0	0.1944	0.3935	0.0915	0.0179	100
6	Tal-i Iblis mit241G Large Prill inclusion	73.631	0.0257	0.5669	0.1799	0.2995	0.0789	25.218	100
7	Tal-i Iblis mit241G Large Prill inclusion	76.502	0.0069	2.0779	0.1967	0.2814	0.0949	20.84	100
8	Tal-i Iblis mit241G Large Prill inclusion	72.146	0.0591	0.1217	0.1325	0.2698	0.0997	27.171	100
9	Tal-i Iblis mit241G Large Prill inclusion	72.245	0.0448	0.1887	0.1953	0.23	0.0759	27.02	100

MDL:EI%

ant#	Label	Cu	Fe	As	Co	Ni	Ag	S	X	Y
1	Tal-i Iblis mit241D Prill1	0.19543	0.11548	0.18728	0.00181	0.14841	0.01194	0.0503	32.473	36.108
2	Tal-i Iblis mit241D Prill2	0.01038	0.00209	0.1873	0.00181	0.14843	0.01195	0.05031	32.465	36.188
3	Tal-i Iblis mit241D Prill3	0.01038	0.00209	0.18733	0.00181	0.14845	0.01195	0.05032	32.48	36.251
4	Tal-i Iblis mit241D Prill4	0.01038	0.00209	0.18727	0.00181	0.1484	0.01194	0.0503	35.362	39.109
5	Tal-i Iblis mit241D Prill5	0.01038	0.00209	0.18736	0.00181	0.14847	0.01195	0.05033	36.755	43.342
6	Tal-i Iblis mit241D Prill6	0.01038	0.00209	0.18736	0.00181	0.14847	0.01195	0.05033	36.603	43.356
7	Tal-i Iblis mit241D Dendrite1	0.01038	0.00209	0.18738	0.00181	0.14849	0.01195	0.05033	36.103	40.529
		MDL:EI%								
ant#	Label	Cu	Fe	As	Co	Ni	Ag	S	X	Y
1	Tal-i Iblis mit241G Large Prill	0.01036	0.00209	0.18697	0.00181	0.14816	0.01192	0.05022	65.949	39.828
2	Tal-i Iblis mit241G Large Prill	0.00518	0.00104	0.09346	0.0009	0.07406	0.00596	0.0251	65.959	39.854
3	Tal-i Iblis mit241G Large Prill	0.00518	0.00104	0.09348	0.0009	0.07408	0.00596	0.02511	65.875	39.757
4	Tal-i Iblis mit241G Large Prill	0.00518	0.00104	0.09346	0.0009	0.07407	0.00596	0.02511	65.971	39.785
5	Tal-i Iblis mit241G Large Prill	0.00518	0.00104	0.09346	0.0009	0.07407	0.00596	0.02511	65.948	39.871
6	Tal-i Iblis mit241G Large Prill inclusion	0.00518	0.00104	0.0935	0.0009	0.07409	0.00596	0.02511	65.936	39.822
7	Tal-i Iblis mit241G Large Prill inclusion	0.00518	0.00104	0.09354	0.0009	0.07413	0.00597	0.02513	65.902	39.799
8	Tal-i Iblis mit241G Large Prill inclusion	0.00519	0.00105	0.09364	0.00091	0.07421	0.00597	0.02515	65.922	39.757
9	Tal-i Iblis mit241G Large Prill inclusion	0.00519	0.00105	0.0937	0.00091	0.07426	0.00598	0.02517	65.984	39.895

Input numbers in the yellow region; see output in the blue region.

All Fe considered as Fe²⁺, and all Cu considered as Cu⁺ (lower oxidation states)

		Si	Al	Fe	Mg	Ca	Na	K	S	Cu	O	To
at-wt		28.09	26.98	55.85	24.31	40.08	22.99	39.10	32.07	63.40	16.00	
		Si	Al	Fe	Mg	Ca	Na	K	S	Cu	O	To
1	Tal-i Iblis mit241D Bright crystal1	0.2018	0.7438	60.33	1.9538	0.41	0	0.0598		7.59	28.52	
2	Tal-i Iblis mit241D Bright crystal2	0.0407	0.8182	62.82	1.616	0.2711	0	0		3.62	28.89	
3	Tal-i Iblis mit241D Bright crystal2 rim	0.1261	0.6641	36.83	0.3412	0.3027	0.0751	0.028		37.67	22.96	
4	Tal-i Iblis mit241D Bright crystal3	0.042	0.7323	62.18	0.8482	0.2246	0	0.0461		5.1	23.77	
5	Tal-i Iblis mit241D Dendrite2	8.17	2.1594	3.18	0.2879	3.62	0.777	1.205		61.06	19.56	
6	Tal-i Iblis mit241D Matrix light phase1	16.77	4.07	17.11	3.38	16.09	0.1489	0		0.6754	40.46	
7	Tal-i Iblis mit241D Matrix light phase1	17.72	4.33	15.76	3.27	15.28	0.2825	0.4586		0.791	40.64	
8	Tal-i Iblis mit241D Matrix light phase3	17.04	3.9	16.52	3.73	16.03	0.1373	0.0018		0.5881	40.31	
9	Tal-i Iblis mit241D Matrix dark phase1	20.67	4.95	4.15	0.3385	14.16	1.1951	2.179		7.79	41.23	
10	Tal-i Iblis mit241D Matrix dark phase2	20.64	4.77	4.8	0.51	15.39	0.9304	1.921		6.62	40.91	
11	Tal-i Iblis mit241D Matrix dark phase2	20.23	4.89	5.06	0.0818	14.95	1.335	2.5699	0.0317	6.29	41.06	
		Si	Al	Fe	Mg	Ca	Na	K	S	Cu	O	To
1	Tal-i Iblis mit241G Matrix dark crystals	19.01	4.08	2.1653	4.81	24.42	1.9955	0.0221	0	0.4255	41.36	
2	Tal-i Iblis mit241G Matrix dark crystals	19.09	3.99	1.7858	5.09	24.84	1.8266	0.0184	0	0.4787	41.97	
3	Tal-i Iblis mit241G Matrix dark crystals	19.08	3.78	1.8595	5.14	24.63	1.8339	0.0062	0	0.4271	41.3	
4	Tal-i Iblis mit241G Matrix light phase	18.99	6.52	7.17	1.1916	14.62	0.6942	0.6711	0.0158	5.31	40.49	
5	Tal-i Iblis mit241G Matrix light phase	18.59	6.31	6.74	1.353	15.16	0.7311	0.6126	0.0135	5.45	40.31	
6	Tal-i Iblis mit241G Matrix light phase	18.99	5.93	8.26	1.7585	15.04	0.5463	0.442	0.0158	3.94	40.47	
		Si	Al	Fe	Mg	Ca	Na	K	S	Cu	O	To
1	Tal-i Iblis mit5277Q Matrix dark phase	24.78	14.12	0.1703	0	6.52	4.47	0.0736	0	0	47.83	
2	Tal-i Iblis mit5277Q Matrix light phase	25.45	7.67	4.55	3.05	5.9	1.9601	2.0292	0	0	46.76	

Output numbers in the yellow region; see output in the blue region.

If Fe considered as Fe2+, and all Cu considered as Cu+ (lower oxidation states)

at-wt

	SiO2	Al2O3	Fe2O3	FeO	MgO	CaO	Na2O	K2O	SO3	CuO	Cu2O	Total
Tal-i Iblis mit241D Bright crystal1	0.43	1.41		77.61	3.24	0.57	0.00	0.07	0.00		8.55	
Tal-i Iblis mit241D Bright crystal2	0.09	1.55		80.82	2.68	0.38	0.00	0.00	0.00		4.08	
Tal-i Iblis mit241D Bright crystal2 rim	0.27	1.25		47.38	0.57	0.42	0.10	0.03	0.00		42.42	
Tal-i Iblis mit241D Bright crystal3	0.09	1.38		79.99	1.41	0.31	0.00	0.06	0.00		5.74	
Tal-i Iblis mit241D Dendrite2	17.48	4.08		4.09	0.48	5.07	1.05	1.45	0.00		68.76	
Tal-i Iblis mit241D Matrix light phase1	35.88	7.69		22.01	5.60	22.51	0.20	0.00	0.00		0.76	
Tal-i Iblis mit241D Matrix light phase1	37.91	8.18		20.27	5.42	21.38	0.38	0.55	0.00		0.89	
Tal-i Iblis mit241D Matrix light phase3	36.45	7.37		21.25	6.19	22.43	0.19	0.00	0.00		0.66	
Tal-i Iblis mit241D Matrix dark phase1	44.22	9.35		5.34	0.56	19.81	1.61	2.62	0.00		8.77	
Tal-i Iblis mit241D Matrix dark phase2	44.15	9.01		6.18	0.85	21.53	1.25	2.31	0.00		7.46	
Tal-i Iblis mit241D Matrix dark phase2	43.28	9.24		6.51	0.14	20.92	1.80	3.10	0.08		7.08	
	SiO2	Al2O3	Fe2O3	FeO	MgO	CaO	Na2O	K2O	SO3	CuO	Cu2O	Total
Tal-i Iblis mit241G Matrix dark crystals	40.67	7.71		2.79	7.98	34.17	2.69	0.03	0.00		0.48	
Tal-i Iblis mit241G Matrix dark crystals	40.84	7.54		2.30	8.44	34.76	2.46	0.02	0.00		0.54	
Tal-i Iblis mit241G Matrix dark crystals	40.82	7.14		2.39	8.52	34.46	2.47	0.01	0.00		0.48	
Tal-i Iblis mit241G Matrix light phase	40.63	12.32		9.22	1.98	20.46	0.94	0.81	0.04		5.98	
Tal-i Iblis mit241G Matrix light phase	39.77	11.92		8.67	2.24	21.21	0.99	0.74	0.03		6.14	
Tal-i Iblis mit241G Matrix light phase	40.63	11.20		10.63	2.92	21.04	0.74	0.53	0.04		4.44	
	SiO2	Al2O3	Fe2O3	FeO	MgO	CaO	Na2O	K2O	SO3	CuO	Cu2O	Total
Tal-i Iblis mit5277Q Matrix dark phase	53.01	26.68		0.22	0.00	9.12	6.03	0.09	0.00		0.00	
Tal-i Iblis mit5277Q Matrix light phase	54.44	14.49		5.85	5.06	8.26	2.64	2.44	0.00		0.00	

All Fe considered as Fe3+, and all Cu considered as Cu2+ (higher oxidation states)

	SiO2	Al2O3	Fe2O3	FeO	MgO	CaO	Na2O	K2O	SO3	CuO	Cu2O	T
1 Tal-i Iblis mit241D Bright crystal1	0.43	1.41	86.25		3.24	0.57	0.00	0.07	0.00	9.51		
2 Tal-i Iblis mit241D Bright crystal2	0.09	1.55	89.81		2.68	0.38	0.00	0.00	0.00	4.53		
3 Tal-i Iblis mit241D Bright crystal2 rim	0.27	1.25	52.66		0.57	0.42	0.10	0.03	0.00	47.18		
4 Tal-i Iblis mit241D Bright crystal3	0.09	1.38	88.90		1.41	0.31	0.00	0.06	0.00	6.39		
5 Tal-i Iblis mit241D Dendrite2	17.48	4.08	4.55		0.48	5.07	1.05	1.45	0.00	76.47		
6 Tal-i Iblis mit241D Matrix light phase1	35.88	7.69	24.46		5.60	22.51	0.20	0.00	0.00	0.85		
7 Tal-i Iblis mit241D Matrix light phase1	37.91	8.18	22.53		5.42	21.38	0.38	0.55	0.00	0.99		
8 Tal-i Iblis mit241D Matrix light phase3	36.45	7.37	23.62		6.19	22.43	0.19	0.00	0.00	0.74		
9 Tal-i Iblis mit241D Matrix dark phase1	44.22	9.35	5.93		0.56	19.81	1.61	2.62	0.00	9.76		
10 Tal-i Iblis mit241D Matrix dark phase2	44.15	9.01	6.86		0.85	21.53	1.25	2.31	0.00	8.29		
11 Tal-i Iblis mit241D Matrix dark phase2	43.28	9.24	7.23		0.14	20.92	1.80	3.10	0.08	7.88		
	SiO2	Al2O3	Fe2O3	FeO	MgO	CaO	Na2O	K2O	SO3	CuO	Cu2O	T
1 Tal-i Iblis mit241G Matrix dark crystals	40.67	7.71	3.10		7.98	34.17	2.69	0.03	0.00	0.53		
2 Tal-i Iblis mit241G Matrix dark crystals	40.84	7.54	2.55		8.44	34.76	2.46	0.02	0.00	0.60		
3 Tal-i Iblis mit241G Matrix dark crystals	40.82	7.14	2.66		8.52	34.46	2.47	0.01	0.00	0.53		
4 Tal-i Iblis mit241G Matrix light phase	40.63	12.32	10.25		1.98	20.46	0.94	0.81	0.04	6.65		
5 Tal-i Iblis mit241G Matrix light phase	39.77	11.92	9.64		2.24	21.21	0.99	0.74	0.03	6.83		
6 Tal-i Iblis mit241G Matrix light phase	40.63	11.20	11.81		2.92	21.04	0.74	0.53	0.04	4.93		
	SiO2	Al2O3	Fe2O3	FeO	MgO	CaO	Na2O	K2O	SO3	CuO	Cu2O	T
1 Tal-i Iblis mit5277Q Matrix dark phase	53.01	26.68	0.24		0.00	9.12	6.03	0.09	0.00	0.00		
2 Tal-i Iblis mit5277Q Matrix light phase	54.44	14.49	6.51		5.06	8.26	2.64	2.44	0.00	0.00		

Activation Laboratories Ltd. Work Order No. A04-0635 Report No. A04-0635

	SiO2	Al2O3	Fe2O3	FeO	MnO	MgO	CaO	Na2O	K2O	TiO2	P2O5	LOI	LOI2	TOTAL2	TOTAL	Ba	Sr	Y	Sc	Zr	Be	V
	%	%	%	%	%	%	%	%	%	%	%	%	%	%	%	ppm	ppm	ppm	ppm	ppm	ppm	ppm
74-1	52.54	15.78	5.04	1.08	0.123	3.21	6.54	2.07	2.92	0.609	0.31	9.10	9.22	99.43	99.43	367	475	16	17	118	2	123
77-1	55.29	15.13	5.30	-0.01	0.107	3.04	8.26	2.64	2.22	0.587	0.22	5.99	5.99	98.79	98.79	427	699	14	13	116	1	105
77-2	55.12	15.32	4.87	0.36	0.109	3.04	8.29	2.63	2.16	0.578	0.20	6.03	6.07	98.76	98.76	427	690	15	13	115	2	106
0-1	56.08	17.97	6.33	0.83	0.150	3.76	6.97	2.16	2.78	0.657	0.25	1.95	2.04	99.96	99.97	387	429	18	20	116	2	140
0b-1	58.21	17.43	4.18	2.16	0.129	3.34	7.57	2.14	2.54	0.665	0.25	0.20	0.44	99.05	99.05	423	507	17	18	132	2	133
1d-1	55.39	17.76	5.23	1.00	0.131	3.22	7.62	2.09	2.63	0.650	0.26	2.60	2.71	98.71	98.71	401	556	17	17	118	1	126
1e-1	55.81	18.03	5.32	1.44	0.141	3.51	7.66	1.88	2.47	0.643	0.26	1.39	1.55	98.71	98.71	398	508	17	19	118	2	137
1h-1	57.25	17.46	4.76	2.01	0.141	3.44	6.72	2.10	2.48	0.661	0.32	0.96	1.19	98.53	98.53	407	498	17	19	137	2	137
5-1	54.99	17.46	5.51	1.24	0.149	3.73	8.20	2.20	2.48	0.640	0.27	1.65	1.79	98.66	98.66	362	446	18	19	122	2	113
CERT	<u>59.62</u>	<u>11.75</u>	<u>6.49</u>	<u>3.59</u>	<u>0.32</u>	<u>2.67</u>	<u>8.26</u>	<u>4.12</u>	<u>4.23</u>	<u>0.15</u>	<u>0.54</u>	1.16				450	<u>302</u>	<u>718</u>	6.8	<u>320</u>	20	50 syenite
	59.60	11.53	6.25	3.59	0.324	2.62	8.22	3.96	4.21	0.133	0.53					440	307	727	8	311	21	50
94 CERT	<u>11.20</u>	<u>1.80</u>	<u>0.79</u>		<u>0.01</u>	<u>0.33</u>	<u>43.60</u>	<u>0.86</u>	<u>0.51</u>	0.11	<u>30.20</u>											1736 western phosphate roc
	11.16	1.87	0.72		0.011	0.32	42.92	0.83	0.54	0.109	29.14					116	961	140	3	94	2	1598
CERT	<u>52.44</u>	<u>15.35</u>	<u>10.74</u>		<u>0.163</u>	<u>6.37</u>	<u>10.87</u>	<u>2.14</u>	<u>0.627</u>	<u>1.06</u>	<u>0.131</u>	0.60				<u>182</u>	<u>194</u>	<u>24</u>	<u>35</u>	<u>94</u>	1.3	262 diabase
	52.42	15.30	10.73		0.163	6.35	10.85	2.17	0.68	1.063	0.15					176	196	18	36	81	1	263
CERT	<u>47.04</u>	<u>18.30</u>	<u>9.93</u>		<u>0.149</u>	<u>10.05</u>	<u>11.27</u>	<u>1.87</u>	<u>0.229</u>	<u>0.48</u>	0.085	0.60				<u>114</u>	<u>145</u>	<u>18</u>	<u>31</u>	<u>41</u>	1	148 dolerite
	46.90	18.28	9.80		0.144	10.11	11.22	1.87	0.23	0.473	0.08					107	143	16	31	32	-1	139
CERT	<u>47.77</u>	<u>15.35</u>	<u>11.26</u>	<u>8.38</u>	<u>0.171</u>	<u>9.68</u>	<u>13.24</u>	<u>1.75</u>	<u>0.027</u>	<u>0.96</u>	0.05					7.7	<u>108</u>	<u>16</u>	<u>44</u>	<u>22</u>	0.58	313 basalt
	47.75	15.32	11.24	8.4	0.169	9.64	13.21	1.77	0.03	0.957	0.02					8	108	13	44	15	-1	322
7113 CERT	<u>72.78</u>	<u>12.96</u>	<u>3.21</u>	<u>1.86</u>	<u>0.140</u>	<u>0.16</u>	<u>0.59</u>	<u>2.57</u>	<u>5.43</u>	<u>0.30</u>	<u>0.05</u>					<u>506</u>	<u>43</u>	<u>42.5</u>	<u>5.2</u>	<u>403</u>	<u>4.09</u>	3.8 granite
	72.78	12.89	3.13	1.82	0.140	0.15	0.59	2.48	5.35	0.282	0.05					495	41	44	5	392	4	34
333b CERT	<u>49.24</u>	<u>28.43</u>	<u>11.13</u>		<u>0.020</u>	<u>0.799</u>	<u>2.11</u>	<u>0.271</u>	2.26	<u>1.32</u>	0.53					<u>709</u>	<u>1041</u>		41			296 fly ash
	49.19	28.42	11.10		0.016	0.79	2.14	0.27	2.32	1.286	0.54					709	1038	81	39	207	12	290
CERT	<u>59.64</u>	<u>18.39</u>	<u>5.22</u>		<u>0.22</u>	<u>0.101</u>	<u>1.09</u>	<u>8.94</u>	<u>4.28</u>	<u>0.135</u>	<u>0.158</u>					560	<u>700</u>	<u>46</u>	<u>0.61</u>	<u>1210</u>	9.6	(8.7 syenite
	59.61	18.06	5.15		0.218	0.10	1.13	8.58	4.18	0.129	0.16					590	700	40	-1	1210	9	-5
CERT	<u>41.20</u>	<u>0.15</u>	<u>55.85</u>		<u>0.042</u>	<u>1.89</u>	<u>1.55</u>	<u>0.032</u>	<u>0.012</u>	<u>0.014</u>	<u>0.063</u>					1.5	3	9	0.38	2.4	4.7	4 Iron form sample
	41.13	0.13	55.80		0.037	1.94	1.54	0.06	0.07	-0.001	0.07					7	4	8	-1	10	5	-5
CERT	<u>65.02</u>	<u>18.61</u>	<u>0.09</u>		<u>0.005</u>	<u>0.01</u>	<u>0.11</u>	<u>2.58</u>	<u>12.81</u>	<u>0.02</u>	<u>0.02</u>					<u>200</u>	<u>39</u>	0.3	0.05	13	1	3 K-feldspar
	65.40	18.42	0.10		0.003	-0.01	0.10	2.46	12.26	-0.001	0.02					203	37	-1	-1	-1	1	-5
CERT			<u>8.66</u>																			
CERT			8.6																			
CERT			<u>1.07</u>																			
CERT			1.04																			

Note: Certificate data underlined are recommended values; other values are proposed except those preceded by a "/" which are information values.
 Note: The Fe2O3 for the standards is Total Fe2O3 and has not been adjusted for the FeO.

C. Douglas Read, B.Sc.
 Laboratory Manager

Appendix C

ActLabs Inc. protocol

Quality Analyses



Innovative Technologies

Code 4B Fusion ICP-OES Whole Rock Analysis

Samples are prepared and analyzed in a batch system. Each batch contains a method reagent blank, certified reference material and 17% replicates. Samples are mixed with a flux of lithium metaborate and lithium tetraborate and fused in an induction furnace. The molten melt is immediately poured into a solution of 5% nitric acid containing an internal standard, and mixed continuously until completely dissolved (~30 minutes). The samples were run for major oxides and selected trace elements (Code 4B) on a combination simultaneous/sequential Thermo Jarrell-Ash ENVIRO II ICP. Calibration is performed using 7 prepared USGS and Canmet certified reference materials. One of the 7 standards is used during the analysis for every group of ten samples.

Totals should be between 98.5% and 101%. If results come out lower, samples are scanned for base metals. Low reported totals may indicate sulphate being present or other elements like Li which won't normally be scanned for. Samples with low totals however are automatically refused and reanalyzed.

Fusion ICP:

Oxide	Detection Limits	Trace Elements:	Detection Limit
SiO ₂	0.01%	Ba	2 ppm
Al ₂ O ₃	0.01%	Sr	2 ppm
Fe ₂ O ₃	0.01%	Y	2 ppm
MgO	0.01%	Zr	2 ppm
MnO	0.01%	Sc	2 ppm
CaO	0.01%	Be	1 ppm
TiO ₂	0.01%	V	5 ppm
Na ₂ O	0.01%		
K ₂ O	0.01%		
P ₂ O ₅	0.01%		
Loss On Ignition	0.01%		

Typical ICP Standards Analysis (Oxides-%, Trace-ppm)

	SY3	Cert	DNC1	Cert	W2	Cert	STMI	Cert	MRG1	Cert	BIR1	Cert	G2	Cert
SiO ₂	59.51	59.68	46.91	47.04	52.58	52.44	59.64	59.64	39.43	39.12	47.78	47.77	68.72	69.14
Al ₂ O ₃	11.62	11.76	18.46	18.3	15.35	15.35	18.07	18.39	8.59	8.47	15.43	15.35	14.95	15.39
Fe ₂ O ₃	6.47	6.49	9.76	9.93	10.72	10.74	5.24	5.22	17.93	17.94	11.52	11.26	2.65	2.66
MnO	0.32	0.32	0.15	0.15	0.16	0.16	0.22	0.22	0.17	0.17	0.17	0.17	0.03	0.03
MgO	2.54	2.67	10.05	10.05	6.37	6.37	0.07	0.1	13.74	13.55	9.7	9.68	0.71	0.75
CaO	8.25	8.25	11.27	11.27	10.98	10.87	1.09	1.09	14.77	14.7	13.75	13.24	1.87	1.96
Na ₂ O	4.17	4.12	1.99	1.87	2.31	2.14	8.87	8.94	0.73	0.74	1.86	1.75	4.08	4.08
K ₂ O	4.23	4.23	0.24	0.23	0.64	0.63	4.24	4.28	0.18	0.18	0.02	0.02	4.48	4.48
TiO ₂	0.14	0.15	0.47	0.48	1.05	1.06	0.13	0.14	3.78	3.77	0.95	0.96	0.48	0.48
P ₂ O ₅	0.32	0.54	0.07	0.08	0.12	0.13	0.16	0.16	0.07	0.08	0.02	0.05	0.13	0.14
Ba	435	450	102	114	170	182	583	560	48	61	7	7	1,882	1,882
Sr	306	302	141	145	194	194	700	700	272	266	107	108	471	478
Y	718	718	16	18	21	24	44	46	13	14	16	16	9	11
Sc	8	6.8	31	31	35	35	-1	0.61	55	55	44	44	3	3.5
Zr	327	320	32	41	86	94	1,210	1,210	96	108	15	15.5	318	309
Be	22	20	-1	1	1	1.3	9	9.6	1	0.62	-1	0.58	2	2.5
V	44	50	141	148	262	262	-5	8.7	528	526	320	313	36	36

1336 Sandhill Drive, Ancaster, Ontario, Canada L9G 4V5
 Tel: +1.905.648.9611 or +1.888.228.5227 Fax: +1.905.648.9613
 E-mail: ancaster@actlabs.com ACTLABS Group Website <http://www.actlabs.com>

References Cited

- Bazin, D and H. Hübner.
1969 *Copper Deposits in Iran*. Geological Survey of Iran, Report No. 13
- Caldwell, Joseph R. and Sadegh Malek Shahmirzadi
1966 "Tal-i Iblis: The Kerman Range and the Beginnings of Smelting," *Illinois State Museum Preliminary Reports* No. 7, pp.1-25
- Caldwell, J. R.
1967 Forward In *Investigations at Tal-i Iblis*. Illinois State Museum Preliminary Reports No. 9, pp.7-14
- Caldwell, Joseph R.
1967 Chapter V "The setting and results of the Kerman Project, in Investigations at Tal-i Iblis," In *Investigations at Tal-i Iblis*. Illinois State Museum Preliminary Reports No. 9, pp.21-40
- Carniglia, S.C. and G. L. Barna
1992 *Handbook of Industrial Refractories Technology: Principles, Types, Properties and Applications*. Noyes Publications, Park Ridge, N.J.
- Charles, J.A.
July 1979 "From Copper to Iron—the Origin of Metallic Materials," *Journal of Metals*. Vol. 31, pp.8-13
- Chase, David W., Joseph R. Caldwell and Iren Fehervari
1967 Chapter X: "The Iblis Sequence and the Exploration of Excavation Areas A, C, and E" In *Investigations at Tal-i Iblis*. Illinois State Museum Preliminary Reports No. 9, pp.111-201
- Craddock, P.T.
2001 "From Hearth to Furnace: Evidences for the Earliest Metal Smelting Technologies in the Eastern Mediterranean," *Paleorient*. Vol. 26/2, pp.151-165
- Craddock, P. T. and M. J. Hughes
1985 *Early Metal Mining and Production*. Smithsonian Institute Press, Washington DC.
- Craig, James R. and David J. Vaughan
1981 *Ore Microscopy and Ore Petrography*. John Wiley & Sons, New York, Chichester, Brisbane, Toronto
- Deer, W.A., R.A Howie, and J. Zussman
1966 *An Introduction to the Rock-Forming Minerals*. Longman Group Ltd, Essex

- Dougherty, Ralph C. and Joseph R Caldwell
1966 "Evidence of early pyrometallurgy in the Kerman Range in Iran, in Investigations at Tal-I Iblis," *Science*, Vol.153, pp.984-5
- Dougherty, Ralph C. and Joseph R Caldwell
1967 "Evidence of early pyrometallurgy in the Kerman Range in Iran, in Investigations at Tal-I Iblis," In *Investigations at Tal-i Iblis*. Illinois State Museum Preliminary Reports No. 9, pp.17-20
- Ehlers, Ernest G.
1987 *Optical Mineralogy Volume 2: Mineral Descriptions*. Blackwell Scientific Publications, Palo Alto, Oxford, London, Edinburgh, Boston, Melbourne
- Evett, Daniel
1967 Chapter XI: "Artifacts and Architecture of the Iblis I Period: Areas D, F and G, in Investigations at Tal-i Iblis," In *Investigations at Tal-i Iblis*. Illinois State Museum Preliminary Reports No. 9, pp.202-219
- Freestone, Ian and David Gaimster
1997 *Pottery in the Making: Ceramic Traditions*. Smithsonian Institution Press, Washington DC
- Haghipour, A. and A. Aghanabati
1985 "Geological Map of Iran" *Ministry of Mines and Metals, Geological Survey of Iran*.
- Kingery, W.D.
1974 "A note on the Differential Thermal Analysis of Archaeological ceramics," *Archaeometry*. Vol.16 No.1 pp.109-112
- Kingery, W.D., H. K. Bowen and D. R. Uhlmann
1976 *Introduction to Ceramics*. John Wiley & Sons, New York, Chichester, Brisbane, Toronto
- Lamberg-Karlovsky, C. C. and Jeremy A. Sabloff
1995 *Ancient Civilizations: The Near East and Mesoamerica*, Waveland Press Inc, Illinois, pp.62-66, 80-84
- Lechtman, Heather and Sabine Klein
1999 "The Production of Copper-Arsenic Alloys (Arsenic Bronze) by Cosmelting: Modern Experiment, Ancient Practice" *Journal of Archaeological Science*. Vol. 26/5, pp.497-526

Lur'ye, A. M.

1986 "Formation Conditions of Copper-Sandstone and Copper-Shale deposits"
Geology and Metallogeny of Copper Deposits. G.H. Friedrich et al (editor),
Springer-Verlag Berlin Heidelberg, pp.477-491

Maddin, R., T. Stech Wheeler and J. D. Muhly

1980 "Distinguishing Artifacts Made of Native Copper" *Journal of Archaeological Science*. Vol.7 pp.211-225

Meanwell, Jennifer

2001 *Technical Choice in Pottery Production: A West Mexican Example*. BS Thesis
MIT, Cambridge, MA

MIT Electron Microprobe Facility

2003, Nov. 21, site visited on Feb 20, 2004 <<http://web.mit.edu/e-probe/www/>>

MIT

2001 3.081 lecture notes

Moore, Duane M., and Robert C. Reynolds, Jr.

1997 *X-Ray Diffraction and the Identification and Analysis of Clay Minerals*. Oxford
University Press, Oxford

Muan, Arnulf and E. F. Osborn

1965 *Phase Equilibria Among Oxides in Steelmaking*. Addison-Wesley Publishing
Company, Inc, Reading , MA

Neff, Hector

2000 "Neutron Activation Analysis for Provenance Determination in Archaeology"
In *Modern Analytical Methods in Art and Archaeology*. Enrico Ciliberto and
Giuseppe Spoto (editors) John Wiley & Sons, New York, Chichester, Brisbane,
Toronto

Obstler, Mimi

1996 *Out of the Earth into the Fire: A Course in Ceramic Materials for the Studio Potter*. The American Ceramic Society, Westerville, OH

Pigott, Vincent

1999 "The Development of Metal Production on the Iranian Plateau," *The Archaeometallurgy of the Asian Old World*. Vincent Pigott (editor); University of Pennsylvania Museum Press, Philadelphia pp.73-106

Pigott, Vincent and Heather Lechtman

2001 "Chalcolithic copper-based metallurgy on the Iranian plateau: a new look at old evidence from Tal-i Iblis," pp.291-312

Pleiner, Radomir

1967 Chapter XVII: "Preliminary evaluation of the 1966 metallurgical investigations in Iran, in Investigations at Tal-i Iblis," *Illinois State Museum Preliminary Reports*. No. 9, pp. 340-401

Rapp, George, Jr.

1988 "On the Origins of Copper and Bronze Alloying" In *The Beginning of the Use of metals and Alloys*. Robert Maddin (editor), MIT Press, Cambridge, MA. pp.21-27

Rice, Prudence M

1987 *Pottery Analysis: A Sourcebook*. The University of Chicago Press, Chicago

Stein, Sir Aurel

1937 *Archaeological Reconnaissances in North-Western India and South-Eastern Iran*. The University Press, Oxford

Thompson, F.C.

1958 "The Early Metallurgy of Copper and Bronze," *Man*. Vol. 58 pp. 1-7

Thornton, Christopher P., C.C. Lamberg-Karlovsky, Martin Liezers, and Suzanne M.Young

2002 "On Pins and Needles: Tracing the Evolution of Copper-base Alloying at Tepe Yahya, Iran via ICP-MS Analysis of Common-place Items," *Journal of Archaeological Science*. Vol. 29, pp.1451-1460

Tite, M.S.

1972 *Methods of Physical Examination in Archaeology*. Seminar Press, London, New York

Touloukian, Y. S. (editor)

1970 *Thermal Conductivity of Nonmetallic Solids*. Vol. 2 in series, Thermophysical Properties of Matter. IFI/Plenum, New York

Tylecote, R. F.

1982 "Metallurgical Crucibles and Crucible Slags," *Archaeological Ceramics*. Smithsonian Institution Press, Washington DC. pp.231-43

Tylecote, R. F.

1976 *A History of Metallurgy*. The Metals Society, London

U.S Department of the Interior, U.S. Geological Survey (USGS)

2001, Oct 10, *A Laboratory Manual for X-Ray Diffraction: Clay minerals*. Site visited on: April 13, 2004 <<http://pubs.usgs.gov/of/of01-041/htmldocs/clay.htm>>

Voigt, M. N. and R. H. Dyson, Jr.

1992 "The Chronology of Iran, ca. 8000-2000 B.C." *Chronologies in Old World Archaeology*. Robert Ehrich (editor), 3rd Edition, 2 Vols., The University of Chicago Press, Chicago

Weast, Robert (editor)

1981 *CRC Handbook of Chemistry and Physics 62nd Edition*. CRC Press, Boca Raton, Fla